Economic Geology, v. 103, pp. 1151–1184

Pericontinental Crustal Growth of the Southwestern Abitibi Subprovince, Canada—U-Pb, Hf, and Nd Isotope Evidence

John W. F. Ketchum,[†,*]

GEMOC ARC National Key Centre, Department of Earth and Planetary Sciences, Macquarie University, NSW 2109, Australia

John A. Ayer,

Precambrian Geoscience Section, Ontario Geological Survey, 933 Ramsay Lake Road, Sudbury, Ontario, Canada P3E 6B5

Otto van Breemen,

Geological Survey of Canada, 601 Booth Street, Ottawa, Ontario, Canada K1A 0E8

Norman J. Pearson,

GEMOC ARC National Key Centre, Department of Earth and Planetary Sciences, Macquarie University, NSW 2109, Australia

and Jens K. Becker

Institute of Geology, University of Tuebingen, Sigwartstr. 10, 72076 Tuebingen, Germany

Abstract

The Abitibi subprovince is widely regarded as a classic example of Neoarchean continental crust formed in an ensimatic setting. However, sialic crust as old as 2.93 Ga occurs in the adjacent Wawa subprovince, and the two subprovinces are thought to have formed a contiguous block since the initiation of Abitibi magmatic activity at 2.75 Ga. A detailed geochemical, U-Pb geochronological, and Nd-Hf isotope study of plutonic and volcanic rocks from the southwestern Abitibi provides evidence for the involvement of older crust during magma genesis near the Abitibi-Wawa boundary (Kapuskasing structural zone). Inherited zircons dated at ca. 2.85 Ga occur both in 2747 Ma tonalite and 2700 Ma granodiorite of the Rice Lake batholith, part of the larger Kenogamissi plutonic complex. Igneous zircons from this batholith display large intrasample variations in $^{176}Hf/^{177}Hf$, which we attribute to mixing of magmas derived from mantle ± juvenile crust and older crustal sources. Nd isotope data for felsic volcanic and plutonic rocks in this region indicate a dominantly juvenile source; however, two older felsic volcanic units (2739 and 2729 Ma) show Nd isotope evidence of significant crustal contamination. Post-tectonic plutonic units that were emplaced at 2676 and 2662 Ma also contain inherited zircons, but none are older than 2.76 Ga. In contrast, tonalitic units dated at 2744 and 2715 Ma from the Round Lake plutonic complex, located 150 km east of the Kapuskasing structural zone, lack zircon inheritance and display less intrasample Hf isotope variability in zircons. Our data suggest that the influence of older sialic crust during Abitibi volcanic and plutonic activity is restricted both in space and time. Similar evidence for an older crustal influence occurs elsewhere in the southwestern Abitibi near the Kapuskasing structural zone. The data collectively suggest that an approximately 75-km-wide belt of Abitibi crust adjacent to this structure was underlain by older Wawa crust from 2.75 Ga onward. This crustal geometry is consistent with development of the Abitibi subprovince at the edge of a Wawa protocraton, perhaps as the result of rifting of this older continental block.

Introduction

Amalgamation of the world's largest Archean craton, the Superior province of the Canadian Shield, is generally attributed to convergent plate tectonic processes similar to those operating on modern Earth. A number of distinctive subprovinces (also termed superterranes; Thurston, 1991) and smaller terranes have been identified throughout the province, and their boundaries are commonly linked to major structures formed during terrane accretion. The Abitibi subprovince (Fig. 1) is thought to represent one of the youngest of these accreted terranes (Corfu and Davis, 1992). It consists of volcanic, volcaniclastic, sedimentary, and plutonic rocks with primary ages between 2750 and 2670 Ma.

[†] Corresponding author: e-mail, john_ketchum@gov.nt.ca

[*] Present address: Northwest Territories Geoscience Office, P.O. Box 1500, Yellowknife, NT, Canada X1A 2R3.

Numerous geochemical and isotopic studies of Abitibi volcanic rocks suggest their derivation from juvenile mantle and/or juvenile crustal sources with no involvement of significantly older crust (e.g., Walker et al., 1988; Corfu and Noble, 1992; Kerrich et al., 1999; Wyman et al., 2002). Based mainly on this evidence, the Abitibi subprovince has been interpreted as a composite of intraoceanic arc and ocean plateau fragments that were tectonically accreted to the Superior province, followed by additional crustal growth (e.g., Ludden et al., 1986; Jackson and Fyon, 1991; Desrochers et al., 1993; Jackson et al., 1994; Wyman et al., 1999). Lithoprobe seismic reflection surveys of the Abitibi subprovince have imaged distinct crustal volumes bounded by north-dipping reflectors interpreted as regional-scale shear zones. These features have been largely attributed to accretionary tectonics (Calvert and Ludden, 1999), supporting the view of an allochthonous origin for most if not all of the subprovince. However, other

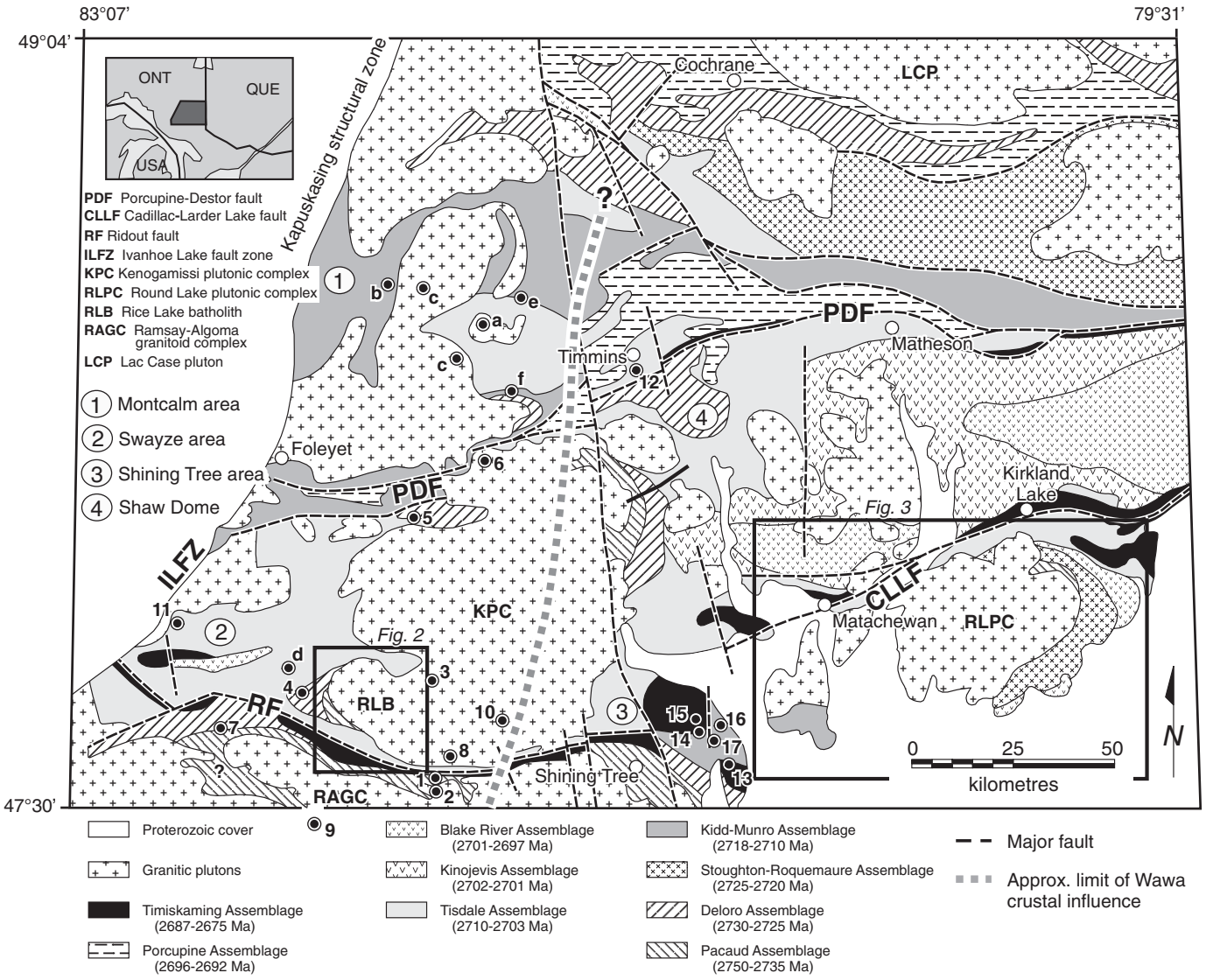

FIG. 1. Geologic map of the southwestern Abitibi subprovince in Ontario (after Ayer at al., 2002a), showing the location of the principal study areas. Numbered locations indicate whole-rock Sm-Nd sample sites (numbers are keyed to Table 6). Lettered locations indicate samples of other workers that are discussed in the text. Dashed line depicts the proposed eastern limit of older Wawa crust at depth that is detected isotopically in Abitibi magmatic and volcanic rocks. See text for further details.

workers have presented evidence favoring more autochthonous models of crustal growth. For example, Ayer et al. (2002a) noted that the regional stratigraphy of the southern Abitibi greenstone belt is largely upward-facing and coherent, with inherited zircons in most volcanic packages yielding U-Pb ages similar to those of stratigraphically lower units. These relationships were interpreted to suggest a mainly autochthonous to parautochthonous crustal development. Bleeker (2002) also highlighted this stratigraphic-isotopic age relationship and, in addition, summarized U-Pb and Nd isotope evidence for the involvement of significantly older crust during Abitibi magmatism. Rare inherited zircons with ages between 2.93 and 2.80 Ga are documented in both volcanic and plutonic protoliths, and whole-rock ε_{Nd} data suggest local involvement of older crust during magma genesis. Bleeker (2002) noted that rocks of similar age to the inherited zircons occur in the adjacent Opatica and Wawa subprovinces, located north and west of the Abitibi subprovince, respectively. He suggested that Abitibi supracrustal assemblages were built in part on highly extended continental crust derived from these neighboring subprovinces. If correct, this model has important implications for the tectonic setting(s) of Abitibi crustal growth. As one of world's most prospective greenstone belts, the model may also have implications for metallogenic evolution and the location of mineral deposits.

Here we add to this debate by presenting geochemical, U-Pb, Nd, and Hf isotope data for plutonic and volcanic rocks from the southwestern Abitibi subprovince. Our study integrates data from a variety of instrumental methods, including thermal ionization mass spectrometry (TIMS), sensitive high-resolution ion microprobe (SHRIMP), inductively coupled plasma mass spectrometry (ICPMS), and multicollector-magnetic

sector-inductively coupled plasma mass spectrometry (MC-ICPMS). The latter two methods were employed for in situ laser ablation (LA) sampling of igneous zircon grains. Our study provides additional evidence for the interaction of Abitibi magmas with significantly older continental crust. This is perhaps best demonstrated by zircon U-Pb and Hf isotope data from the Kenogamissi plutonic complex, located near the Abitibi-Wawa subprovince boundary in Ontario. Whole-rock Nd isotope data from the adjacent Swayze greenstone belt also provide some supporting evidence. In contrast, zircon isotope data from the more easterly Round Lake plutonic complex lack comparable evidence for the involvement of older continental crust during magma genesis.

Regional Geology

Figure 1 depicts part of the southwestern Abitibi subprovince of Ontario. This region lies mainly within the Southern Volcanic Zone described by Dimroth et al. (1982) and Ludden et al. (1986). The Abitibi greenstone belt underlies much of the area and is known for its well-preserved and geochemically varied volcanic lithologic units, economic mineral deposits, and relative abundance of komatiite and komatiitic basalt. The Abitibi greenstone belt is truncated to the west by the Kenogamissi plutonic complex, beyond which occur supracrustal rocks of the Swayze greenstone belt. The western border of the Swayze belt is defined in part by the Kapuskasing structural zone, a northeast-trending belt of high-grade plutonic and minor sedimentary rocks of the Wawa subprovince that were tectonically exhumed from the midcrust during the Late Archean and Paleoproterozoic (e.g., Percival and West, 1994).

The Abitibi and Swayze greenstone belts, and the smaller Shining Tree and Montcalm belts (Fig. 1), contain supracrustal assemblages of comparable lithology, U-Pb age, and depositional setting. Ayer et al. (2002a) regarded these belts as exposures of a single large greenstone belt consisting of nine volcano-sedimentary assemblages. The seven oldest assemblages contain mainly ultramafic, mafic, and felsic volcanic rocks, whereas the youngest two assemblages are dominantly sedimentary. The regional distribution and ages of these assemblages are depicted in Figure 1. Plutonic rocks within the Abitibi subprovince are mainly of granitic (sensu lato) composition. They are broadly divided into synvolcanic, syntectonic, and late- or post-tectonic suites (e.g., Sutcliffe et al., 1993; Chown et al., 2002).

The Kenogamissi plutonic complex has not been extensively studied, but its southwestern lobe was mapped at 1:50,000 scale by Heather and Shore (1999) and was termed the Rice Lake batholith by Becker and Benn (2003). Heather and Shore (1999) defined five principal map units within this batholith (Fig. 2), one of which they interpreted as a mafic

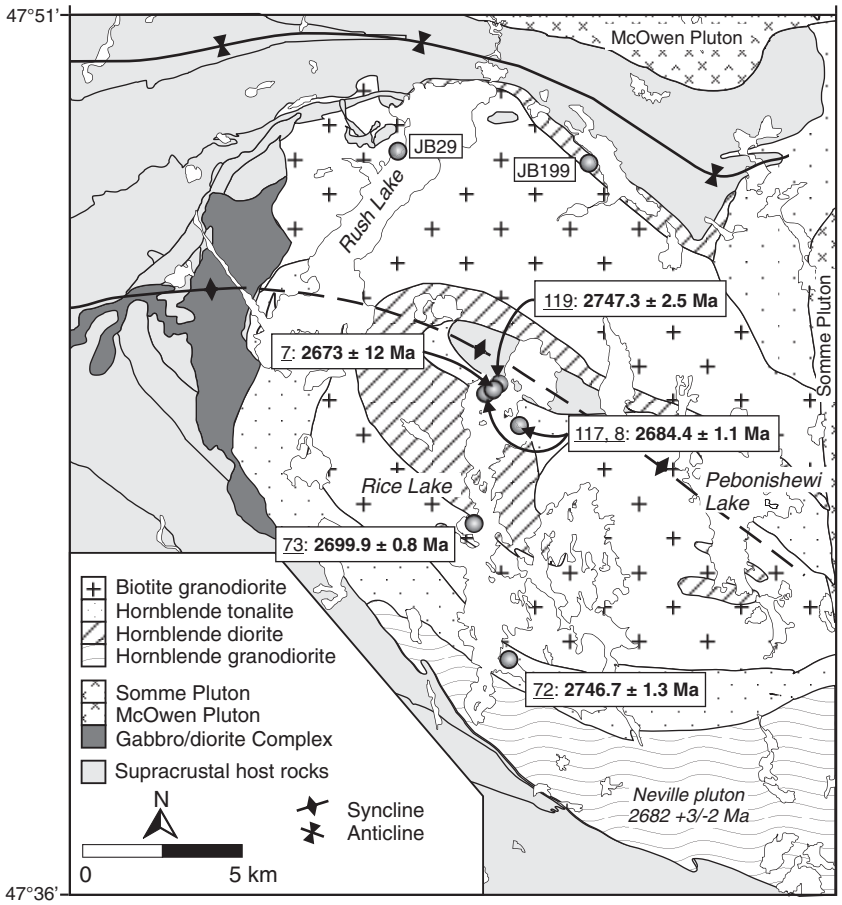

FIG. 2. Map of the Rice Lake batholith (after Becker and Benn, 2003), showing sample locations, abbreviated sample numbers, and primary crystallization ages based on U-Pb zircon data. The locations of two samples processed for Sm-Nd isotope geochemistry are also shown.

supracrustal enclave. These metamorphosed and variably deformed units are truncated to the east by the Somme granite pluton, a post-tectonic phase of the Kenogamissi plutonic complex. Elsewhere, the Rice Lake batholith is in contact with either the Swayze greenstone belt or with an Archean gabbro-diorite complex (Heather and Shore, 1999). The southern portion of the batholith is underlain by hornblende granodiorite of the Neville pluton, for which van Breemen et al. (2006) reported a U-Pb zircon age of 2682 $^{+3}_{-2}$ Ma. This unit is strongly deformed within the Ridout high-strain zone which occurs along the southern margin of the Kenogamissi plutonic complex (RF, Fig. 1).

West of the Rice Lake batholith, rocks of the Swayze greenstone belt are mainly assigned to the Tisdale assemblage (2710–2703 Ma), with older rocks of the Pacaud and Deloro assemblages (2750–2735 and 2730–2725 Ma, respectively) confined to the southern and eastern margins (Fig. 1). The stratigraphically highest volcanic package is exposed in the core of the Brett Lake syncline and consists of ca. 2670 Ma alkalic volcanic breccia that is correlated with the Timiskaming assemblage (Ayer et al., 2002b). As for the Abitibi belt, inherited zircon ages suggest a largely intact stratigraphic sequence for the Swayze belt (Heather, 1998; Ayer et al., 2002a; van Breemen et al., 2006). Clastic sedimentary rocks of the Timiskaming assemblage occur locally as unconformity bounded elongate panels, the largest of which occurs within the Ridout high-strain zone. South of this structural zone, the Swayze greenstone belt is in contact with the Chester granitoid complex and the more regionally extensive Ramsey-Algoma granitoid complex. An emplacement age of 2740 ± 2 Ma has been obtained for biotite trondjemite of the Chester complex (van Breemen et al., 2006).

The Round Lake plutonic complex is situated 100 km east of the Rice Lake study area (Figs. 1, 3). It is characterized by deformed tonalite and leucotonalite, and younger bodies of deformed and undeformed granodiorite (Harrap and Helmstaedt, 1992; Chown et al., 2002). Tonalitic units near the complex margin are typically highly strained and exhibit margin-parallel foliations. No age data have been published for tonalite members but two granodiorite bodies are dated at 2697.6 ± 4 and 2696.9 ± 1.5 Ma (Mortensen, 1993a; Fig. 3). The eastern granodiorite body also contains inherited zircons as old as ca. 2715 Ma. The emplacement ages appear to bracket a phase of late deformation that is related either to faulting (Chown et al., 2002) or solid-state diapirism (Jackson and Fyon, 1991). Where not obscured by Proterozoic cover rocks or mafic intrusions, host rocks to the batholith include the Pacaud, Stoughton-Roquemaure, and Tisdale assemblages. Strongly deformed Pacaud felsic tuff near the batholith margin is dated at 2746.9 ± 0.8 Ma (Mortensen, 1993a) and represents one of the oldest known volcanic units in the Abitibi subprovince.

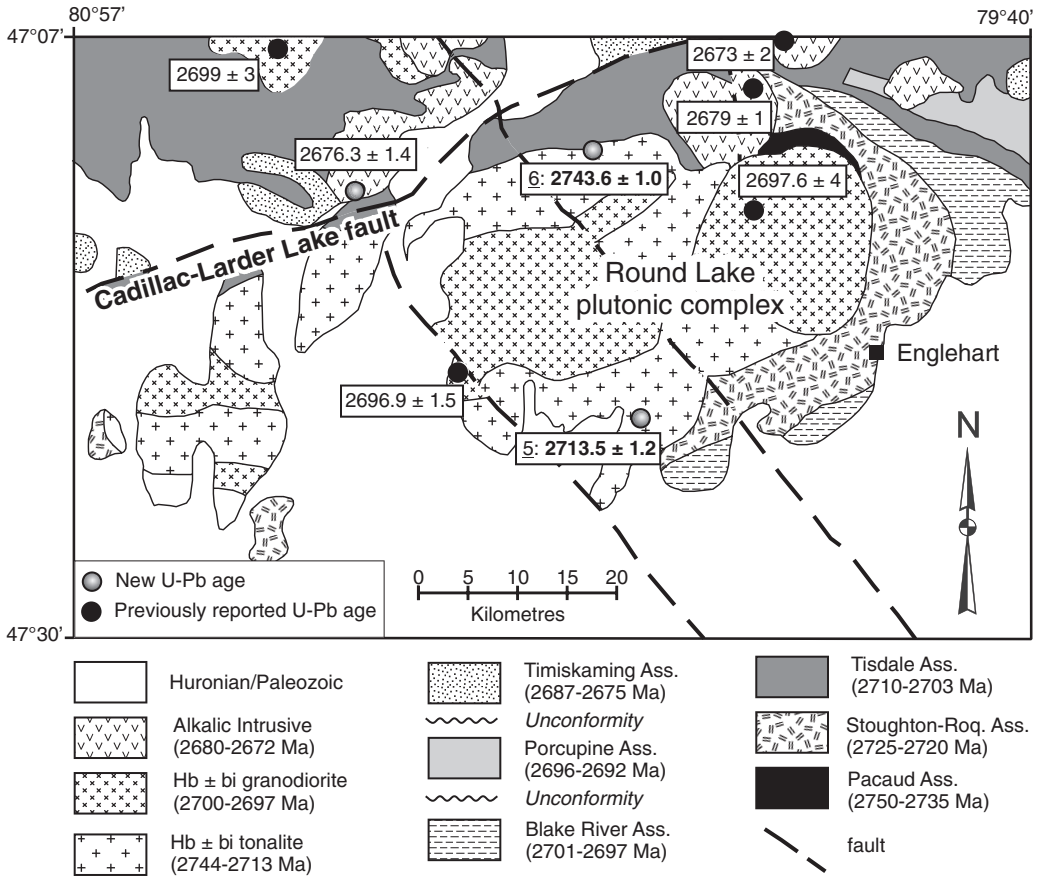

FIG. 3. Map of the Round Lake plutonic complex. Two new U-Pb zircon ages for this complex are shown in bold text, along with published ages for plutonic rocks in this region.

Sample Locations and Descriptions

Plutonic rocks

The majority of samples for U-Pb and Hf isotope analyses were collected from shoreline exposures of the Rice Lake batholith along Rice Lake (Fig. 2). The hornblende tonalite map unit was sampled in two areas. One sample (01JAA-72) consists of strongly foliated hornblende-biotite tonalite, whereas the other (JB119) is from a network of tonalite veins that intrude fine-grained amphibolite of possible supracrustal origin (Heather and Shore, 1999). The biotite granodiorite unit was sampled in central Rice Lake (01JAA-73) where this unit is only weakly foliated. The hornblende diorite was sampled in two locations. At both sample sites (JB117, 02JAA-8), the diorite is cut by two generations of tonalitic to granodioritic veins which were avoided during sampling. Near one of these locations, a small, weakly foliated body of tonalitic to granodioritic composition cuts the hornblende diorite and may be equivalent to one of the crosscutting phases. This body, which cuts a contorted foliation in the diorite, was also sampled (02JAA-7).

The U-Pb geochronology sample from the Somme pluton (92-HNB-26b; loc. 3, Fig. 1) is a medium-grained, unfoliated biotite granite. To the south, the Bardney batholith of the Ramsey-Algoma granitoid complex was also sampled (92-HNB-132f). This unit occurs outside the area shown in Figure 1. The sample consists of pink, massive, medium- to coarse-grained biotite granite. Both samples were dated by SHRIMP and no Hf isotope analyses were carried out.

The Round Lake batholith was sampled in two locations (Fig. 3). Highly strained hornblende-biotite tonalite gneiss (02JAA-6) crops out along Highway 66 near the northern margin of the batholith. The tonalite is cut by variably deformed veins of tonalite, granodiorite, and granite and contains large amphibolite enclaves of probable supracrustal origin. A vein- and enclave-free sample of tonalite gneiss was collected. Near the southern margin of the batholith, a large exposure of foliated tonalite was sampled along Highway 560 (02JAA-5). This sample is representative of a major map unit of the Round Lake batholith (Chown et al., 2002; Fig. 3).

Most of the Rice Lake samples and the Somme pluton sample were also processed for whole-rock Sm-Nd isotope geochemistry. From the Rice Lake batholith we also report Nd data for two additional samples that were not dated (JB29, JB199; Fig. 2). Several units of the Kenogamissi and Ramsay-Algoma plutonic complexes (locations 2, 6, 8, 10 in Fig. 1) and two intrusive bodies from the Shining Tree greenstone belt (locs. 16, 17) were also sampled for Nd isotope geochemistry. Reported U-Pb ages for all these samples range from 2740 to 2685 Ma (e.g., van Breemen et al., 2006; this study). The Nd isotope data are used here to investigate the source characteristics of Abitibi magmatism at various times and to compare with zircon Hf isotope data from the same area.

Volcanic rocks

A variety of volcanic samples were collected from the Swayze, Shining Tree, and Abitibi belts for whole-rock Sm-Nd isotope geochemistry. Sample locations are shown in Figure 1. The samples range in composition from felsic to ultramafic and have U-Pb zircon primary ages between 2730 and 2687 Ma.

Analytical Methods

Complete analytical methods are presented in the Appendix; however, a brief summary is provided here. Samples used in this study were collected over a ten-year period (1992–2002) by the authors and by other Abitibi workers including Kevin Heather (Geological Survey of Canada) and Glen Johns (Ontario Geological Survey). Whole-rock geochemical data (Table 1) were obtained by wavelength-dispersive X-ray fluorescence spectrometry (WD-XRFS) and ICPMS methods at the Geoscience Laboratories, Ontario Geological Survey, Sudbury. Samples collected for U-Pb geochronology were dated by TIMS (Jack Satterly Geochronology Lab, Royal Ontario Museum, Toronto; Table 2), LA-ICPMS (Macquarie University, Sydney; Table 3), and/or SHRIMP (Geological Survey of Canada, Ottawa; Table 4). The latter two methods were performed in situ on imaged zircons in polished grain mounts. The laser ablation data were used in most instances both to confirm the TIMS age of the sample and to search for older inherited zircon components. Most of the mounted zircons were subsequently analyzed in situ for Lu and Hf isotopes by LA-MC-ICPMS at Macquarie University (Table 5). Sm-Nd isotope analyses of whole-rock samples (Table 6) were carried out using TIMS by Brian Cousens at Carleton University, Ottawa (on contract to the Ontario Geological Survey) and by workers at the Geological Survey of Canada.

Whole-Rock Geochemical Data

Samples from the Kenogamissi and Round Lake plutonic complexes were analyzed for major and trace elements. The analyses are grouped with respect to both age and rock type in order to compare the geochemical characteristics of the plutonic complexes. In general, there is an overall enrichment trend in alkalis (in particular K_2O) for progressively younger samples of the same rock type, with the exception of the diorites which have a uniform age but variable K_2O (Table 1). Trace elements are shown as chondrite-normalized rare earth element (REE) plots and primitive mantle-normalized spidergrams in Figure 4. The 2747 Ma tonalites from the Rice Lake batholith have less light REE enrichment than the 2744 and 2714 Ma tonalites from the Round Lake plutonic complex ($[La/Yb]_{CN}$ = 7–8 vs. 18–27) and also have less depletion in Nb. Similar to the REE patterns for tonalites, granodiorite samples from the Rice Lake batholith are less light REE enriched than a single sample of Round Lake granodiorite ($[La/Yb]_{CN}$ = 8–16 vs. 26) but with equivalent Nb and Ti depletions. The 2684 Ma diorite samples from the Rice Lake batholith are relatively primitive, with lower SiO_2 and higher MgO, Ni, Cr, and Co than the other groups (Table 3). Their REE patterns show greater fractionation than the tonalite and granodiorite suites ($[La/Yb]_{CN}$ = 27–58), with typically pronounced negative Nb and Ti anomalies. They also have Zr and Hf depletions in contrast to the other groups which show moderate enrichments of these elements (Fig. 4). Youngest granitoid rocks of the Kenogamissi plutonic complex include a granodiorite sample from the 2682 Ma Neville pluton, a 2675 Ma tonalite dike, and granite from the 2676 Ma Somme pluton. These samples have variable REE fractionation ($[La/Yb]_{CN}$ = 14–36) and pronounced depletions in both Nb and Ti.

TABLE 1. Whole-Rock Geochemical Data, Kenogamissi and Round Lake Plutonic Complexes

Sample no.	JB119	01JAA-72	02JAA-5	02JAA-6	JB97	01JAA-73	02JAA-4	JB23	JB117	02JAA-8	JB79	JB100	02JAA-7	92-HNB-26b
Intrusion	RLB	RLB	RLPC	RLPC	RLB	RLB	RLPC	RLB	RLB	RLB	RLB-N	RLB-N	RLB	SP
Rock name	hb ton	hb ton	bi ton	hb-bi ton	bi gdi	bi gdi	hb-bi gdi	hb dio	hb dio	hb-qz dio	gdi	gdi	gdi	gdi
Easting	414199	414570	560503	555107	417896	413503	554823	414261	414555	413971	413490	418670	414031	425664
Northing	5288190	5279524	5289086	5318037	5280740	5283989	5306958	5298128	5287174	5288055	5277837	5277471	5288088	5292110
SiO_2	64.2	66.4	64.7	68.0	67.9	68.0	65.8	59.1	52.3	52.2	64.2	63.6	63.6	75.3
TiO_2	0.35	0.41	0.48	0.34	0.46	0.21	0.37	0.57	0.96	0.97	0.40	0.42	0.18	0.11
Al_2O_3	18.7	16.8	17.4	15.5	15.9	16.8	16.0	15.2	16.9	13.5	15.9	14.9	19.3	14.0
Fe_2O_3	3.19	4.01	4.55	3.62	3.72	1.75	3.36	5.45	9.12	9.96	4.08	3.97	1.81	0.60
MnO	0.04	0.06	0.06	0.05	0.04	0.03	0.05	0.08	0.13	0.16	0.07	0.08	0.03	0.03
MgO	1.12	1.15	2.08	1.53	0.89	0.64	2.24	4.24	5.09	8.13	2.15	3.68	1.13	0.26
CaO	3.98	4.58	4.93	4.27	2.62	2.19	3.70	5.37	7.25	8.25	4.03	3.84	1.83	0.97
Na_2O	6.70	5.15	4.41	5.44	5.91	7.61	6.14	4.85	5.59	4.67	5.19	5.56	8.45	3.70
K_2O	0.87	0.81	1.39	0.99	1.51	1.45	1.36	3.47	0.88	1.01	2.96	2.75	1.92	4.67
P_2O_5	0.09	0.09	0.13	0.06	0.11	0.06	0.13	0.43	0.43	0.63	0.21	0.24	0.08	
LOI	0.71	0.77	1.01	0.83	0.69	0.70	1.13	0.67	1.13	1.42	0.93	0.94	1.44	
Cr	25	5	35	28	10		80	178	89	331	55	159	40	
Co			21	15			17			53			10	
Ni			27	30			44			140			15	
Rb	20	22	33	27	46	24	23.36	100	11	24	64	51	53	
Sr	795	276	450	261	511	450	829	1349	1283	777	928	683	762	220
Cs	1.73	0.79	0.72	0.66	1.26	0.31	0.55	2.76	0.30	0.34	1.03	0.39	0.90	3.60
Ba	373	233	346	217	533	302	504	1501	676	436	1243	1658	535	760
Pb	9.0	3.0	9.0	8.0	6.0	10.4	13	13.0	5.0	8.0	15.0	7.0	13.0	
Ga	22.0	19.8	20.0	17.0	23.0	22.1	22	20.0	23.0	19.0	22.0	21.0	19.0	
Nb	2.2	4.7	4.3	7.7	4.6	3.5	2.84	8.5	6.0	4.9	6.7	5.3	1.5	9.6
Cu			15	6			18			12			14	
Sc			6	6			6			21			3	1
V			62	45			54			161			23	
Zn			65	51			73			142			53	27
Ta		0.38	0.31	0.80	0.36			0.40			0.42	0.34		0.91
Y	5.2	7.8	7.3	9.0	4.4	5.8	6.73	15.5	17.1	22.7	14.0	15.9	3.5	7.0
Zr	129.9	117.1	119.0	88.8	145.9	102.9	108.24	216.1	34.5	156.7	175.4	137.3	62.9	100.0
Hf	3.33	2.83	3.03	2.85	3.71	2.55	2.81	5.24	1.16	3.80	4.68	3.76	1.55	3.10
Th	0.48	0.40	3.44	3.60	2.14	1.09	1.54	13.67	0.51	2.15	6.41	6.14	0.53	19.00
U	0.30	0.14	0.35	1.03	0.39	0.40	0.35	2.35	0.12	0.64	1.22	0.86	0.20	4.40
La	5.86	6.72	24.58	18.85	10.00	5.60	19.05	80.94	47.75	59.41	37.61	49.49	5.75	29.00
Ce	13.23	12.83	49.36	36.58	24.03	13.62	40.71	169.33	111.83	131.18	77.02	107.71	13.03	57.00
Pr	1.73	1.70	5.74	4.13	2.52	1.73	5.33	20.55	15.10	18.24	9.10	12.74	1.82	5.60
Nd	7.76	7.56	19.73	14.74	9.71	7.10	21.42	78.65	63.68	76.70	34.90	50.52	7.52	19.00
Sm	1.70	1.88	2.94	2.77	1.91	1.71	3.8	12.47	11.35	14.25	6.28	8.88	1.52	2.80
Eu	0.65	0.75	0.91	0.78	0.59	0.46	1.11	2.86	3.00	3.84	1.50	2.10	0.66	0.53
Gd	1.49	1.84	2.09	2.24	1.46	1.51	2.63	7.25	7.34	9.24	4.46	5.86	1.15	1.00
Tb	0.17	0.26	0.27	0.32	0.19	0.22	0.3	0.74	0.79	1.10	0.55	0.69	0.14	0.25
Dy	1.00	1.49	1.41	1.66	1.02	1.06	1.38	3.48	3.84	5.00	2.77	3.41	0.68	1.20
Ho	0.19	0.28	0.27	0.31	0.18	0.19	0.24	0.54	0.61	0.87	0.48	0.58	0.12	0.21
Er	0.53	0.75	0.77	0.87	0.47	0.50	0.6	1.36	1.56	1.90	1.28	1.51	0.36	0.00
Tm	0.08	0.11	0.11	0.11	0.07	0.08	0.09	0.17	0.20	0.26	0.18	0.22	0.05	0.08
Yb	0.50	0.72	0.66	0.74	0.44	0.48	0.52	1.00	1.16	1.58	1.14	1.31	0.29	0.58
Lu	0.08	0.11	0.10	0.11	0.07	0.07	0.072	0.16	0.17	0.21	0.18	0.19	0.04	0.08
$(La/Yb)_{CN}$	8	7	27	18	16	8	26	58	30	27	24	27	14	36

Abbreviations: RLB = Rice Lake batholith (-N indicates Neville pluton); SP = Somme pluton; both are components of the larger Kenogamissi plutonic complex; RLPC = Round Lake plutonic complex; UTM coordinates are based on zone 17 and NAD 83.

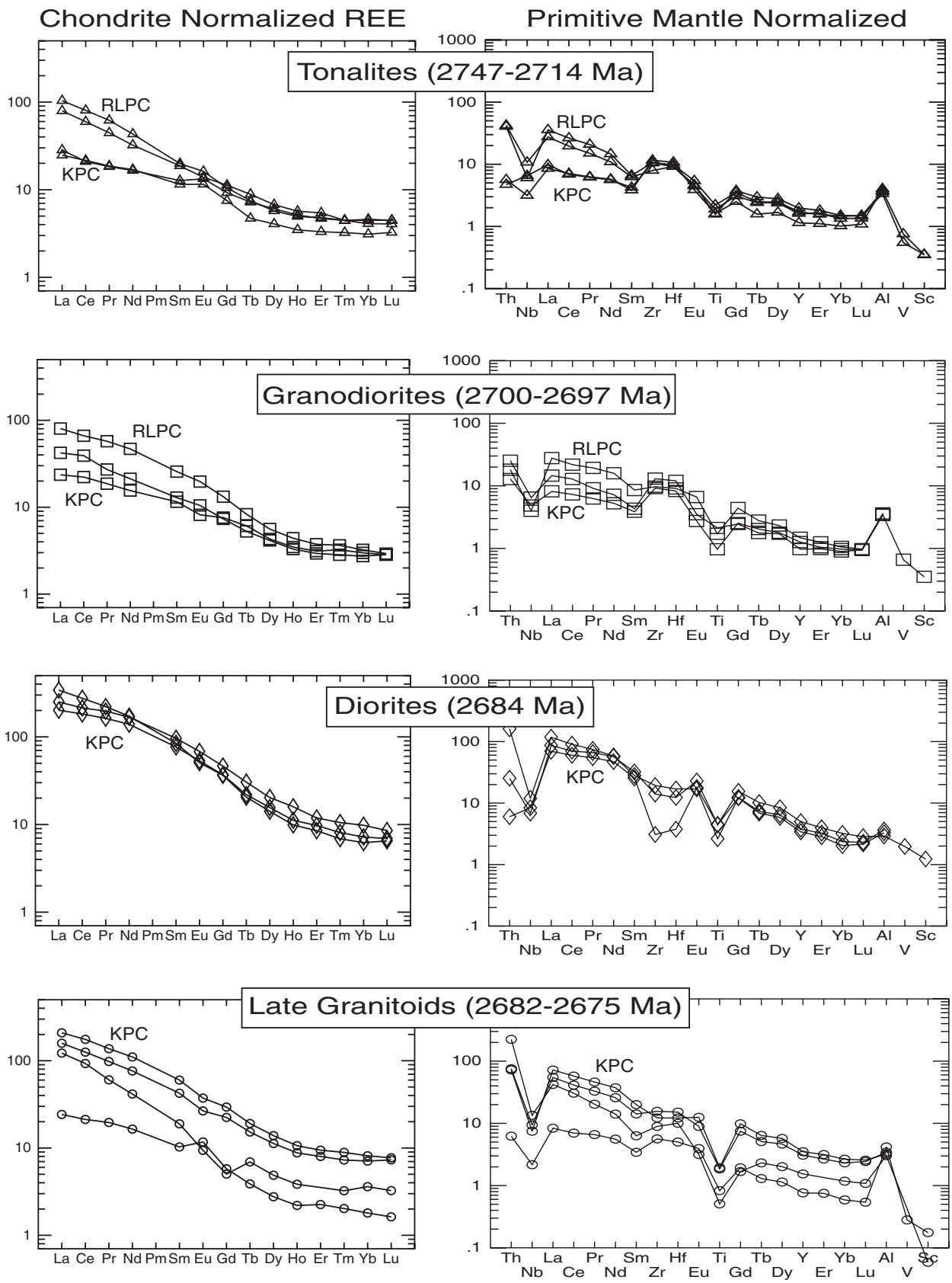

FIG. 4. Chondrite-normalized rare earth element plots and primitive mantle-normalized spider diagrams for representative plutonic rocks from the Kenogamissi plutonic complex (includes the Rice Lake batholith) and Round Lake plutonic complex. Geochemical data are provided in Table 1.

Zircon Characteristics and U-Pb Ages (TIMS and LA-ICPMS)

Sample JB119—biotite tonalite, Rice Lake batholith

Colorless, euhedral to slightly rounded prismatic zircons ranging from equant to 4/1 (length/breadth) occur in the least paramagnetic mineral separate. BSE and/or CL images reveal cores with patchy sector or oscillatory zoning and relatively thin, unzoned or oscillatory zoned rims that are typically cracked. Truncation of oscillatory zoning in cores is evident in several grains, as are recrystallized, BSE bright domains that occur adjacent to cracks, inclusions, and prismatic terminations. The best quality 3/1 and 4/1 prisms lacking visible evidence of cores were selected for TIMS analysis (Table 2), whereas all morphologies were selected for LA-ICPMS dating (Table 3).

Five single- and multigrain zircon fractions were analyzed by TIMS. Four fractions overlap within analytical uncertainty and provide a weighted average $^{207}Pb/^{206}Pb$ age of 2742.1 ± 1.7 Ma. The remaining fraction is 4 percent discordant. Regression of all data yields a discordia line with an upper intercept age of 2747.3 ± 2.6 Ma (Fig. 5a).

Interior portions of polished grains were targeted for LA-ICPMS dating. Nearly all the analyses are concordant at ca. 2750 Ma (Fig. 5b). Excluding one negatively discordant analysis, a weighted average $^{207}Pb/^{206}Pb$ age of 2755 ± 12 Ma is obtained from nine zircons. A cracked, high U grain tip (Table 3) was also analyzed and has a $^{207}Pb/^{206}Pb$ age of 2577 Ma. It is uncertain whether this dates a metamorphic overgrowth or a magmatic component that has lost Pb. Based on similar Th/U for core and rim analyses, the latter interpretation is preferred.

Given that near-concordant zircons analyzed by TIMS have younger $^{207}Pb/^{206}Pb$ ages with increasing discordance (suggesting a component of ancient Pb loss) and laser ablation analyses suggest a relatively old age for the sample, we suggest that the upper intercept age of 2747.3 ± 2.6 Ma provides the best estimate for tonalite emplacement. This age closely agrees with that for another tonalite sample from the Rice Lake batholith (see below).

Sample 01JAA-72—tonalite gneiss, Rice Lake batholith

Gem-quality, euhedral, 2/1 colorless zircon prisms are predominant in this sample. They are oscillatory zoned in BSE/CL and resemble pristine igneous zircons (e.g., Corfu et al., 2003), with sector zoning and evidence of minor magmatic resorption observed in some grains. Rare unzoned grain tips may indicate either local recrystallization or the presence of late magmatic or metamorphic overgrowths.

TIMS data for six strongly abraded single grains are concordant to 4.9 percent discordant with $^{207}Pb/^{206}Pb$ ages mainly between 2749 and 2741 Ma. Two concordant analyses provide a weighted mean age of 2746.7 ± 1.4 Ma, whereas a third is distinctly younger (2741.3 ± 1.8 Ma). Two discordant fractions with broadly similar ages to these suggest a component of recent Pb loss. A light pink grain has a significantly older age of 2846.8 ± 1.6 Ma and is interpreted as a zircon xenocryst.

LA-ICPMS analyses are concordant, with 10 grains yielding a weighted mean $^{207}Pb/^{206}Pb$ age of 2746 ± 11 Ma. One slightly older analysis was excluded from this calculation.

TABLE 2. Zircon and Titanite U-Pb Data (TIMS)

Lab ref.	Fraction[1]	Weight (mg)	U (ppm)	Th/U[2]	Total Pb (pg)	Pb^3 (pg)[c]	$^{207}Pb/^{204}Pb^4$	$^{206}Pb/^{238}U$	2 σ	$^{207}Pb/^{235}U$	2 σ	$^{207}Pb/^{206}Pb$ (Ma)	2 σ	Discord.[5] (%)	Corr. Coeff.
JB119 biotite tonalite, Rice Lake batholith															
jk7p14	Z1 clr euh 3:1 pr	0.004	68	0.39	160.1	0.5	3293	0.5267	0.0015	13.790	0.043	2741.3	1.4	0.6	0.961
jk7p15	Z2 clr euh 3:1 pr	0.002	55	0.34	60.2	3.8	189	0.5007	0.0047	12.826	0.130	2705.1	5.1	4.0	0.979
jk7p16	Z3 2 sm euh 3:1 lpr	0.002	57	0.53	68.8	0.5	1579	0.5260	0.0016	13.775	0.044	2741.7	2.0	0.8	0.924
jk7p42	Z4 2 sm clr lpr	0.004	33	0.51	79.9	0.2	4172	0.5293	0.0017	13.874	0.047	2743.2	1.9	0.2	0.942
jk9p90	Z5 lrg clr core? incl	0.003	86	0.34	125.5	0.4	3297	0.5281	0.0025	13.847	0.066	2743.6	2.7	0.4	0.942
jk10p55	T1 br frags (4)	0.069	82	0.14	3109.9	80.5	380	0.5141	0.0011	13.000	0.039	2684.0	2.9	0.5	0.815
jk10p56	T2 lbr to clr frag (6)	0.072	60	0.20	2643.5	286.2	92	0.5115	0.0027	12.912	0.116	2680.9	12.8	0.8	0.517
01JAA-72 tonalite gneiss, Rice Lake batholith															
jk7p121	Z1 clr euh 2:1 pr	0.001	35	0.43	29.2	0.3	1082	0.5285	0.0021	13.837	0.057	2741.3	1.8	0.3	0.966
jk7p123	Z2 lpk euh 2:1 pr	0.003	48	0.31	72.9	0.2	5017	0.5515	0.0015	15.401	0.045	2846.8	1.6	0.7	0.945
jk8p13	Z3 2:1 clr euh pr	0.004	62	0.41	123.2	0.2	7540	0.5059	0.0036	13.305	0.095	2748.6	2.6	4.9	0.975
jk8p14	Z4 2:1 clr pr	0.002	33	0.42	29.6	0.2	2575	0.5294	0.0035	13.918	0.090	2747.8	2.9	0.4	0.964
jk8p15	Z5 2:1 clr pr	0.001	43	0.41	25.8	0.2	2249	0.5307	0.0020	13.946	0.055	2746.3	1.6	0.1	0.970
jk8p70	Z6 3:1 euh clr pr	0.003	36	0.46	64.0	1.3	564	0.5227	0.0037	13.708	0.099	2743.8	2.6	1.5	0.976
02JAA-6 gneissic hornblende-biotite tonalite, Round Lake batholith															
jk9p133	Z3 clr 3:1 euh pr	0.003	26	0.51	50.9	1.4	412	0.5282	0.0021	13.855	0.061	2744.2	3.4	0.5	0.883
jk9p134	Z4 clr euh tab pr incl	0.002	70	0.64	95.4	0.7	1443	0.5272	0.0019	13.819	0.052	2743.0	1.9	0.6	0.951
jk9p131	Z1 lpk 2:1 euh pr	0.006	55	0.68	206.0	1.2	1798	0.5300	0.0017	13.895	0.048	2743.6	1.7	0.1	0.954
jk9p132	Z2 clr 3:1 euh pr	0.003	43	0.51	88.5	1.0	941	0.5287	0.0018	13.866	0.051	2743.9	1.9	0.4	0.948
jk10p53	T1 br frags (6)	0.028	161	0.27	2251.5	28.7	771	0.4575	0.0053	11.516	0.126	2676.3	6.9	11.1	0.933

TABLE 2. *(Cont)*

Lab ref.	Fraction[1]	Weight (mg)	U (ppm)	Th/U[2]	Total Pb (pg)	Pb[3] (pg)[c]	$^{207}Pb/^{204}Pb$[4]	$^{206}Pb/^{238}U$	2 σ	$^{207}Pb/^{235}U$	2 σ	$^{207}Pb/^{206}Pb$ (Ma)	2 σ	Discord.[5] (%)	Corr. Coeff.
02JAA-5 hornblende-biotite tonalite, Round Lake batholith															
jk9p128	Z1 3:1 clr euh pr	0.002	31	0.76	32.7	0.7	517	0.5176	0.0034	13.333	0.090	2714.3	3.4	1.1	0.953
jk9p129	Z2 4:1 clr euh pr	0.001	26	0.54	14.3	0.4	364	0.5253	0.0032	13.490	0.087	2709.4	3.4	–0.6	0.946
jk9p130	Z3 tab euh clr pr	0.001	82	0.50	48.5	0.6	870	0.5227	0.0018	13.460	0.050	2713.8	2.2	0.1	0.934
jk10p19	Z4 tab euh pr	0.001	147	0.39	67.9	0.2	3353	0.5200	0.0016	13.382	0.043	2713.0	1.9	0.6	0.931
01JAA-73 granodiorite, Rice Lake batholith															
jk7p124	Z1 clr euh 2:1 pr	0.003	51	0.26	76.6	0.2	4714	0.5491	0.0013	15.268	0.040	2839.8	1.5	0.8	0.940
jk7p125	Z2 clr euh 2:1 pr	0.002	30	0.22	27.0	0.3	1327	0.5521	0.0019	15.388	0.056	2843.6	2.3	0.4	0.922
jk7p126	Z3 clr eq euh pr	0.004	26	0.39	67.6	12.9	76	0.5507	0.0019	15.339	0.164	2842.6	13.0	0.6	0.849
jk8p16	Z4 3:1 clr euh pr	0.002	68	0.58	82.1	0.2	5378	0.5192	0.0012	13.278	0.035	2702.6	1.7	0.3	0.915
jk8p17	Z5 3:1 clr euh pr	0.002	40	0.71	37.3	0.1	2686	0.5187	0.0017	13.248	0.047	2700.3	1.8	0.3	0.954
jk8p18	Z6 2:1 clr euh pr	0.002	28	0.40	24.0	0.2	1157	0.5209	0.0023	13.302	0.061	2700.2	2.0	–0.1	0.965
jk8p71	Z7 clr eq euh pr	0.005	54	0.55	201.2	1.2	1402	0.5181	0.0025	13.231	0.066	2700.2	1.5	0.4	0.982
jk8p72	Z8 2:1 euh clr pr	0.006	55	0.64	200.7	2.3	912	0.5154	0.0018	13.182	0.050	2702.4	2.1	1.0	0.945
jk9p88	Z9 clr mf euh pr core?	0.015	22	0.40	192.0	0.4	5843	0.5173	0.0025	13.204	0.064	2699.2	2.1	0.5	0.965
jk9p89	Z10 clr core	0.003	44	0.41	76.8	0.3	3069	0.5190	0.0021	13.249	0.055	2699.5	1.7	0.2	0.967
jk10p57	T1 br frags (5)	0.064	59	2.04	3000.7	954.1	40	0.5288	0.0032	13.347	0.339	2680.6	33.2	–2.6	0.926
jk10p58	T2 lbr tablets (10)	0.071	27	2.80	1673.4	443.7	42	0.5117	0.0030	12.834	0.308	2670.2	31.3	0.3	0.904
JB117 hornblende diorite, Rice Lake batholith															
jk7p47	Z1 clr lrg irreg lpr	0.003	17	0.95	33.6	0.2	1391	0.5178	0.0019	13.101	0.049	2684.8	2.2	–0.2	0.937
jk7p48	Z2 3 sm anh clr pr	0.002	13	0.75	20.1	0.5	353	0.5168	0.0028	13.057	0.076	2682.5	3.9	–0.1	0.916
jk7p49	Z3 lbr anh pr frag	0.001	103	0.54	61.0	0.4	1772	0.5153	0.0020	13.023	0.048	2683.0	3.5	0.2	0.846
02JAA-8 hornblende diorite, Rice Lake batholith															
jk9p86	Z1 br euh 2:1 pr	0.000	308	1.40	84.9	0.7	1057	0.5107	0.0024	12.917	0.059	2684.2	3.5	1.1	0.895
jk9p87	Z2 clr anh 2:1 pr (3)	0.001	112	1.09	51.5	0.4	1278	0.5154	0.0016	13.042	0.044	2685.0	1.9	0.2	0.938
jk10p51	T1 lrg lyel pr frag (3)	0.083	9	2.41	699.9	95.1	56	0.5128	0.0020	12.905	0.177	2676.1	22.3	0.4	0.223
jk10p52	T2 sm lyel pr frags (4)	0.061	13	2.46	735.5	103.3	54	0.5134	0.0026	12.908	0.192	2674.4	23.8	0.2	0.278
02JAA-7 cross-cutting granodiorite, Rice Lake batholith															
jk10p37	Z1 euh 2:1 clr pr	0.004	24	0.67	57.3	0.4	1591	0.5167	0.0024	13.215	0.061	2702.6	2.5	0.8	0.945
jk10p38	Z2 euh 2:1 clr pr incl	0.003	20	0.68	37.3	0.9	434	0.5168	0.0020	13.192	0.056	2699.6	3.2	0.6	0.889
jk10p39	Z3 eq euh clr pr	0.003	24	0.50	48.5	0.8	674	0.5193	0.0021	13.266	0.057	2700.7	2.8	0.2	0.922
jk10p71	Z4 lpk subh eq pr	0.006	26	0.42	89.7	0.6	1661	0.5135	0.0035	13.131	0.088	2702.4	3.0	1.4	0.964
jk10p72	Z5 clr core	0.002	14	0.44	16.8	0.5	357	0.5205	0.0037	13.275	0.096	2698.1	5.3	–0.1	0.900
jk10p50	T1 euh lyel pr frag (4)	0.069	14	2.82	1013.0	160.7	46	0.5133	0.0021	12.930	0.232	2677.6	29.7	0.3	0.130

Notes: Data are from single grains unless otherwise noted by number of grains (bracketed) in fraction description; decay constants used are from Jaffey et al. (1971); for sample locations (UTM coordinates) see Table 3

[1] Abbreviations: Z = zircon, T = titanite; anh = anhedral, br = brown, clr = colorless, eq = equant, euh = euhedral, frag = fragment, incl = inclusions, irreg = irregular, lbr = light brown, lpr = long prismatic, lrg = large, mf = multifaceted, ovrgrth = overgrowth, pr = prismatic, rnd = rounded, sm = small, subh = subhedral, turb = turbid

[2] Th/U calculated from radiogenic $^{208}Pb/^{206}Pb$ ratio and $^{207}Pb/^{206}Pb$ age

[3] Total common Pb in fraction; blank isotopic composition: 206/204 = 18.221, 207/204 = 15.612, 208/204 = 39.36

[4] Corrected for spike and fractionation but not procedural blank

[5] Percent discordance for the given $^{207}Pb/^{206}Pb$ age

TABLE 3. Zircon U-Pb

Analysis no.[1]	Th (ppm)	U (ppm)	Th/U	$^{206}Pb^{C}$ (%)[2]	± 1σ (%)	Ratios (common-Pb corrected) $^{207}Pb/^{206}Pb$	± 1σ	$^{207}Pb/^{235}U$	± 1σ	$^{206}Pb/^{238}U$	± 1σ
JB119-02	39	95	0.42			0.19435	0.00209	14.921	0.192	0.5569	0.0069
JB119-03	26	53	0.49			0.18992	0.00200	13.979	0.167	0.5339	0.0063
JB119-04c	29	61	0.46			0.19093	0.00199	14.055	0.167	0.5340	0.0063
JB119-04r	92	286	0.32			0.17195	0.00181	11.304	0.134	0.4768	0.0056
JB119-07	47	88	0.54			0.18976	0.00200	13.831	0.173	0.5287	0.0065
JB119-08	33	75	0.44			0.19349	0.00204	13.964	0.172	0.5234	0.0063
JB119-09	40	89	0.45			0.19159	0.00202	14.541	0.181	0.5505	0.0067
JB119-10	31	74	0.43			0.19244	0.00204	14.441	0.178	0.5443	0.0065
JB119-14	12	82	0.15			0.19261	0.00203	14.273	0.174	0.5375	0.0064
JB119-15	21	59	0.35			0.19126	0.00204	14.077	0.169	0.5338	0.0062
JB119-17	35	71	0.49			0.19168	0.00202	13.780	0.167	0.5215	0.0062
01JAA-72-01	23	57	0.40			0.19142	0.00200	14.097	0.167	0.5342	0.0062
01JAA-72-03	21	46	0.45			0.18949	0.00200	14.101	0.169	0.5398	0.0064
01JAA-72-04c	22	55	0.40			0.19119	0.00201	13.789	0.165	0.5232	0.0062
01JAA-72-04r	12	33	0.35			0.19379	0.00226	14.662	0.196	0.5489	0.0070
01JAA-72-07	9	30	0.28			0.19087	0.00209	13.823	0.170	0.5253	0.0063
01JAA-72-08	28	68	0.41			0.18985	0.00197	14.072	0.167	0.5377	0.0063
01JAA-72-09	15	45	0.34			0.19020	0.00201	14.234	0.171	0.5429	0.0064
01JAA-72-10	20	50	0.41			0.19159	0.00202	14.235	0.172	0.5391	0.0064
01JAA-72-13	28	51	0.56			0.18866	0.00199	14.324	0.173	0.5509	0.0066
01JAA-72-14	10	55	0.18			0.19161	0.00201	14.436	0.174	0.5467	0.0065
01JAA-72-15	38	64	0.60			0.18987	0.00200	14.146	0.172	0.5404	0.0064
02JAA-6-01	29	39	0.73			0.18885	0.00200	13.875	0.172	0.5327	0.0066
02JAA-6-02	32	43	0.73			0.18703	0.00196	13.625	0.169	0.5281	0.0066
02JAA-6-03	20	28	0.71			0.18672	0.00200	13.801	0.171	0.5358	0.0067
02JAA-6-04	20	38	0.53			0.18626	0.00193	14.326	0.175	0.5576	0.0069
02JAA-6-05	21	51	0.41			0.18826	0.00194	13.517	0.164	0.5206	0.0064
02JAA-6-07	27	34	0.78			0.18780	0.00198	13.768	0.171	0.5316	0.0066
02JAA-6-08	19	29	0.65			0.19035	0.00206	13.789	0.173	0.5254	0.0065
02JAA-6-09	14	23	0.63			0.19047	0.00209	13.961	0.177	0.5316	0.0066
02JAA-6-11	21	54	0.38			0.19099	0.00196	13.794	0.169	0.5239	0.0065
02JAA-6-12	24	45	0.53			0.18909	0.00198	13.909	0.171	0.5336	0.0066
02JAA-5-01	27	71	0.38			0.18652	0.00191	13.424	0.161	0.5220	0.0063
02JAA-5-02	43	83	0.52			0.18738	0.00193	13.469	0.165	0.5214	0.0064
02JAA-5-03	44	79	0.56			0.18531	0.00187	12.618	0.142	0.4940	0.0056
02JAA-5-04	34	43	0.77			0.18399	0.00191	13.655	0.165	0.5382	0.0066
02JAA-5-05	29	46	0.64			0.18635	0.00193	13.413	0.162	0.5220	0.0064
02JAA-5-07	51	120	0.43			0.18542	0.00184	13.407	0.159	0.5244	0.0064
02JAA-5-10	18	39	0.47			0.18375	0.00192	13.206	0.161	0.5211	0.0064
02JAA-5-11	46	85	0.53			0.18366	0.00184	13.186	0.155	0.5206	0.0062
02JAA-5-13	34	45	0.75			0.18274	0.00190	13.407	0.164	0.5320	0.0066
02JAA-5-16	51	55	0.93			0.18204	0.00201	13.158	0.162	0.5244	0.0064
01JAA-73-01	44	87	0.51			0.18389	0.00189	13.822	0.158	0.5462	0.0062
01JAA-73-03	7	14	0.49			0.18247	0.00217	13.638	0.175	0.5435	0.0066
01JAA-73-04	60	106	0.56			0.17943	0.00181	13.602	0.157	0.5513	0.0064
01JAA-73-05	52	89	0.58			0.18450	0.00187	13.743	0.161	0.5415	0.0064
01JAA-73-07	14	60	0.23			0.18424	0.00188	13.401	0.156	0.5276	0.0062
01JAA-73-08	60	190	0.32			0.18450	0.00184	13.239	0.153	0.5204	0.0061
01JAA-73-09m	52	138	0.37	4.27	0.17	0.18127	0.00379	12.955	0.215	0.5183	0.0066
01JAA-73-09r	76	150	0.51	7.19	0.26	0.17865	0.00433	12.634	0.259	0.5129	0.0066
01JAA-73-10	83	158	0.53			0.18476	0.00185	13.538	0.156	0.5315	0.0062
01JAA-73-11	34	90	0.38			0.18586	0.00189	13.676	0.160	0.5336	0.0063
01JAA-73-13	72	142	0.51			0.18373	0.00186	13.465	0.155	0.5316	0.0061
01JAA-73-14	61	127	0.48			0.18450	0.00187	13.280	0.154	0.5220	0.0061
01JAA-73-15	11	27	0.42			0.18457	0.00201	13.135	0.161	0.5160	0.0061
01JAA-73-18	78	125	0.62			0.18633	0.00190	13.144	0.151	0.5115	0.0058
01JAA-73-19	41	73	0.56			0.18640	0.00193	13.473	0.161	0.5240	0.0062
01JAA-73-21	53	116	0.46			0.18571	0.00190	13.559	0.158	0.5296	0.0061
01JAA-73-22	114	145	0.79			0.18631	0.00190	13.286	0.154	0.5172	0.0059
01JAA-73-26	41	83	0.50			0.18540	0.00193	13.322	0.161	0.5212	0.0062

Data (LA-ICPMS)

		Ages (common-Pb corrected, Ma)									
$^{208}Pb/^{232}Th$	± 1σ	$^{207}Pb/^{206}Pb$	± 1σ	$^{207}Pb/^{235}U$	± 1σ	$^{206}Pb/^{238}U$	± 1σ	$^{208}Pb/^{232}Th$	± 1σ	Disc.[3] %	Correction type[4]
0.1576	0.0021	2779	18	2810	12	2854	29	2958	36	–3.3	None
0.1551	0.0020	2741	18	2748	11	2758	26	2914	34	–0.7	None
0.1535	0.0019	2750	18	2753	11	2758	26	2886	33	–0.3	None
0.1334	0.0017	2577	18	2549	11	2513	24	2531	31	3.0	None
0.1486	0.0018	2740	18	2738	12	2736	27	2801	32	0.2	None
0.1524	0.0019	2772	18	2747	12	2714	27	2866	33	2.6	None
0.1625	0.0020	2756	18	2786	12	2827	28	3044	35	–3.2	None
0.1602	0.0020	2763	18	2779	12	2801	27	3004	35	–1.7	None
0.1568	0.0023	2765	18	2768	12	2773	27	2944	40	–0.4	None
0.1541	0.0020	2753	18	2755	11	2758	26	2896	35	–0.2	None
0.1506	0.0019	2757	18	2735	12	2705	26	2835	33	2.3	None
0.1558	0.0020	2754	18	2756	11	2759	26	2927	34	–0.2	None
0.1572	0.0020	2738	18	2757	11	2782	27	2952	35	–2.0	None
0.1552	0.0020	2752	18	2735	11	2713	26	2915	34	1.8	None
0.1720	0.0029	2775	20	2794	13	2820	29	3208	51	–2.0	None
0.1651	0.0026	2750	18	2738	12	2722	26	3088	44	1.3	None
0.1579	0.0019	2741	17	2755	11	2774	26	2963	34	–1.5	None
0.1646	0.0022	2744	18	2765	11	2796	27	3079	38	–2.3	None
0.1650	0.0021	2756	18	2766	11	2780	27	3086	37	–1.0	None
0.1660	0.0021	2731	18	2771	11	2829	27	3103	36	–4.4	None
0.1672	0.0024	2756	18	2779	11	2811	27	3124	42	–2.4	None
0.1597	0.0020	2741	18	2760	12	2785	27	2994	35	–2.0	None
0.1560	0.0020	2732	18	2741	12	2753	28	2931	35	–1.0	None
0.1569	0.0020	2716	18	2724	12	2733	28	2946	35	–0.8	None
0.1563	0.0020	2713	18	2736	12	2766	28	2935	35	–2.4	None
0.1550	0.0020	2709	17	2772	12	2857	28	2912	36	–6.8	None
0.1429	0.0019	2727	17	2716	11	2702	27	2700	33	1.1	None
0.1464	0.0018	2723	18	2734	12	2748	28	2762	32	–1.2	None
0.1428	0.0019	2745	18	2735	12	2722	28	2698	34	1.0	None
0.1480	0.0020	2746	18	2747	12	2748	28	2790	36	–0.1	None
0.1474	0.0019	2751	17	2736	12	2716	27	2779	34	1.6	None
0.1505	0.0019	2734	18	2743	12	2757	28	2834	34	–1.0	None
0.1470	0.0018	2712	17	2710	11	2708	27	2772	32	0.2	None
0.1484	0.0018	2719	17	2713	12	2705	27	2797	32	0.7	None
0.1376	0.0015	2701	17	2652	11	2588	24	2605	27	5.1	None
0.1463	0.0018	2689	18	2726	11	2776	27	2759	31	–4.0	None
0.1460	0.0018	2710	17	2709	11	2707	27	2754	31	0.1	None
0.1477	0.0017	2702	17	2709	11	2718	27	2784	30	–0.7	None
0.1478	0.0019	2687	18	2695	12	2704	27	2786	34	–0.8	None
0.1485	0.0017	2686	17	2693	11	2702	26	2799	30	–0.7	None
0.1415	0.0017	2678	18	2709	12	2750	28	2676	31	–3.3	None
0.1450	0.0019	2672	19	2691	12	2718	27	2737	33	–2.1	None
0.1532	0.0018	2688	17	2738	11	2809	26	2881	32	–5.4	None
0.1612	0.0026	2675	20	2725	12	2798	27	3021	46	–5.4	None
0.1502	0.0017	2648	17	2722	11	2831	27	2829	30	–8.3	None
0.1516	0.0018	2694	17	2732	11	2790	27	2852	31	–4.2	None
0.1612	0.0020	2691	17	2708	11	2731	26	3021	35	–1.8	None
0.1536	0.0017	2694	17	2697	11	2701	26	2888	30	–0.3	None
0.1427	0.0023	2665	35	2676	16	2692	28	2696	41	–1.3	Disc
0.1414	0.0025	2640	41	2653	19	2669	28	2673	45	–1.3	Disc
0.1548	0.0017	2696	17	2718	11	2748	26	2910	29	–2.3	None
0.1666	0.0019	2706	17	2728	11	2757	26	3114	33	–2.3	None
0.1562	0.0017	2687	17	2713	11	2748	26	2933	30	–2.8	None
0.1533	0.0017	2694	17	2700	11	2708	26	2883	30	–0.6	None
0.1555	0.0022	2694	18	2689	12	2682	26	2921	38	0.5	None
0.1517	0.0017	2710	17	2690	11	2663	25	2854	30	2.1	None
0.1534	0.0018	2711	17	2713	11	2716	26	2885	32	–0.3	None
0.1529	0.0018	2705	17	2719	11	2740	26	2876	31	–1.6	None
0.1519	0.0017	2710	17	2700	11	2687	25	2858	30	1.0	None
0.1562	0.0019	2702	18	2703	11	2704	26	2933	34	–0.1	None

TABLE 3.

Analysis no.[1]	Th (ppm)	U (ppm)	Th/U	$^{206}Pb^{C}$ (%)[2]	± 1σ (%)	Ratios (common-Pb corrected) $^{207}Pb/^{206}Pb$	± 1σ	$^{207}Pb/^{235}U$	± 1σ	$^{206}Pb/^{238}U$	± 1σ
02JAA-8-02	37	52	0.71			0.18829	0.00219	13.845	0.188	0.5336	0.0069
02JAA-8-03	364	377	0.97			0.17998	0.00180	12.531	0.151	0.5049	0.0061
02JAA-8-04	118	133	0.88			0.18779	0.00202	13.855	0.183	0.5352	0.0069
02JAA-8-06	602	434	1.39			0.18420	0.00187	13.588	0.161	0.5350	0.0063
02JAA-8-08	677	553	1.23			0.18304	0.00185	13.680	0.169	0.5422	0.0067
02JAA-8-09	275	250	1.10			0.17042	0.00174	11.031	0.129	0.4696	0.0055
02JAA-8-10	266	247	1.08			0.18369	0.00182	12.952	0.151	0.5113	0.0061
02JAA-8-11	224	153	1.46			0.18336	0.00182	13.390	0.158	0.5297	0.0064
02JAA-8-12	424	378	1.12			0.18164	0.00179	13.332	0.156	0.5323	0.0064
02JAA-8-14	933	572	1.63			0.18075	0.00177	13.559	0.162	0.5442	0.0067
02JAA-8-15	815	582	1.40			0.18258	0.00180	13.608	0.161	0.5405	0.0065
02JAA-8-16	516	472	1.10			0.17196	0.00176	10.969	0.129	0.4627	0.0054
02JAA-7-01	97	60	1.62			0.18179	0.00190	12.630	0.152	0.5039	0.0060
02JAA-7-02	44	113	0.39			0.18364	0.00187	13.029	0.154	0.5145	0.0061
02JAA-7-03	89	66	1.35			0.18217	0.00189	13.109	0.159	0.5219	0.0063
02JAA-7-04	25	64	0.38			0.18131	0.00187	12.733	0.153	0.5093	0.0061
02JAA-7-05	60	41	1.44			0.18372	0.00193	13.024	0.158	0.5141	0.0061
02JAA-7-06	103	83	1.24			0.18280	0.00187	13.066	0.154	0.5184	0.0061
02JAA-7-08	161	90	1.79	1.26	0.51	0.17377	0.00595	11.731	0.358	0.4896	0.0076
02JAA-7-09	5	13	0.40			0.18010	0.00221	12.811	0.171	0.5158	0.0064
02JAA-7-11	171	108	1.59			0.18260	0.00184	12.577	0.149	0.4995	0.0060
02JAA-7-15	55	43	1.29			0.18101	0.00193	13.234	0.165	0.5303	0.0066

Notes: For rock types and sample locations see Tables 1 and 2

[1] c = core, m = middle, r = rim

[2] Percent common ^{206}Pb, calculated by the method of Andersen (2002)

[3] Disc. = percent discordance toward 0 Ma; negative number indicates that ellipse center lies above concordia

[4] Common Pb correction type (Andersen 2002); none = no common Pb correction; disc = common Pb corrected

These data compare favorably with the TIMS age of 2746.7 ± 1.4 Ma which, based on duplicate concordant analyses, we suggest represents the best age estimate for the tonalite gneiss protolith. The reason for the younger concordant TIMS age of 2741 Ma is uncertain, but it could be due either to Pb loss or to incomplete removal of a younger metamorphic overgrowth during laboratory abrasion.

Sample 02JAA-6—gneissic hornblende-biotite tonalite, Round Lake plutonic complex

Abundant euhedral and subhedral, faceted, colorless and light brown zircons are present in this sample. Broad oscillatory zoning or faint sector zoning (and in some cases both) are observed in individual grains, as are narrow, BSE/CL bright rims. A metamorphic versus igneous origin for the zircon rims is not readily apparent.

The weighted average $^{207}Pb/^{206}Pb$ age of four single abraded zircons analyzed by TIMS is 2743.6 ± 1.0 Ma, which we interpret as the emplacement age of the tonalite protolith. Excluding one negatively discordant analysis, a LA-ICPMS age of 2732 ± 12 Ma is obtained from 10 grains, which just overlaps the TIMS result within uncertainty. The zircon rims are too thin to analyze and were avoided during laser sampling. A scattering of LA-ICPMS analyses along concordia and their nominally younger age suggest that some of these zircons may have experienced a minor degree of Pb loss.

Sample 02JAA-5—hornblende-biotite tonalite, Round Lake plutonic complex

Colorless and light brown, high-quality euhedral zircons ranging from equant to 4/1 are abundant in the sample. Thin tip overgrowths are observed on some grains both in heavy mineral separates and in BSE/CL. Oscillatory zoning is typically well developed although variably truncated by patchy and sector-zoned domains, suggesting partial internal recrystallization.

Four single abraded grains were analyzed by TIMS; of these, three have a weighted average $^{207}Pb/^{206}Pb$ age of 2713.5 ± 1.3 Ma. The fourth analysis is slightly younger (2709.4 ± 3.4 Ma) and negatively discordant. The exact significance of this younger age is uncertain. LA-ICPMS data are predominantly concordant and provide a weighted mean $^{207}Pb/^{206}Pb$ age of 2696 ± 11 Ma. However, the analyses are somewhat dispersed along concordia, indicating that Pb loss may have variably influenced the zircon population. If this interpretation is correct, then the age of the four oldest concordant analyses (2711 ± 17 Ma) may better estimate the true zircon age. This age is in good agreement with the TIMS age of 2713.5 ± 1.3 Ma, which we suggest dates primary crystallization of the hornblende-biotite tonalite. Based on this result, the tonalite represents a possible source of ~2715 Ma zircon inheritance noted by Mortensen (1993a) and Chown et al. (2002) in the eastern granodiorite body of the Round Lake plutonic complex.

(Cont.)

Ages (common-Pb corrected, Ma)											
$^{208}Pb/^{232}Th$	± 1σ	$^{207}Pb/^{206}Pb$	± 1σ	$^{207}Pb/^{235}U$	± 1σ	$^{206}Pb/^{238}U$	± 1σ	$^{208}Pb/^{232}Th$	± 1σ	Disc.[3] %	Correction type[4]
0.1523	0.0022	2727	20	2739	13	2756	29	2865	39	–1.3	None
0.1382	0.0015	2653	17	2645	11	2635	26	2617	26	0.8	None
0.1427	0.0019	2723	18	2740	12	2763	29	2696	33	–1.8	None
0.1510	0.0017	2691	17	2721	11	2763	26	2843	30	–3.3	None
0.1543	0.0019	2681	17	2728	12	2792	28	2901	33	–5.1	None
0.1213	0.0013	2562	17	2526	11	2482	24	2313	24	3.8	None
0.1393	0.0015	2686	17	2676	11	2662	26	2635	26	1.1	None
0.1379	0.0015	2683	17	2708	11	2740	27	2611	26	–2.6	None
0.1459	0.0015	2668	17	2703	11	2751	27	2753	27	–3.8	None
0.1455	0.0015	2660	17	2719	11	2801	28	2745	26	–6.5	None
0.1461	0.0015	2676	17	2723	11	2785	27	2756	26	–5.0	None
0.1275	0.0015	2577	17	2520	11	2451	24	2425	26	5.9	None
0.1395	0.0015	2669	18	2652	11	2630	26	2639	27	1.8	None
0.1473	0.0017	2686	17	2682	11	2676	26	2777	30	0.4	None
0.1450	0.0016	2673	18	2688	11	2707	27	2737	28	–1.6	None
0.1476	0.0018	2665	17	2660	11	2654	26	2783	32	0.5	None
0.1479	0.0017	2687	18	2681	11	2674	26	2788	29	0.6	None
0.1494	0.0016	2678	17	2684	11	2692	26	2814	29	–0.6	None
0.1353	0.0020	2594	58	2583	29	2569	33	2565	35	1.2	Disc
0.1423	0.0028	2654	21	2666	13	2682	27	2689	49	–1.3	None
0.1470	0.0016	2677	17	2648	11	2612	26	2772	28	2.9	None
0.1499	0.0018	2662	18	2696	12	2743	28	2822	31	–3.7	None

Sample 01JAA-73—granodiorite, Rice Lake batholith

Colorless and light brown, euhedral and subhedral 2/1 prisms comprise the zircon population. Most grains are cracked and a few appear to contain distinctive core and rim components. Most of the imaged zircons are oscillatory zoned with minor evidence of resorption and local recrystallization. The remaining grains exhibit weakly zoned or unzoned cores and thin, BSE/CL bright rims. Colorless euhedral prisms, grains with apparent cores and overgrowths, and rare, high-clarity colorless euhedral grains were abraded separately for TIMS analysis.

Seven single-grain TIMS fractions provide a weighted mean $^{207}Pb/^{206}Pb$ age of 2700.6 ± 1.2 Ma but with a low 6 percent probability of fit. In detail, two age populations appear to be present. Five zircons yield an average $^{207}Pb/^{206}Pb$ age of 2699.9 ± 0.8 Ma, whereas two others are slightly but distinctly older with an average age of 2702.5 ± 1.3 Ma. The reproducibility of $^{207}Pb/^{206}Pb$ age argues for two distinct populations, but neither age group is morphologically distinct. Three additional single grains analyzed by TIMS are significantly older, with $^{207}Pb/^{206}Pb$ ages ranging from 2844 to 2840 Ma. A discordia line for these fractions has an imprecise upper intercept age of 2848 Ma, which is identical to the age of the interpreted xenocrystic zircon in sample 01JAA-72. The data therefore suggest that ca. 2850 to 2840 Ma inheritance occurs within at least two units of the Rice Lake batholith.

LA-ICPMS analyses are concordant or negatively discordant, with two common Pb-corrected data yielding relatively young ages most likely due to removal of supported uranogenic Pb during the correction procedure (Andersen, 2002). Excluding these data and two relatively young, negatively discordant analyses, a weighted average $^{207}Pb/^{206}Pb$ age of 2699 ± 18 Ma is obtained from 14 grains, identical to the TIMS age. Crystallization of the granodiorite is suggested here to have occurred at 2699.9 ± 0.8 Ma, with all older zircons interpreted as inherited. The 2702.5 Ma zircons may be derived from a slightly older phase of the Rice Lake batholith.

Samples JB117 and 02JAA-8— hornblende diorite, Rice Lake batholith

These samples were collected from the same map unit of hornblende diorite. Both yielded colorless to light brown, subhedral and anhedral zircons ranging from equant to 4/1. Some grains preserve crystal faces but most appear to be strongly resorbed. BSE/CL images show cracked and variably resorbed zircons, with anhedral grains typically exhibiting evidence of internal recrystallization and alteration (e.g., patchy and/or bulbous unzoned domains). Euhedral grains and grain fragments are characterized mainly by diffuse oscillatory zoning, which may be a relict igneous feature ("ghost zoning" of Hoskin and Schaltegger, 2003).

Single- and multigrain TIMS analyses for both samples have been combined in Figure 6c. The analyses are mostly concordant and provide an average $^{207}Pb/^{206}Pb$ age of 2684.4 ± 1.2 Ma. Only sample (02JAA-08) was dated by LA-ICPMS,

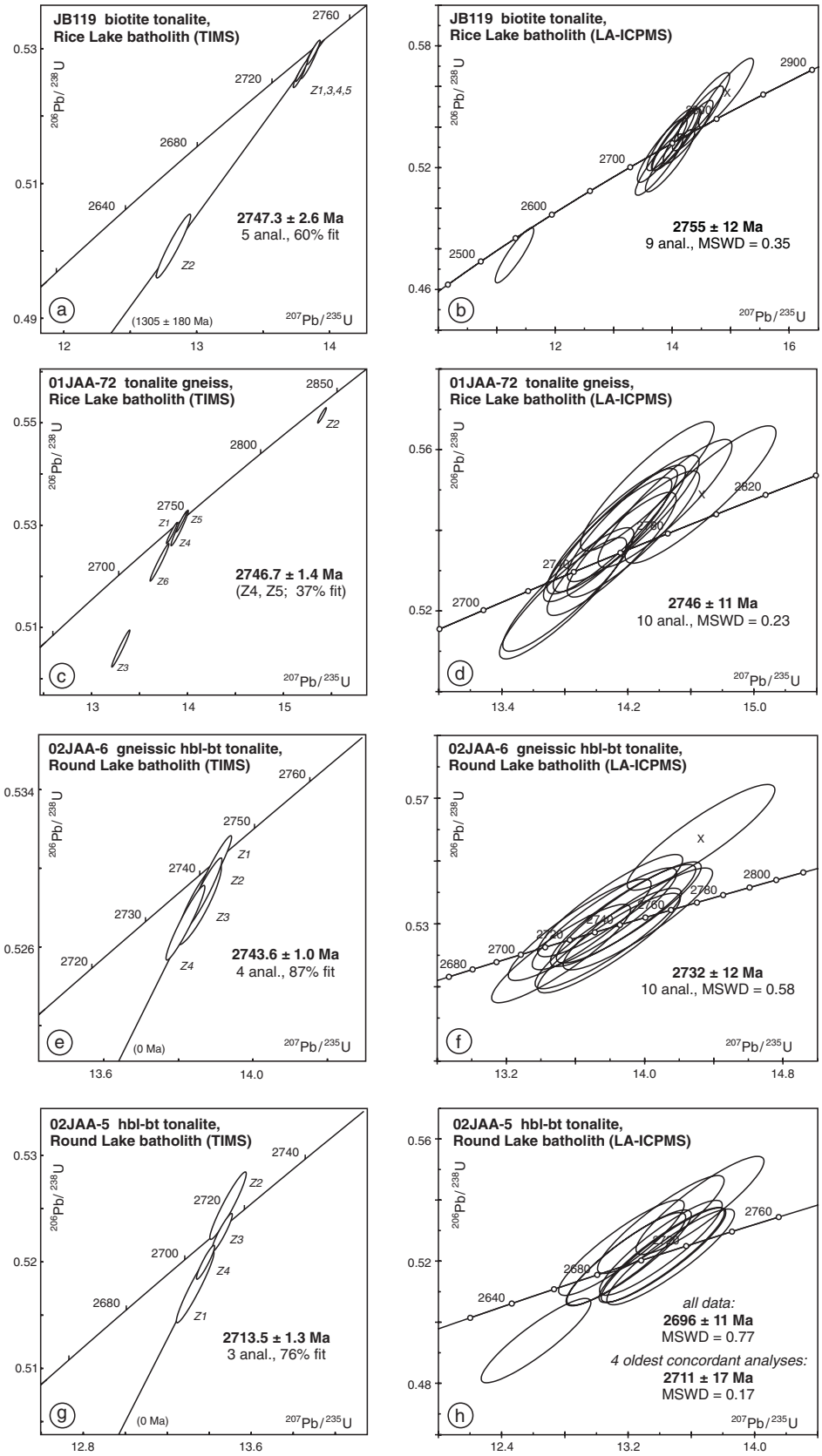

FIG. 5. Zircon U-Pb concordia diagrams. TIMS data in left-hand column, LA-ICPMS data from the same sample are shown opposite. LA-ICPMS analyses that plot near the main population but were not used in an age calculation are shown with an "x" at their center. All error ellipses are 2σ.

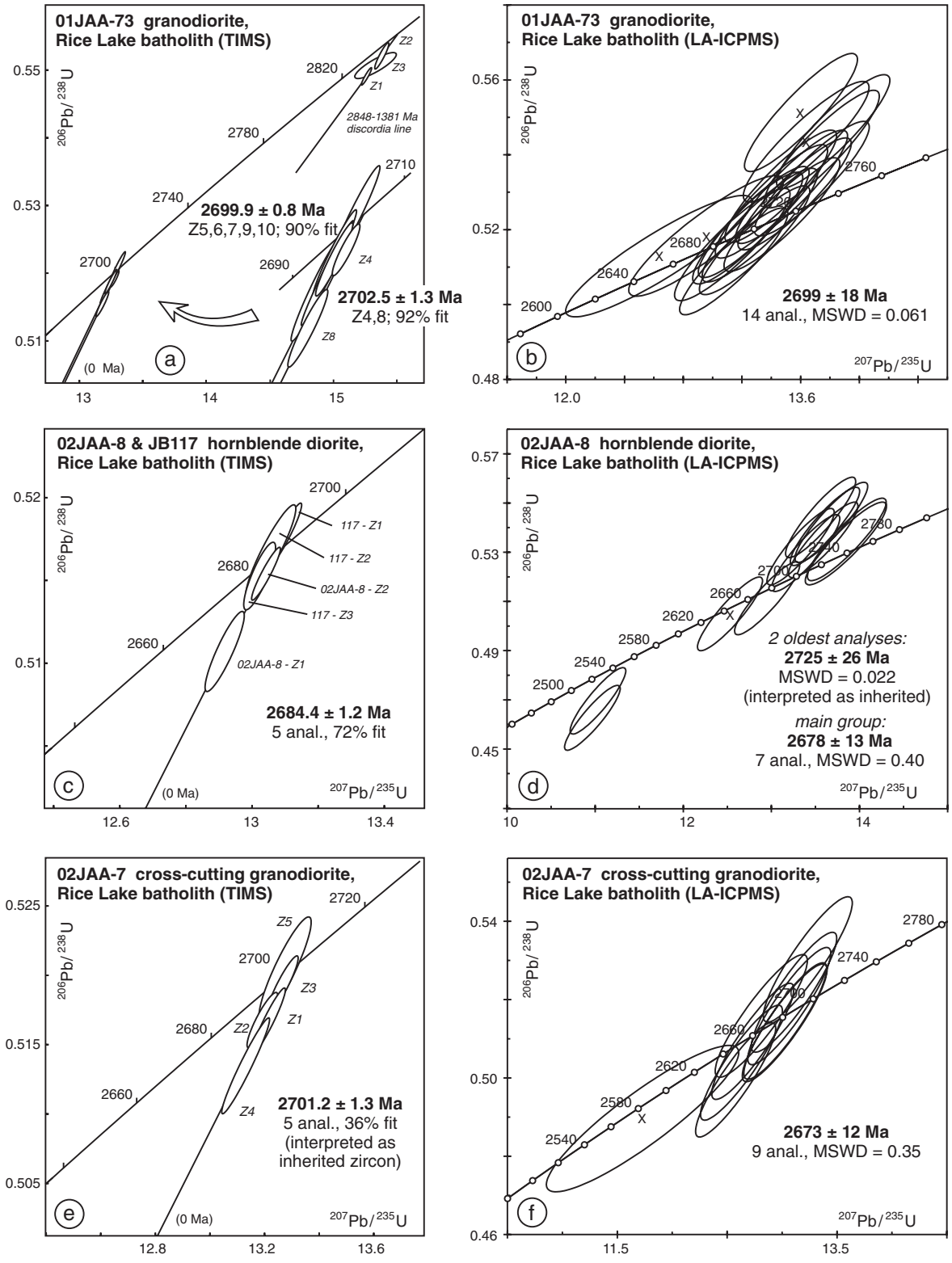

FIG. 6. Zircon U-Pb concordia diagrams. TIMS data in left-hand column, LA-ICPMS data from the same sample are shown opposite. See caption to Figure 6 for additional details.

with the data providing a more complex age distribution. The analyses are concordant or near concordant, with seven grains yielding a weighted mean age of 2678 ± 13 Ma, in good agreement with the TIMS age. Three cracked and/or resorbed and altered grains have younger ages (most likely due to the influence of Pb loss), whereas two oscillatory zoned, elongate subhedral prisms have a weighted mean $^{207}Pb/^{206}Pb$ age of 2725 ± 26 Ma. We suggest that this older age may date an inherited zircon population, with the TIMS age of 2684.4 ± 1.2 Ma interpreted as the primary crystallization age of the hornblende diorite.

Sample 02JAA-7—crosscutting granodiorite, Rice Lake batholith

The zircon population is varied, consisting mainly of poor quality, colorless and light pink, euhedral and anhedral prisms. The best quality zircons are colorless, euhedral, 2/1 faceted prisms that are relatively rare. Only this grain type was selected for TIMS analysis due to the poor quality of the other morphologies. Internal structures in the remaining zircon types selected for LA-ICPMS dating range from well-developed oscillatory zoning to unstructured. Roughly half of the BSE/CL-imaged grains exhibit internal features consistent with partial recrystallization.

Five single grains were analyzed by TIMS. These data are ≤1.4 percent discordant and yield an average $^{207}Pb/^{206}Pb$ age of 2701.2 ± 1.3 Ma. However, this age is inconsistent with field relationships and U-Pb data, indicating a primary age that must be younger than 2684 Ma, the age of the hornblende diorite host. LA-ICPMS data for nine zircons are concordant and provide a weighted mean $^{207}Pb/^{206}Pb$ age of 2673 ± 12 Ma. The laser ablation data, in conjunction with field relationships and the U-Pb age of the hornblende diorite, suggest that the TIMS age of 2701 Ma most likely dates an inherited zircon population. We therefore consider the best age estimate for the granodiorite intrusion to be 2673 ± 12 Ma.

Titanite U-Pb analyses, Rice Lake batholith and Round Lake plutonic complex

Five samples from the Rice Lake and Round Lake study areas yielded titanite, typically as light yellow, light brown, or brown fragments of prismatic grains. Due to the metamorphic and deformation state of all samples, it is unlikely that these represent fragments of original igneous crystals. Igneous titanite, if once present, has likely been completely recrystallized and hence original crystallization ages are not expected. Eight multigrain titanite fractions from the five samples were analyzed by TIMS. All the fractions have comparable $^{207}Pb/^{206}Pb$ ages and yield an upper intercept age of 2683.7 ± 2.8 Ma. One analysis lies above concordia which may indicate disturbance of the uranium isotope composition. The six most concordant analyses have a weighted mean $^{207}Pb/^{206}Pb$ age of 2683.4 ± 2.7 Ma.

Although titanite ages are similar, only one analysis ($^{207}Pb/^{206}Pb$ age of 2684.0 ± 2.9 Ma) can be considered to be precise, with analytical imprecision for the other fractions possibly masking real age differences. For instance, excluding the precise analysis, the remaining fractions yield a weighted average $^{207}Pb/^{206}Pb$ age of 2677.9 ± 8.9 Ma. Therefore, some of the titanite fractions may be younger than 2683 Ma. This is significant because granodiorite sample 02JAA-7, for which we suggest a primary crystallization age of ca. 2673 Ma, also contains titanite. In summary, although U-Pb data suggest a common episode of new titanite growth and/or recrystallization and isotopic resetting of older grains at ca. 2684 Ma, analytical imprecision limits confidence in this hypothesis, and at least one sample contains titanite that is probably younger than this age.

A regional thermal event is suggested by these data and by comparable titanite ages from north of the Swayze greenstone belt (Percival and West, 1994). A possible heat source for this event is suggested by the widespread occurrence of plutonic rocks of appropriate age, including 2684 ± 1 Ma

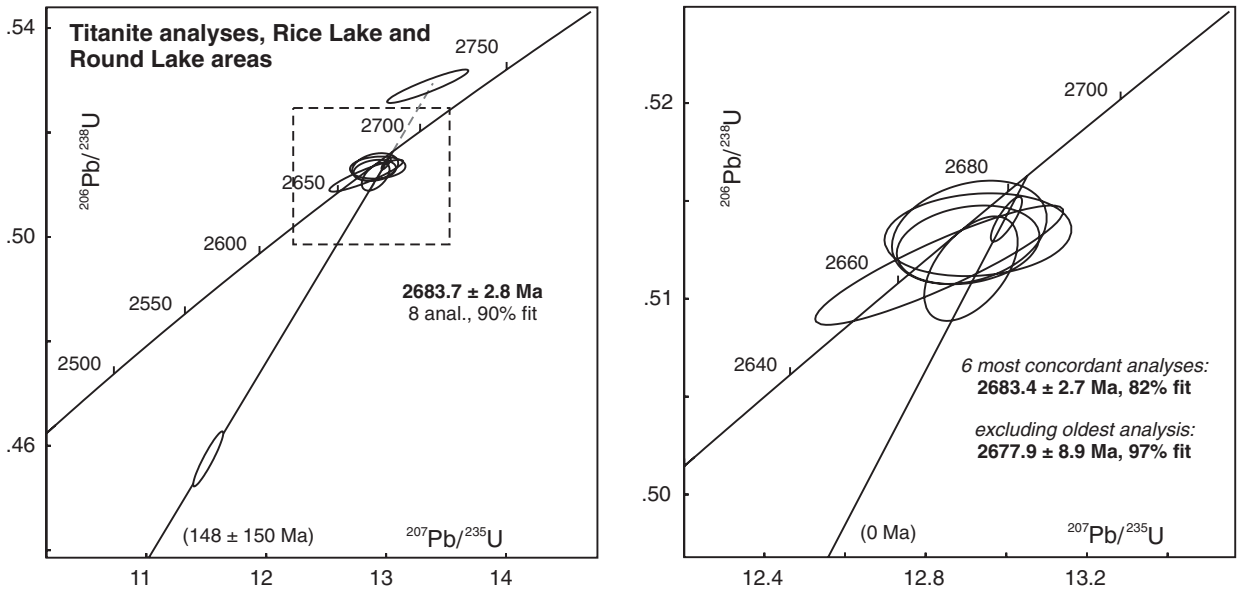

FIG. 7. Titanite U-Pb concordia diagrams. Analyses from five plutonic samples from the Rice Lake batholith and Round Lake plutonic complex are plotted together. Dashed-line box indicates the location of the enlarged figure shown on the right.

hornblende diorite (this study), the 2682 $^{+3}_{-2}$ Ma Neville pluton located at the southern margin of the Rice Lake batholith (van Breemen et al., 2006) and the 2686 ± 3 Ma Adams stock north of the Kenogamissi batholith (see summary in Corfu, 1993). Alternatively, the similarity of titanite ages may be related to regional tectonic burial and heating.

U-Pb Ages (SHRIMP)

Sample 92-HNB-26b—Somme pluton, Kenogamissi plutonic complex

Zircons isolated from this sample are prismatic and range from elongate to stubby, with weak oscillatory zoning typically observed in CL images. The grains are commonly cracked, and in many cases these cracks highlight the presence of a distinctive rounded core resembling an older inherited component. The age data confirm this relationship.

Eighteen analyses of zircons of the "main" population (Fig. 8a) provide a weighted mean $^{207}Pb/^{206}Pb$ age of 2676 ± 4 Ma, which we interpret as the igneous crystallization age of the Somme pluton. Six analyses of zircon cores yield $^{207}Pb/^{206}Pb$ ages ranging from ca. 2765 to 2700 Ma with a weighted mean age of ca. 2740 Ma. The cores have significantly lower concentrations of both U and Th, although there is some overlap with the widely ranging values for the igneous zircons (Fig. 8a). The cores are interpreted as inherited grains that probably crystallized from less-evolved igneous rocks during the early stages of Swayze greenstone belt construction.

Sample 92-HNB-132f—Bardney batholith, Ramsey-Algoma granitoid complex

Zircons are prismatic and range from elongate to equant. CL images of some grains reveal well-developed oscillatory zoning and distinctive cores.

Nineteen zircon grains were analyzed. The youngest analysis of 2564 ± 22 Ma is clearly an outlier. If the oldest analysis is also excluded, the remaining 17 analyses yield a weighted mean $^{207}Pb/^{206}Pb$ age of 2662 ± 4 Ma, which is interpreted as

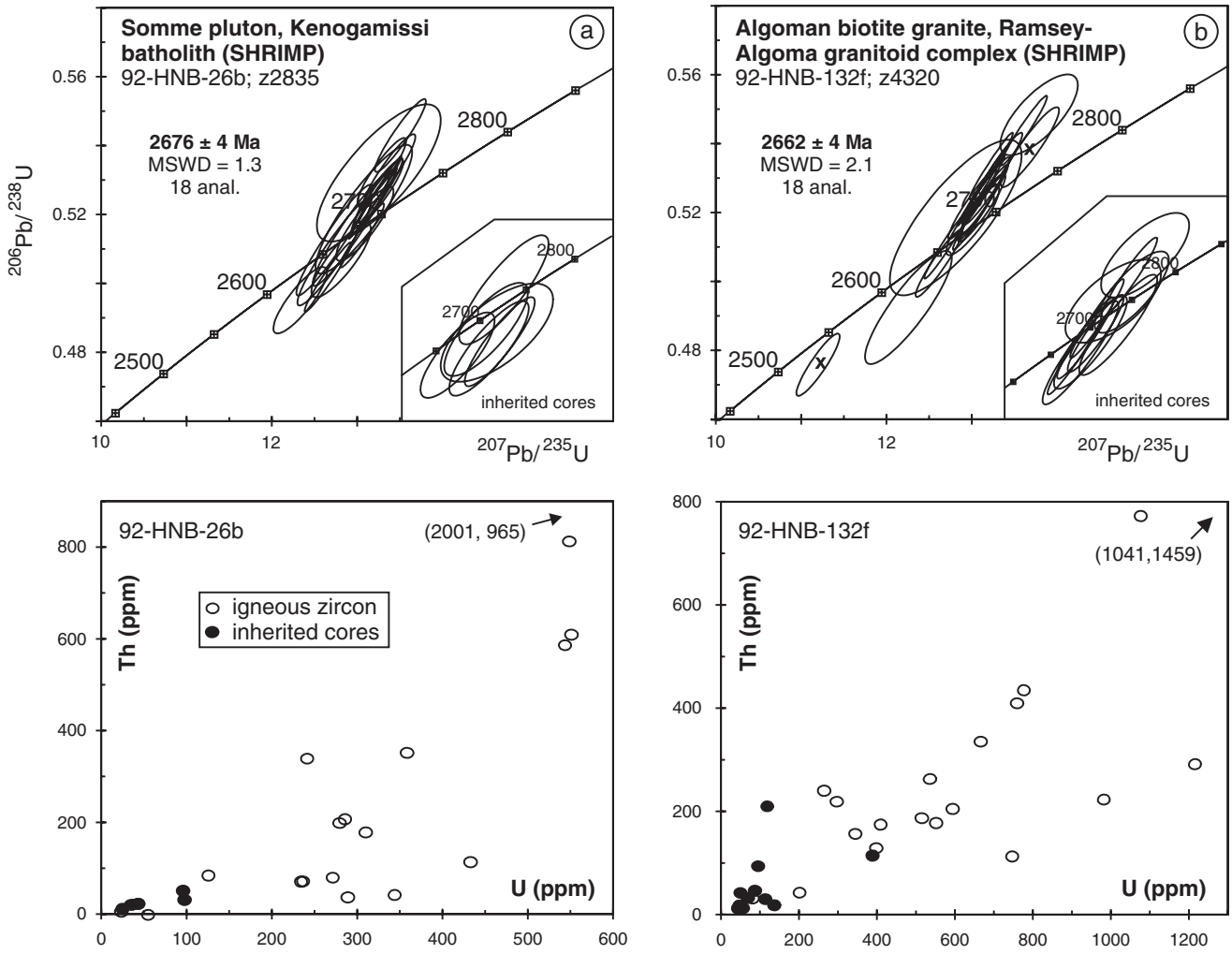

FIG. 8. U-Pb concordia diagrams for igneous and inherited zircons analyzed by SHRIMP from (a) the Somme pluton, Kenogamissi plutonic complex (92-HNB-26b) and (b) the Barney batholith, Ramsey-Algoma granitoid complex (92-HNB-132f). Error envelopes are shown at the 1σ confidence level. The lower diagrams show that zircon cores interpreted as inherited are not only older but also have distinctly lower U and Th concentrations (Table 4). Bracketed U and Th concentrations, respectively (shown next to arrows), represent single data points that plot outside of the graphs.

the igneous crystallization age. Eleven analyses of imaged cores provide $^{207}Pb/^{206}Pb$ ages ranging from ca. 2766 to 2702 Ma, with a weighted mean age of ca. 2710 Ga. As for sample 92-HNB-26b, these cores have significantly lower U and Th concentrations than the interpreted igneous overgrowth and igneous grains (Fig. 8b).

Zircon Hf Isotope Data

Initial $^{176}Hf/^{177}Hf$ ratios and initial ε_{Hf} values ("initial" indicates at the time of zircon primary crystallization and is implied but not stated henceforth) were calculated for zircons using the (mainly TIMS) protolith ages presented above. This approach is preferable to using the $^{207}Pb/^{206}Pb$ age determined for each grain by LA-ICPMS as more precise TIMS data are available for most samples, and in nearly all cases the ICPMS data clearly indicate whether individual zircons belong to the primary igneous population or have "anomalous" ages. Igneous grains are therefore assigned the more precise TIMS age, with the LA-ICPMS $^{207}Pb/^{206}Pb$ age only used in instances where this age is clearly anomalous. In detail, the choice of TIMS versus LA-ICPMS age has little effect on the calculated $^{176}Hf/^{177}Hf$ for zircons analyzed in this study. However, ε_{Hf} is more sensitive to this choice.

The Hf isotope data can also be used to assess the significance of a U-Pb age. For instance, Hf data for anomalously young zircons may indicate whether this age is more likely to be due to Pb loss ($^{176}Hf/^{177}Hf$ is similar to the igneous population) or to a secondary growth event ($^{176}Hf/^{177}Hf$ will typically vary from the igneous population). For example, two relatively young zircons in sample 02JAA-8 (grains 3 and 16, Table 4) have $^{176}Hf/^{177}Hf$ ratios that fall within the range defined by igneous zircons. Therefore their younger LA-ICPMS ages are probably best attributed to Pb loss, and in calculating $^{176}Hf/^{177}Hf$ and ε_{Hf} we use the TIMS-determined sample age of 2684 Ma.

Hf data are reported in Table 5 and plotted against U-Pb age in Figure 9. Zircons from all samples have $^{176}Hf/^{177}Hf$ ranging from 0.28097 to 0.28135, corresponding to ε_{Hf} of –3.6 to +11.4. For zircons from individual samples, ε_{Hf} varies by 3 to 12 epsilon units, with oldest tonalitic samples from the Rice Lake batholith yielding the largest range and 2673 Ma granodiorite from this batholith having the smallest range. ε_{Hf} is positive for most analyses; the exceptions are two zircons from the two samples of Rice Lake tonalite, and the majority of analyzed zircons from hornblende diorite sample 02JAA-8 (Fig. 9). Average ε_{Hf} values for all but the hornblende diorite sample lie between the depleted mantle and chondrite evolution curves. Although several analyses plot above the model depleted mantle, all lie within error of the ±3 ε_{Hf} unit uncertainty commonly assigned to its composition (comparable to that for modern MORB; e.g., White and Patchett, 1984).

With the exception of sample 02JAA-7, the range of ε_{Hf} recorded by primary igneous zircons from individual samples exceeds analytical uncertainty. This range is unlikely

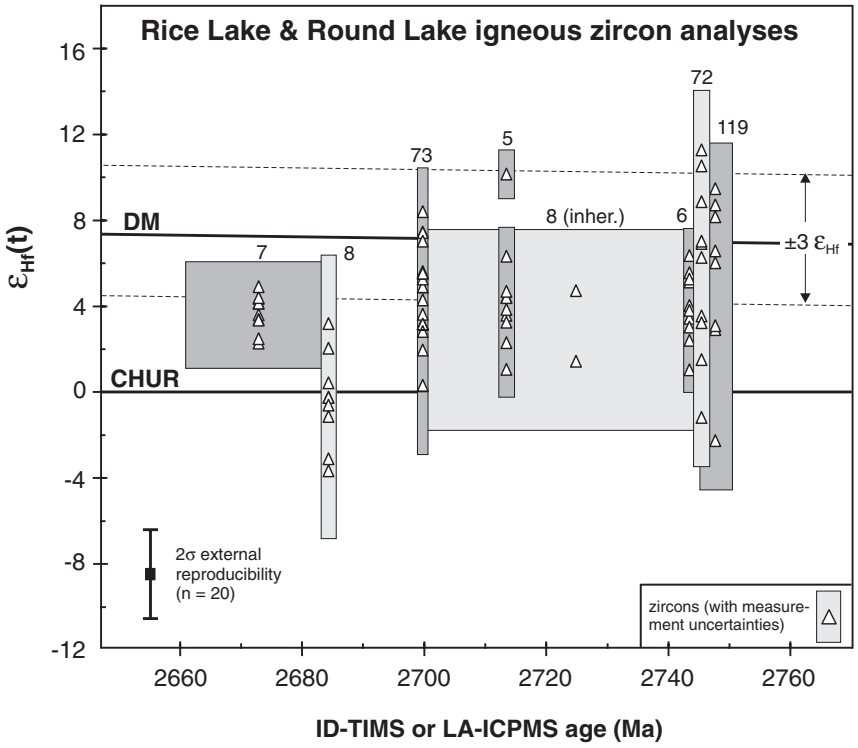

FIG. 9. Initial ε_{Hf} for individual zircons (triangles) plotted against plutonic host-rock age. Abbreviated sample numbers are shown above data rectangles, which illustrate 2σ age uncertainties and the range of 2 standard errors from $^{176}Hf/^{177}Hf$ measurements. Host-rock ages are based mainly on precise isotope dilution TIMS data and confirmed by LA-ICPMS age dating. However, two zircons from sample 02JAA-8 with distinctly older laser ablation ages are interpreted as inherited and are shown separately. For some samples from the Rice Lake batholith, the influence of older crust during Abitibi magmatic activity is suggested by the relatively wide range of ε_{Hf} and negative ε_{Hf} values. Additional details are in the text and footnotes to Table 5.

to reflect disturbances in primary Hf isotope composition as in most cases relatively pristine igneous zircons have been analyzed. In instances where recrystallized domains have been analyzed, there is no systematic variation in $^{176}Hf/^{177}Hf$ relative to unrecrystallized grains in the sample. In fact, no such relationship is expected as Hf is an essential structural constituent of zircon and remains relatively immobile during internal recrystallization (e.g., Hoskin and Schaltegger, 2003).

As discussed by Griffin et al. (2002) and Andersen et al. (2002), the observed intrasample isotopic range more likely reflects Hf isotope variations in the magma during igneous zircon growth, similar to that demonstrated by Sr isotope data from igneous feldspars (e.g., Waight et al., 2000; Gagnevin et al., 2005). This variation is due to one or more processes that can occur in the magma source region or magma chamber. For instance, individual magma batches that reach zircon saturation can crystallize and then transport isotopically distinct igneous grains (± inherited grains) to the magma chamber. Zircon crystallization during magma mixing episodes can yield both inter- and intragrain variations in Hf isotope composition. Magma interaction with isotopically dissimilar wall rocks may also generate isotopic heterogeneity during zircon crystallization. The ε_{Hf} ranges for individual samples suggest that such processes may have been more important in samples from the Rice Lake batholith.

Due to the current precision of the technique, LA-ICPMS U-Pb dating cannot resolve early- from late-crystallizing magmatic zircons, or magmatic from slightly older xenocrystic zircons. However, despite this limitation, we note that the nominally oldest or youngest igneous zircons in some of our samples also have the highest or lowest $^{176}Hf/^{177}Hf$ for that sample. For example, the two oldest zircons in sample 01JAA-72 (grains 10 and 14, with LA-ICPMS ages of 2756 Ma) have the highest $^{176}Hf/^{177}Hf$ and also the lowest Hf concentrations (Tables 3, 5, 7). Similarly, the oldest zircon in sample 02JAA-5 has elevated $^{176}Hf/^{177}Hf$ relative to all other grains, whereas the three oldest zircons in sample 02JAA-6 have the lowest $^{176}Hf/^{177}Hf$ for that sample. These relationships suggest that "end-member" zircons, derived from isotopically distinct magma batches that may have formed at different times, may be present in some of our samples. The presence of such end members supports the hypothesis that intrasample Hf isotope variations reflect (at least in part) mixing and/or assimilation processes during generation and accumulation of the protolith magma. This suggests that some igneous zircon populations may consist of several generations that grew during a long-lived, deep-seated magmatic event. As mentioned earlier, we consider this a possible explanation for some of the age variation observed in the TIMS-dated zircon population from sample 01JAA-73. This may also provide an alternate explanation for the range of TIMS and LA-ICPMS ages observed in other samples.

Whole-Rock Nd Isotope Data

Nd isotope data for the plutonic and volcanic samples shown in Figure 1 are presented in Table 6. Initial ε_{Nd} ranges from 0.6 to 5.7, with most samples overlapping the composition of the Abitibi model depleted mantle at 2.7 Ga (~2.5–3.0; Machado et al., 1986; Vervoort et al., 1994). Only two samples have distinctly lower ε_{Nd}; both are from felsic volcanic units in the Rice Lake area (samples 1 and 4, Fig. 1). A 2739 Ma lapilli tuff of the Pacaud assemblage (van Breemen et al., 2006) has an ε_{Nd} of 0.6, whereas a 2729 Ma volcanic flow from the Deloro assemblage has a comparable ε_{Nd} of 0.7. The $T_{DM(Nd)}$ model ages (DePaolo, 1980) for these samples are 2.94 and 2.88 Ga, respectively, in contrast to T_{DM} ages for all other samples that more closely compare with their zircon crystallization ages. A sample of intermediate lapilli tuff from the Shining Tree greenstone belt has an unusually high ε_{Nd} of 5.7, which may potentially indicate syn- or postdepositional disturbance of the Sm-Nd system (e.g., McDaniel et al., 1994). Apart from this sample, we have no reason to suspect that our Nd data is significantly influenced by such disturbances.

Most of the Nd isotope results reported here are consistent with existing Nd data from the Ontario and Québec segments of the Abitibi belt (for an overview see Ayer et al., 2002a, b). These data have been suggested to indicate little or no involvement of significantly older crust during magma genesis. However, the low ε_{Nd} for two relatively old felsic volcanic units in the Rice Lake area suggests a contribution of older crustal material during early volcanic activity. Other samples from this area, of similar or younger primary age, lack Nd isotope evidence for this older crustal component, which suggests either that melting and assimilation of older crust was episodic or that this process was common to magma generation but the relative crustal input varied over time. It is important to recall that a small or even moderate contribution of felsic crustal material to an isotopically juvenile magma can go undetected by the Sm-Nd system if this crust is both young (<~150 m.y. old) and was itself largely juvenile at the time of formation.

Summary of Analytical Data

The analytical results presented above, in conjunction with previously reported data, can be used to highlight a number of similarities and differences between the Rice Lake and Round Lake areas:

1. The plutonic complexes in both areas have comparable intrusion ages ranging between 2750 and 2660 Ma. Xenocrystic zircons (ca. 2850 Ma) have been found in two samples from the Rice Lake batholith; however, pre-Abitibi zircon inheritance has not been documented in the Round Lake plutonic complex or in surrounding rocks.
2. Rice Lake tonalites and granodiorites are geochemically less fractionated than rocks of comparable lithology and age in the Round Lake plutonic complex (Fig. 4).
3. Zircon Hf isotope data suggest larger intrasample variations in $^{176}Hf/^{177}Hf$ for the Rice Lake batholith in contrast to zircons from the Round Lake plutonic complex. These isotopic variations likely record different stages of magmatic zircon crystallization, perhaps during magma-mixing episodes or perhaps reflecting crystallization within individual magma batches. The wide range of ε_{Hf} and negative ε_{Hf} values for some Rice Lake samples probably reflects the variable mixing of both depleted mantle and older crustal sources during magma genesis. In contrast, ε_{Hf} data for the Round Lake plutonic complex are not as suggestive of an older crustal component in the magma source region, although our Hf data alone do not exclude this possibility.

TABLE 4. Zircon U-

Sample Spotname[1]	U (ppm)	Th (ppm)	Th/U	Pb (ppm)	^{204}Pb (ppb)	^{204}Pb/^{206}Pb	± 1σ	f^{206}	^{208}Pb/^{206}Pb	± 1σ
92-HNB-26b Somme pluton, Kenogamissi batholith (z2835; Zone 17, Easting 425691, Northing 5292290)										
26B-21.5	543	587	1.12	378	5	0.000018	0.000011	0.00032	0.3078	0.0019
26B-21.4	240	340	1.46	141	2	0.000017	0.000018	0.00030	0.2002	0.0018
26B-21.6	551	610	1.14	377	9	0.000034	0.000003	0.00059	0.3120	0.0017
26B-21.1	285	209	0.76	182	1	0.000010	0.000034	0.00017	0.2133	0.0028
26B-3.1	309	180	0.60	183	4	0.000027	0.000009	0.00047	0.1334	0.0011
26B-21.7	548	813	1.53	372	7	0.000028	0.000006	0.00048	0.3124	0.0018
26B-9.1	358	353	1.02	237	2	0.000014	0.000010	0.00024	0.2835	0.0024
26B-124.1	288	38	0.14	159	4	0.000029	0.000008	0.00050	0.0374	0.0008
26B-5.1	432	115	0.27	245	2	0.000011	0.000009	0.00019	0.0752	0.0007
26B-66.2	270	81	0.31	148	1	0.000010	0.000010	0.00017	0.0855	0.0012
26B-21.2	278	200	0.74	168	4	0.000031	0.000010	0.00053	0.2041	0.0028
26B-66.1	233	73	0.32	132	4	0.000041	0.000015	0.00071	0.0916	0.0010
26B-124.2	343	44	0.13	185	4	0.000024	0.000003	0.00041	0.0365	0.0004
26B-14.1	2001	965	0.50	1164	8	0.000009	0.000005	0.00016	0.1395	0.0012
26B-88.1	22	7	0.34	13	7	0.000668	0.000239	0.01157	0.0790	0.0112
26B-49.1	236	73	0.32	131	2	0.000018	0.000014	0.00030	0.0880	0.0009
26B-93.1	125	86	0.71	76	2	0.000045	0.000026	0.00078	0.1913	0.0016
26B-52.1	54	0	0.01	29	3	0.000118	0.000081	0.00205	0.0014	0.0035
cores:										
26B-39.1	96	33	0.35	54	6	0.000140	0.000024	0.00242	0.0961	0.0046
26B-94.1	33	22	0.68	21	2	0.000123	0.000098	0.00213	0.1881	0.0062
26B-44.1	95	53	0.58	57	4	0.000097	0.000025	0.00168	0.1626	0.0016
26B-100.1	36	23	0.66	22	5	0.000314	0.000231	0.00544	0.1761	0.0109
26B-17.1	24	13	0.58	14	0	0.000010	0.000118	0.00017	0.1605	0.0103
26B-128.1	42	25	0.61	25	4	0.000230	0.000118	0.00399	0.1714	0.0053
92-HNB-132f Algoman biotite granite, Ramsey-Algoma granitoid complex (z4320; Zone 17, Easting 396179, Northing 5245074)										
132-24.1	981	224	0.24	514	249	0.000618	0.000034	0.01071	0.1126	0.0013
132-10.6	664	336	0.52	392	2	0.000008	0.000015	0.00013	0.1440	0.0036
132-104.1	1076	773	0.74	682	68	0.000138	0.000007	0.00239	0.2022	0.0012
132-129.1	295	220	0.77	186	1	0.000007	0.000005	0.00012	0.2141	0.0020
132-126.1	342	158	0.48	197	2	0.000016	0.000003	0.00029	0.1308	0.0006
132-10.1	593	206	0.36	341	7	0.000027	0.000013	0.00047	0.0998	0.0009
132-128.1	78	33	0.44	43	1	0.000036	0.000115	0.00049	0.1292	0.0059
132-83.1	745	114	0.16	413	6	0.000018	0.000007	0.00030	0.0431	0.0010
132-7.1	534	264	0.51	324	2	0.000010	0.000009	0.00017	0.1404	0.0007
132-10.5	775	436	0.58	452	3	0.000010	0.000010	0.00017	0.1597	0.0014
132-10.3	758	410	0.56	459	0	0.000001	0.000004	0.00001	0.1573	0.0007
132-94.1	1041	1459	1.45	771	5	0.000010	0.000004	0.00017	0.3982	0.0011
132-19.1	407	176	0.45	240	9	0.000049	0.000008	0.00085	0.1284	0.0017
132-10.4	513	188	0.38	296	2	0.000010	0.000010	0.00017	0.1041	0.0008
132-99.1	199	44	0.23	110	3	0.000038	0.000015	0.00066	0.0636	0.0021
132-42.1	396	131	0.34	235	11	0.000059	0.000049	0.00103	0.0755	0.0021
132-83.2	1215	293	0.25	677	12	0.000022	0.000004	0.00037	0.0685	0.0004
132-10.2	550	179	0.34	317	45	0.000184	0.000040	0.00318	0.1018	0.0018
132-53.1	262	241	0.95	176	5	0.000038	0.000016	0.00065	0.2613	0.0019
Cores										
132-31.1	134	20	0.15	74	2	0.000030	0.000044	0.00042	0.0424	0.0019
132-17.1	116	211	1.89	67	12	0.000231	0.000060	0.00315	0.1408	0.0050
132-20.1	93	95	1.06	56	16	0.000382	0.000072	0.00520	0.1772	0.0040
132-21.1	66	34	0.53	43	85	0.002749	0.000340	0.03742	0.2458	0.0143
132-109.1	53	14	0.28	29	2	0.000101	0.000116	0.00138	0.0756	0.0053
132-7.2	386	116	0.31	229	5	0.000030	0.000013	0.00041	0.0840	0.0009
132-72.1	44	20	0.45	28	0	0.000010	0.000010	0.00014	0.1353	0.0034
132-53.2	84	48	0.59	50	0	0.000010	0.000010	0.00014	0.1623	0.0030
132-75.1	111	31	0.29	62	1	0.000018	0.000030	0.00024	0.0762	0.0023
132-13.1	42	13	0.33	24	0	0.000024	0.000043	0.00033	0.0913	0.0016
132-14.1	47	44	0.96	31	0	0.000010	0.000127	0.00014	0.2721	0.0068

[1] Zircon grain number followed by analysis number; uncertainties are reported at one sigma and are calculated by numerical propagation of all known outlined in Stern (1997); concordance = 100 x (^{206}Pb/^{238}U age)/(^{207}Pb/^{206}Pb age)

Pb Data (SHRIMP)

						Age (Ma)				
$^{207}Pb/^{235}U$	± 1σ	$^{206}Pb/^{238}U$	± 1σ	$^{207}Pb/^{206}Pb$	± 1σ	$^{206}Pb/^{238}U$	± 1σ	$^{207}Pb/^{206}Pb$	± 1σ	Conc. (%)
13.496	0.197	0.5427	0.0071	0.18035	0.00092	2795	30	2656	9	105.2
12.317	0.207	0.4945	0.0065	0.18066	0.00163	2590	28	2659	15	97.4
13.279	0.189	0.5323	0.0065	0.18095	0.00108	2751	27	2662	10	103.4
13.363	0.202	0.5325	0.0071	0.18202	0.00105	2752	30	2671	10	103.0
13.152	0.174	0.5227	0.0068	0.18248	0.00032	2711	29	2676	3	101.3
13.256	0.168	0.5269	0.0065	0.18249	0.00037	2728	27	2676	3	102.0
13.223	0.198	0.5251	0.0072	0.18264	0.00082	2721	30	2677	7	101.6
13.247	0.189	0.5260	0.0065	0.18265	0.00108	2725	27	2677	10	101.8
13.194	0.171	0.5237	0.0064	0.18271	0.00054	2715	27	2678	5	101.4
12.644	0.181	0.5012	0.0067	0.18296	0.00066	2619	29	2680	6	97.7
12.799	0.231	0.5061	0.0071	0.18343	0.00178	2640	31	2684	16	98.3
13.077	0.223	0.5169	0.0072	0.18350	0.00153	2686	30	2685	14	100.0
13.045	0.169	0.5134	0.0062	0.18427	0.00064	2671	26	2692	6	99.2
12.718	0.292	0.5121	0.0108	0.18013	0.00129	2665	46	2654	12	100.4
13.239	0.481	0.5318	0.0133	0.18057	0.00424	2749	56	2658	39	103.4
12.719	0.288	0.5087	0.0104	0.18135	0.00136	2651	45	2665	12	99.5
12.910	0.296	0.5150	0.0108	0.18181	0.00130	2678	46	2669	12	100.3
13.066	0.375	0.5211	0.0124	0.18184	0.00242	2704	53	2670	22	101.3
12.921	0.384	0.5062	0.0110	0.18512	0.00328	2640	47	2699	30	97.8
13.646	0.463	0.5317	0.0141	0.18613	0.00340	2749	59	2708	30	101.5
13.369	0.434	0.5162	0.0120	0.18782	0.00374	2683	51	2723	33	98.5
13.538	0.582	0.5150	0.0127	0.19066	0.00615	2678	54	2748	54	97.5
13.413	0.413	0.5089	0.0122	0.19116	0.00315	2652	52	2752	27	96.4
13.583	0.363	0.5115	0.0115	0.19262	0.00231	2663	49	2765	20	96.3
11.177	0.167	0.4750	0.0060	0.17068	0.00109	2505	26	2564	11	97.7
12.799	0.513	0.5181	0.0151	0.17917	0.00435	2691	64	2645	41	101.7
13.218	0.167	0.5332	0.0064	0.17978	0.00048	2755	27	2651	4	103.9
13.091	0.181	0.5264	0.0071	0.18037	0.00032	2726	30	2656	3	102.6
12.685	0.169	0.5099	0.0064	0.18042	0.00055	2656	27	2657	5	100.0
12.993	0.185	0.5220	0.0068	0.18053	0.00081	2708	29	2658	7	101.9
12.240	0.337	0.4917	0.0110	0.18054	0.00247	2578	48	2658	23	97.0
13.124	0.167	0.5267	0.0065	0.18073	0.00036	2727	27	2660	3	102.5
13.303	0.183	0.5329	0.0067	0.18105	0.00075	2754	28	2662	7	103.4
12.602	0.180	0.5047	0.0065	0.18109	0.00086	2634	28	2663	8	98.9
13.154	0.181	0.5258	0.0066	0.18145	0.00079	2724	28	2666	7	102.2
13.603	0.180	0.5436	0.0068	0.18149	0.00059	2798	28	2667	5	104.9
13.142	0.178	0.5236	0.0066	0.18203	0.00065	2715	28	2671	6	101.6
13.075	0.170	0.5209	0.0064	0.18205	0.00059	2703	27	2672	5	101.2
12.999	0.206	0.5173	0.0067	0.18226	0.00138	2687	29	2674	13	100.5
13.779	0.302	0.5483	0.0078	0.18227	0.00273	2818	32	2674	25	105.4
13.024	0.170	0.5182	0.0063	0.18228	0.00058	2692	27	2674	5	100.7
13.105	0.181	0.5208	0.0065	0.18250	0.00086	2703	28	2676	8	101.0
13.670	0.225	0.5388	0.0077	0.18403	0.00118	2778	32	2689	11	103.3
13.387	0.309	0.5236	0.0113	0.18544	0.00113	2714	48	2702	10	100.5
12.990	0.309	0.5077	0.0113	0.18557	0.00117	2647	48	2703	10	97.9
13.184	0.325	0.5150	0.0116	0.18566	0.00145	2678	49	2704	13	99.0
13.670	0.551	0.5312	0.0120	0.18666	0.00573	2746	51	2713	52	101.2
13.100	0.437	0.5087	0.0148	0.18677	0.00244	2651	64	2714	22	97.7
13.958	0.319	0.5415	0.0114	0.18696	0.00128	2790	48	2716	11	102.7
14.229	0.508	0.5511	0.0121	0.18725	0.00477	2830	51	2718	43	104.1
13.368	0.324	0.5171	0.0111	0.18749	0.00169	2687	47	2720	15	98.8
13.274	0.421	0.5133	0.0134	0.18757	0.00282	2671	57	2721	25	98.1
13.996	0.428	0.5351	0.0117	0.18971	0.00357	2763	49	2740	31	100.8
13.757	0.452	0.5208	0.0144	0.19157	0.00278	2703	61	2756	24	98.1

sources of error (Stern, 1997); F^{206} refers to mole fraction of total ^{206}Pb that is due to common Pb; data are common-Pb corrected according to procedures

TABLE 5. Zircon Lu-Hf Isotope Data (LA-MC-ICPMS)

Analysis no.	TIMS age[1] (Ma)	$^{176}Hf/^{177}Hf$	± 1 se	$^{176}Lu/^{177}Hf$	± 1 se	$^{176}Yb/^{177}Hf$	± 1 se	$^{176}Hf/^{177}Hf(t)$	$\varepsilon_{Hf}(t)$	± 1 se
JB119-03	2747	0.281240	0.000040	0.000769	0.000008	0.02474	0.00017	0.281200	6.15	1.42
JB119-04	2747	0.281229	0.000035	0.000261	0.000012	0.00751	0.00038	0.281215	6.71	1.25
JB119-07	2747	0.281337	0.000029	0.001473	0.000044	0.04232	0.00140	0.281260	8.29	1.03
JB119-08	2747	0.281166	0.000048	0.001024	0.000017	0.03449	0.00087	0.281112	3.04	1.71
JB119-09	2747	0.281002	0.000032	0.000668	0.000005	0.01864	0.00012	0.280967	–2.13	1.14
JB119-10	2747	0.281342	0.000030	0.000863	0.000031	0.02239	0.00082	0.281297	9.61	1.07
JB119-14	2747	0.281132	0.000027	0.000280	0.000003	0.00623	0.00006	0.281117	3.23	0.96
JB119-15	2747	0.281299	0.000028	0.000453	0.000003	0.01185	0.00009	0.281275	8.85	1.00
01JAA-72-01	2747	0.281264	0.000029	0.000767	0.000013	0.01871	0.00025	0.281224	7.00	1.03
01JAA-72-03	2747	0.281155	0.000034	0.000495	0.000006	0.01215	0.00016	0.281129	3.63	1.21
01JAA-72-04	2747	0.281039	0.000032	0.000819	0.000014	0.01973	0.00034	0.280996	–1.10	1.14
01JAA-72-07	2747	0.281271	0.000030	0.000844	0.000017	0.02080	0.00041	0.281227	7.11	1.07
01JAA-72-08	2747	0.281143	0.000044	0.001359	0.000026	0.03794	0.00066	0.281072	1.59	1.57
01JAA-72-09	2747	0.281163	0.000033	0.000817	0.000002	0.02136	0.00008	0.281120	3.31	1.17
01JAA-72-10	2747	0.281419	0.000037	0.001790	0.000010	0.05950	0.00028	0.281325	10.60	1.32
01JAA-72-13	2747	0.281242	0.000041	0.000698	0.000012	0.02461	0.00032	0.281205	6.35	1.46
01JAA-72-14	2747	0.281400	0.000039	0.001029	0.000021	0.03838	0.00043	0.281346	11.35	1.39
01JAA-72-15	2747	0.281355	0.000025	0.001460	0.000022	0.05156	0.00140	0.281278	8.94	0.89
02JAA-6-01	2744	0.281171	0.000015	0.000539	0.000017	0.01751	0.00052	0.281143	4.05	0.53
02JAA-6-02	2744	0.281157	0.000018	0.000593	0.000008	0.01740	0.00030	0.281126	3.45	0.64
02JAA-6-03	2744	0.281210	0.000015	0.000467	0.000010	0.01363	0.00032	0.281185	5.57	0.53
02JAA-6-04	2744	0.281240	0.000018	0.000615	0.000009	0.01693	0.00022	0.281208	6.36	0.64
02JAA-6-05	2744	0.281162	0.000015	0.000492	0.000006	0.01291	0.00015	0.281136	3.81	0.53
02JAA-6-07	2744	0.281202	0.000021	0.000546	0.000018	0.01477	0.00044	0.281173	5.14	0.75
02JAA-6-08	2744	0.281082	0.000015	0.000448	0.000002	0.01242	0.00007	0.281058	1.05	0.53
02JAA-6-09	2744	0.281124	0.000018	0.000515	0.000005	0.01450	0.00006	0.281097	2.42	0.64
02JAA-6-11	2744	0.281133	0.000016	0.000356	0.000002	0.01011	0.00004	0.281114	3.04	0.57
02JAA-6-12	2744	0.281205	0.000013	0.000528	0.000002	0.01523	0.00005	0.281177	5.28	0.46
02JAA-5-01	2714	0.281191	0.000017	0.000331	0.000003	0.00792	0.00006	0.281174	4.45	0.61
02JAA-5-02	2714	0.281380	0.000016	0.000872	0.000010	0.02092	0.00028	0.281335	10.18	0.57
02JAA-5-03	2714	0.281184	0.000017	0.000658	0.000011	0.01685	0.00026	0.281150	3.60	0.61
02JAA-5-04	2714	0.281181	0.000017	0.000452	0.000012	0.01231	0.00038	0.281158	3.88	0.61
02JAA-5-05	2714	0.281160	0.000014	0.000371	0.000005	0.00934	0.00019	0.281141	3.28	0.50
02JAA-5-07	2714	0.281212	0.000021	0.000751	0.000016	0.01801	0.00039	0.281173	4.43	0.75
02JAA-5-10	2714	0.281097	0.000018	0.000340	0.000001	0.00840	0.00004	0.281079	1.09	0.64
02JAA-5-11	2714	0.281236	0.000021	0.001054	0.000015	0.02609	0.00024	0.281181	4.72	0.75
02JAA-5-13	2714	0.281282	0.000019	0.001057	0.000023	0.02635	0.00056	0.281227	6.35	0.68
02JAA-5-16	2714	0.281143	0.000018	0.000556	0.000019	0.01493	0.00051	0.281114	2.33	0.64
01JAA-73-01	2700	0.281219	0.000028	0.000468	0.000003	0.01152	0.00006	0.281195	4.89	1.00
01JAA-73-03	2700	0.281229	0.000039	0.000464	0.000001	0.01234	0.00002	0.281205	5.25	1.39
01JAA-73-04	2700	0.281177	0.000022	0.000583	0.000009	0.01486	0.00023	0.281147	3.18	0.78
01JAA-73-05	2700	0.281191	0.000028	0.000860	0.000014	0.02511	0.00037	0.281147	3.17	1.00
01JAA-73-07	2700	0.281302	0.000024	0.000685	0.000006	0.01830	0.00018	0.281267	7.44	0.85
01JAA-73-08	2700	0.281089	0.000045	0.000443	0.000015	0.01389	0.00048	0.281066	0.31	1.60
01JAA-73-09	2700	0.281187	0.000034	0.000543	0.000002	0.01637	0.00008	0.281159	3.61	1.21
01JAA-73-10	2700	0.281246	0.000028	0.000600	0.000001	0.01545	0.00006	0.281215	5.60	1.00
01JAA-73-11	2700	0.281231	0.000027	0.000359	0.000008	0.01023	0.00019	0.281212	5.51	0.96
01JAA-73-13	2700	0.281337	0.000039	0.001373	0.000006	0.03941	0.00028	0.281266	7.42	1.39
01JAA-73-14	2700	0.281171	0.000028	0.000479	0.000005	0.01445	0.00010	0.281146	3.16	1.00
01JAA-73-15	2700	0.281187	0.000028	0.000178	0.000002	0.00529	0.00008	0.281178	4.28	1.00
01JAA-73-18	2700	0.281234	0.000037	0.000408	0.000019	0.01052	0.00042	0.281213	5.53	1.32
01JAA-73-19	2700	0.281297	0.000036	0.000817	0.000006	0.02268	0.00016	0.281255	7.02	1.28
01JAA-73-21	2700	0.281319	0.000029	0.000495	0.000010	0.01240	0.00021	0.281293	8.40	1.03
01JAA-73-22	2700	0.281174	0.000025	0.000725	0.000034	0.01897	0.00080	0.281137	2.81	0.89
01JAA-73-26	2700	0.281121	0.000027	0.000168	0.000003	0.00435	0.00007	0.281112	1.95	0.96
02JAA-8-02	2725	0.281193	0.000040	0.000355	0.000006	0.00954	0.00017	0.281175	4.75	1.42
02JAA-8-03	2684	0.281092	0.000046	0.000589	0.000002	0.01777	0.00007	0.281062	–0.21	1.64
02JAA-8-04	2725	0.281110	0.000045	0.000539	0.000016	0.01571	0.00051	0.281082	1.45	1.60
02JAA-8-06	2684	0.280993	0.000037	0.000539	0.000006	0.01447	0.00015	0.280965	–3.64	1.32
02JAA-8-08	2684	0.281099	0.000040	0.000358	0.000007	0.01015	0.00032	0.281081	0.46	1.42
02JAA-8-10	2684	0.281173	0.000039	0.000292	0.000005	0.00944	0.00030	0.281158	3.22	1.39
02JAA-8-11	2684	0.281092	0.000041	0.000598	0.000013	0.01980	0.00036	0.281061	–0.22	1.46
02JAA-8-12	2684	0.281071	0.000050	0.000382	0.000003	0.01338	0.00019	0.281051	–0.58	1.78

TABLE 5. *(Cont.)*

Analysis no.	TIMS age[1] (Ma)	$^{176}Hf/^{177}Hf$	± 1 se	$^{176}Lu/^{177}Hf$	± 1 se	$^{176}Yb/^{177}Hf$	± 1 se	$^{176}Hf/^{177}Hf(t)$	$\varepsilon_{Hf}(t)$	± 1 se
02JAA-8-14	2684	0.281023	0.000052	0.000813	0.000060	0.03306	0.00240	0.280981	–3.07	1.85
02JAA-8-15	2684	0.281173	0.000061	0.000918	0.000006	0.03768	0.00055	0.281126	2.07	2.17
02JAA-8-16	2684	0.281052	0.000058	0.000303	0.000004	0.01154	0.00020	0.281036	–1.11	2.06
02JAA-7-01	2673	0.281250	0.000022	0.001438	0.000011	0.03837	0.00019	0.281177	3.61	0.78
02JAA-7-02	2673	0.281197	0.000020	0.000515	0.000004	0.01311	0.00014	0.281171	3.40	0.71
02JAA-7-03	2673	0.281219	0.000016	0.000414	0.000020	0.01083	0.00056	0.281198	4.37	0.57
02JAA-7-04	2673	0.281182	0.000018	0.000239	0.000003	0.00625	0.00010	0.281170	3.37	0.64
02JAA-7-05	2673	0.281209	0.000021	0.000338	0.000003	0.00868	0.00010	0.281192	4.15	0.75
02JAA-7-06	2673	0.281204	0.000018	0.000239	0.000000	0.00591	0.00002	0.281192	4.16	0.64
02JAA-7-08	2673	0.281220	0.000015	0.000410	0.000015	0.01056	0.00043	0.281199	4.41	0.53
02JAA-7-09	2673	0.281164	0.000017	0.000479	0.000015	0.01259	0.00034	0.281139	2.30	0.60
02JAA-7-11	2673	0.281232	0.000017	0.000365	0.000001	0.00998	0.00004	0.281213	4.92	0.60
02JAA-7-15	2673	0.281161	0.000018	0.000307	0.000005	0.00729	0.00010	0.281145	2.50	0.64

Notes: Lu decay constant = 1.865×10^{-11} (Scherer et al. 2001); for rock types and sample locations see Tables 1 and 2; the Mudtank zircon was used as an external standard; during our analytical sessions we obtained $^{176}Hf/^{177}Hf = 0.282537 \pm 0.000060$ (2σ, $n = 20$), with an average one standard error of the mean of 0.000018

[1] U-Pb ages of 2725 Ma for sample 02JAA-8 and 2673 Ma for 02JAA-7 are LA-ICPMS data

4. Whole-rock Nd data generally conform to a model of isotopically juvenile crustal growth of the Abitibi subprovince. However, two felsic volcanic samples from the Rice Lake area with ages of 2739 and 2729 Ma have low ε_{Nd} values, suggesting that they contain melted older crustal material.

Discussion

Comparison of whole-rock Nd and zircon Hf data

In many respects the Hf and Nd isotope data presented here tell a similar story: Late Archean magmatism in the southwestern Abitibi subprovince was predominantly juvenile and was largely dominated by depleted mantle and/or juvenile crustal sources. The extent to which ε_{Nd} and ε_{Hf} scatter about their respective depleted mantle growth curves suggests that this mantle was probably heterogeneous, which is consistent both with the conclusions of earlier workers (e.g., Shirey and Hanson, 1986; Vervoort et al., 1994; Thorpe, 1999; Walker and Stone, 2001) and with tectonomagmatic models that invoke varied mantle sources (e.g., Dostal and Mueller, 1997; Wyman et al., 2002). For the three Rice Lake map units (tonalite, granodiorite, hornblende diorite) with both Nd and Hf isotope data, there is a general but imperfect positive correlation of ε_{Nd} and average $\varepsilon_{Hf(zircon)}$, suggesting that these isotopic systems exhibit coherent geochemical behavior, as expected (Vervoort and Blichert-Toft, 1999).

A significant difference, however, is the varying degrees to which ε_{Nd} and ε_{Hf} indicate the involvement of a relatively unradiogenic component. Based on the presence of ca. 2850 Ma xenocrystic zircons in the Rice Lake batholith, this component probably consists of sialic continental crust. The zircon ε_{Hf} data for some Rice Lake samples span a considerable range and extend to negative values. In contrast, ε_{Nd} values for the southwestern Abitibi subprovince largely overlap the depleted mantle composition (Ayer et al., 2002a, b; this study). It appears that the large ε_{Hf} range and low to negative ε_{Hf} values are due to variable contamination of juvenile magmas by older continental crust, at least in the source region to the Rice Lake batholith. However, whole-rock Nd data from the Rice Lake region, including data from samples containing negative ε_{Hf} zircons, are less demonstrative of crustal contamination, which in our opinion highlights two probable influences: the Lu-Hf isotope system has more resolving power than Sm-Nd due to the shorter half-life of Lu, greater parent-daughter fractionation during mantle separation, and resistance of zircon to Hf isotope resetting (Patchett, 1983; Vervoort et al., 1996); and, in situ Hf measurements of igneous zircons allow the isotopic signatures of magma mixing and assimilation processes to be recognized, thereby increasing the chance of detecting a relatively unradiogenic crustal component. In particular, crustal melts that crystallize zircon prior to magma accumulation and mixing will provide the strongest isotopic evidence of older crust in the source region. In contrast, whole-rock Nd data will indicate its presence only when this crust is both light REE enriched and relatively old (i.e., isotopically evolved from mantle compositions) and forms a component of the magma that is volumetrically sufficient to influence its isotopic composition.

The ε_{Hf} values for zircons from 2684 Ma hornblende diorite sampled at Rice Lake (02JAA-8) are distinctly lower than those of other samples (Fig. 9). As noted earlier, diorite samples from the Rice Lake batholith have relatively high MgO, Ni, Cr, and Co contents and strongly fractionated REE patterns with negative Nb and Ti anomalies (Fig. 4). These characteristics and the 2684 Ma age are typical of sanukitoid-suite granitoid plutons of the Superior province (Shirey and Hanson, 1984, 1986; Stern et al., 1989). The combined geochemical and isotopic characteristics of this suite can be interpreted to indicate a mantle source that was enriched in light REE and large ion lithophile elements by slab-derived melts or fluids (Stern et al., 1989; Smithies and Champion, 2000), with an additional contribution from assimilated older continental crust (Stevenson et al., 1999). As suggested by Corfu and Noble (1992) for other post-2.7 Ga plutons in the southern Abitibi, the low ε_{Hf} of the hornblende diorite could reflect

TABLE 6. Whole-Rock Sm-Nd Isotope Data

Fig. 1 loc.	Sample no.	Unit	Description	Township	Easting (Zone 17,	Northing NAD 83)	Age (Ma)	Nd (ppm)	Sm (ppm)	$^{147}Sm/^{144}Nd$	$^{143}Nd/^{144}Nd$	ε_{Nd}	T_{DM} (Ga) (Goldstein)	T_{DM} (Ga) (DePaolo)
1	92-HNB-46e2	Chester felsic volcanic[1]	Quartz eye-bearing felsic lapilli tuff	Chester	428190	5269305	2739	21.70	5.05	0.1407	0.511658	0.6	3.10	2.94
2	92-HNB-68a1	Chester trondhjemite[1]	Magnetite-bearing trondhjemite	Yeo	427675	5266766	2740	44.26	9.23	0.1261	0.511495	2.6	2.86	2.72
3	92-HNB-26b	Somme pluton[1]	Layered biotite granite/granodiorite	Desrosiers	425681	5292323	2676	17.97	2.85	0.0958	0.510960	2.0	2.82	2.71
4	92-HNB-59a3	Marion felsic volcanic[1]	Quartz, feldspar-phyric massive flow	Heenan	398101	5292443	2729	11.93	2.39	0.1209	0.511310	0.7	3.01	2.88
5	93-HNB-208a2	Hanrahan volcanic[1]	Felsic lapilli tuff	Kenogaming	424462	5331924	2730	20.21	3.26	0.0974	0.510966	2.3	2.85	2.74
6	92-HNB-125	Hillary pluton[1]	Foliated, K-feldspar megacrystic hornblende granodiorite	Hillary	440249	5345799	2680	29.91	5.30	0.1071	0.511176	2.4	2.81	2.69
7	93-HNB-77a1	Shunsby-Cunningham volcanic[1]	Felsic tuff with pyritic and monolithic fragments	Blamey	377451	5280556	2730	16.33	2.74	0.1014	0.511061	2.7	2.82	2.71
8	92-HNB-123a	Neville pluton, Rice Lake batholith[1]	Foliated, K-feldspar-hornblende granodiorite	Neville	430080	5273617	2682	25.40	4.43	0.1055	0.511122	1.9	2.84	2.73
9	94-HNB-267	Bisco Arm felsic volcanic[1]	Schistose felsic volcanic flow	Joffre	405521	5251386	2716	15.68	2.30	0.0886	0.510841	2.8	2.80	2.70
10	95-HNB-274a1	Kenogamissi batholith[1]	Hornblende-biotite gneissic tonalite	Jack	445056	5283304	2723	12.23	2.47	0.1219	0.511383	1.7	2.92	2.78
11	95-HNB-1089a	Raney Township komatiite[1]	Massive komatiite with olivine spinifex and polygonal jointing	Raney	366106	5306749	2705	1.40	0.48	0.2067	0.512988	3.4	-	-
12	99JAA-61	Porcupine assemblage, Krist formation[2]	Dacitic bedded tuff	Deloro	476300	5365940	2688	15.69	2.83	0.1090	0.511226	2.8	2.79	2.67
13	97GWJ-289	Porcupine assemblage, Indian Lake group[2]	Massive felsic flow	Tyrrell	499750	5272535	2687	15.75	2.59	0.0993	0.511037	2.5	2.80	2.69
14	98GWJ-308	Porcupine assemblage, Natal group[2]	Andesite flow	McMurchy	493454	5278668	2687	21.05	4.07	0.1169	0.511333	2.2	2.85	2.72
15	98HSO-205	Porcupine assemblage, Natal group[2]	Intermediate lapilli tuff	Natal	493499	5280038	2687	17.24	3.10	0.1088	0.511372	5.7	2.57	2.44
16	97GWJ-233	Millie Creek stock[2]	Hornblende monzonite	Knight	498808	5279430	2685	46.05	7.59	0.0997	0.511066	2.9	2.77	2.66
17	96GWJ-14	Unnamed sill[2]	Fine-grained syenite	Tyrrell	488038	5274695	2685	10.08	2.09	0.1252	0.511524	3.0	2.79	2.64
	JB29	Rice Lake batholith[2]	Biotite granodiorite	(Study area)	411475	5295861	2700	10.71	1.71	0.0962	0.510998	2.9	2.78	2.67
	JB117	Rice Lake batholith[2]	Hornblende diorite	(Study area)	414555	5287174	2684	62.18	10.82	0.1052	0.511133	2.3	2.82	2.70
	JB119	Rice Lake batholith[2]	Biotite-hornblende tonalite	(Study area)	414207	5288221	2747	7.87	1.73	0.1332	0.511637	2.9	2.85	2.69
	JB199	Rice Lake batholith[2]	Hornblende diorite	(Study area)	417644	5295505	2684	11.42	2.52	0.1334	0.511651	2.6	2.83	2.66
	01JAA-72	Rice Lake batholith[2]	Biotite-hornblende tonalite	(Study area)	414570	5279524	2747	8.02	1.99	0.1497	0.511922	2.7	2.91	2.70
	01JAA-73	Rice Lake batholith[2]	Biotite granodiorite	(Study area)	413503	5283989	2700	7.46	1.82	0.1477	0.511869	2.0	2.94	2.74

Notes: Nd isotope compositions were normalized to $^{146}Nd/^{144}Nd = 0.7219$ and corrected to LaJolla $^{143}Nd/^{144}Nd = 0.511860$; measurements of LaJolla standard yielded $^{143}Nd/^{144}Nd = 0.511842 \pm 10$ (2σ error); external precision for the ε^{143}_{Nd} values is estimated to be within ± 0.5 e units; $^{147}Sm/^{144}Nd$ ratios are reproducible to 0.3%; total procedural blanks were approximately 200 pg for Nd and 100 pb for Sm

[1] Analyses done at the Geological Survey of Canada

[2] Analyses done at Carleton University

TABLE 7. Zircon Major and Trace Element Data

	ZrO_2	SiO_2	HfO_2	Y_2O_3	U_2O_3	ThO_2	Total	Hf[1]	Y[1]	Th[2]	U[2]	Lu[3]	Yb[3]
Analysis no.	Wt % oxides (electron microprobe)							Parts per million					
01JAA-72-01	66.34	32.04	1.14	0.03	n.d.	n.d.	99.54	9684	197	23	57	53	266
01JAA-72-03	67.07	31.79	1.02	0.12	0.02	0.05	100.06	8658	929	21	46	31	154
01JAA-72-04	66.08	31.90	1.16	0.21	n.d.	0.02	99.36	9871	1654	22	55	58	285
01JAA-72-07	65.82	32.29	0.96	0.08	0.03	0.04	99.23	8175	646	9	30	50	249
01JAA-72-08	65.99	31.84	1.06	0.16	0.02	0.08	99.14	8963	1244	28	68	87	498
01JAA-72-09	66.52	31.43	1.08	0.09	n.d.	n.d.	99.11	9124	709	15	45	54	285
01JAA-72-10	66.36	31.50	0.92	0.21	0.03	n.d.	99.02	7836	1622	20	50	101	683
01JAA-72-13	66.68	31.45	1.03	0.09	0.05	0.08	99.39	8751	717	28	51	44	315
01JAA-72-14	66.08	31.66	0.90	0.04	n.d.	0.01	98.70	7624	323	10	55	56	429
01JAA-72-15	65.98	31.43	1.43	n.d.	n.d.	0.01	98.85	12143	n.d.	38	64	127	917
01JAA-73-1	65.08	32.06	1.34	0.06	0.02	0.02	98.57	11372	480	44	87	38	192
01JAA-73-3	66.42	31.70	1.37	0.10	0.03	n.d.	99.62	11592	819	7	14	39	210
01JAA-73-4	65.75	31.72	1.43	0.08	n.d.	n.d.	98.97	12101	606	60	106	51	263
01JAA-73-5	65.84	31.21	1.44	0.14	0.09	0.02	98.74	12169	1110	52	89	75	448
01JAA-73-7	66.00	31.87	1.53	0.07	0.00	n.d.	99.47	12991	520	14	60	64	348
01JAA-73-8	62.95	30.08	1.28	0.25	0.20	0.32	*95.08*	10888	1969	60	190	35	222
01JAA-73-9	66.28	31.70	1.46	0.15	0.06	0.01	99.66	12364	1205	52	138	48	296
01JAA-73-10	67.21	31.84	1.46	0.04	0.05	n.d.	100.60	12372	347	83	158	53	280
01JAA-73-11	67.17	31.30	1.46	0.12	n.d.	n.d.	100.05	12355	937	34	90	32	185
01JAA-73-13	65.25	31.29	1.12	0.22	0.02	n.d.	97.91	9532	1764	72	142	94	550
01JAA-73-14	66.11	31.63	1.38	0.08	0.03	0.01	99.23	11668	599	61	127	40	247
01JAA-73-15	66.32	31.65	1.09	0.05	n.d.	0.03	99.14	9243	410	11	27	12	72
01JAA-73-18	67.73	31.69	1.35	0.06	n.d.	0.03	100.86	11423	473	78	125	33	176
01JAA-73-19	66.43	31.57	1.46	0.04	0.01	n.d.	99.52	12389	339	41	73	73	412
01JAA-73-21	66.06	32.10	1.44	0.10	0.11	0.01	99.82	12245	795	53	116	44	222
01JAA-73-22	66.16	31.47	1.31	0.24	n.d.	0.03	99.21	11117	1874	114	145	58	309
01JAA-73-26	67.42	31.60	1.26	0.03	0.04	n.d.	100.34	10651	213	41	83	13	68
02JAA-5-01	65.91	31.72	1.18	0.06	0.05	0.03	98.95	9998	473	27	71	24	116
02JAA-5-02	65.67	31.85	1.14	0.14	n.d.	0.06	98.86	9650	1071	43	83	60	296
02JAA-5-03	66.67	31.56	1.12	0.01	0.08	n.d.	99.44	9506	102	44	79	45	235
02JAA-5-04	66.40	31.69	1.33	0.07	n.d.	0.04	99.52	11253	551	34	43	37	203
02JAA-5-05	65.78	31.71	1.22	0.18	0.02	0.01	98.91	10312	1386	29	46	28	141
02JAA-5-07	65.59	31.78	0.91	0.02	0.05	0.02	98.36	7700	189	51	120	42	203
02JAA-5-10	65.74	31.70	1.27	0.10	n.d.	n.d.	98.81	10778	772	18	39	26	133
02JAA-5-11	66.00	31.64	1.15	0.19	0.07	n.d.	99.04	9710	1496	46	85	74	371
02JAA-5-13	66.68	31.59	1.13	0.02	n.d.	n.d.	99.42	9557	189	34	45	73	369
02JAA-5-16	65.73	31.92	1.12	0.02	0.12	n.d.	98.91	9532	165	51	55	38	208
02JAA-6-01	65.61	31.54	1.13	0.02	n.d.	0.01	98.32	9608	173	29	39	37	246
02JAA-6-02	64.70	31.65	1.01	0.28	0.06	0.03	97.74	8599	2237	32	43	37	219
02JAA-6-03	64.79	31.48	1.41	0.10	n.d.	n.d.	97.78	11991	788	20	28	40	239
02JAA-6-04	66.97	32.20	1.10	0.08	n.d.	0.03	100.38	9336	622	20	38	41	232
02JAA-6-05	65.55	31.62	1.13	0.07	n.d.	n.d.	98.37	9557	528	21	51	34	181
02JAA-6-07	64.94	31.61	1.27	0.12	0.03	0.03	97.99	10770	921	27	34	42	233
02JAA-6-08	65.85	31.71	1.20	0.11	n.d.	0.07	98.94	10168	835	19	29	33	185
02JAA-6-09	65.86	31.78	1.33	0.04	n.d.	0.00	99.02	11312	347	14	23	42	240
02JAA-6-11	65.69	31.94	1.21	0.10	0.04	0.04	99.02	10261	748	21	54	26	152
02JAA-6-12	66.22	32.11	1.13	0.13	0.05	0.00	99.65	9599	1024	24	45	36	214
02JAA-7-01	66.10	31.56	0.85	0.14	n.d.	0.05	98.70	7200	1126	97	60	74	405
02JAA-7-02	65.13	31.84	1.51	0.12	n.d.	0.01	98.60	12771	914	44	113	47	245
02JAA-7-03	65.81	31.55	1.02	0.13	0.00	0.01	98.53	8684	1055	89	66	26	138
02JAA-7-04	66.31	31.42	1.13	0.06	0.07	n.d.	98.98	9565	457	25	64	16	88
02JAA-7-05	65.58	31.75	1.06	0.07	n.d.	n.d.	98.47	9014	575	60	41	22	115
02JAA-7-06	65.51	31.64	1.21	0.02	0.00	n.d.	98.38	10252	134	103	83	18	89
02JAA-7-08	65.16	31.57	0.99	0.13	0.02	0.01	97.87	8353	1008	161	90	25	129
02JAA-7-09	65.47	31.53	1.21	0.04	n.d.	0.02	98.27	10218	299	5	13	35	188
02JAA-7-11	64.89	31.54	1.15	0.10	n.d.	0.00	97.68	9735	748	171	108	26	142
02JAA-7-15	65.59	31.68	0.99	0.09	0.01	0.02	98.39	8412	732	55	43	19	90
02JAA-8-02	65.64	31.70	1.25	0.01	n.d.	n.d.	98.59	10600	39	37	52	27	148
02JAA-8-03	65.85	31.45	1.09	0.14	n.d.	n.d.	98.53	9235	1103	364	377	39	240
02JAA-8-04	66.77	31.38	1.35	0.06	n.d.	0.07	99.63	11440	473	118	133	44	263
02JAA-8-06	65.79	31.92	1.21	0.14	n.d.	0.03	99.09	10286	1134	602	434	40	218
02JAA-8-08	65.67	31.83	1.00	0.11	0.00	0.04	98.64	8463	843	677	553	22	126

TABLE 7. *(Cont.)*

Analysis no.	ZrO_2	SiO_2	HfO_2	Y_2O_3	U_2O_3	ThO_2	Total	Hf[1]	Y[1]	Th[2]	U[2]	Lu[3]	Yb[3]
	Wt % oxides (electron microprobe)							Parts per million					
02JAA-8-09	55.86	27.74	0.88	0.52	0.23	0.53	*85.76*	7488	4079	275	250	105	677
02JAA-8-10	66.03	32.11	0.89	0.18	0.05	0.14	99.39	7505	1410	266	247	16	104
02JAA-8-11	65.87	31.91	1.18	0.07	0.00	0.02	99.05	10015	583	224	153	43	290
02JAA-8-12	64.88	31.44	0.84	0.16	0.03	0.06	97.41	7157	1229	424	378	20	140
02JAA-8-14	64.93	31.42	1.22	0.01	n.d.	0.04	97.62	10303	110	933	572	60	499
02JAA-8-15	65.13	31.13	1.31	0.13	0.02	0.04	97.76	11083	1055	815	582	73	612
02JAA-8-16	65.78	31.65	0.94	0.15	0.00	0.07	98.60	7971	1197	516	472	17	135
JB119-02	66.27	31.78	0.97	0.08	n.d.	n.d.	99.11	8260	662	39	95	68	378
JB119-03	66.49	31.51	1.09	0.02	n.d.	n.d.	99.11	9243	189	26	53	51	335
JB119-04	65.74	31.73	0.92	0.05	n.d.	0.01	98.46	7836	402	29	61	15	86
JB119-07	66.23	31.46	1.12	0.11	0.01	n.d.	98.92	9455	843	47	88	100	586
JB119-08	66.44	31.52	1.38	0.09	n.d.	n.d.	99.43	11702	685	33	75	86	591
JB119-09	65.81	31.59	1.06	0.07	n.d.	n.d.	98.52	8972	536	40	89	43	245
JB119-10	66.55	31.89	1.00	0.20	0.03	0.03	99.70	8514	1583	31	74	53	279
JB119-14	65.03	31.36	1.75	0.05	0.04	n.d.	98.24	14874	425	12	82	30	136
JB119-15	66.19	31.62	1.25	0.10	n.d.	n.d.	99.15	10625	748	21	59	35	184
JB119-17	66.23	31.35	1.28	0.09	n.d.	n.d.	98.94	10837	669	35	71	n.a.	n.a.

Abbreviations: n.a. = not analyzed, n.d. = not detected

[1] Electron microprobe (EMP) analysis; two analyses have significantly low totals (italicized)

[2] LA-ICPMS analysis; determined by calibration against average within-run value for GJ-1 standard

[3] MC-ICPMS analysis; calculated from $^{176}Lu/^{177}Hf$ and $^{176}Yb/^{177}Hf$ ratios and Hf concentration determined by EMP

fluxing of the mantle wedge by fluids derived from subducted sediments, perhaps equivalent to those exposed in the Pontiac subprovince south of the Abitibi belt. Therefore, the anomalous Hf isotope signature of the hornblende diorite could indicate the influence of a distinctive magma contamination process.

Abitibi early crustal history

Most tectonic models for the Abitibi subprovince do not highlight the earliest stages of crustal growth, mainly due to a relative paucity of data. However, our new geochronological data, combined with available information from the Pacaud assemblage and adjacent plutonic areas (see, for example, Ayer et al., 2002a), suggest that a major early volcanic-plutonic event can now be clearly distinguished. This event is similar to three younger volcanic-plutonic events described by Chown et al. (2002) in that tholeiitic, komatiitic, and calc-alkaline volcanic rocks were erupted at the same time as tonalitic and dioritic plutons were being emplaced at depth. A genetic linkage is inferred from the close spatial association and comparable ages of these rocks.

During the interval 2747 to 2740 Ma, tonalite-trondhjemite ± diorite magmatism occurred in both the Kenogamissi and Round Lake plutonic complexes, as well as within the Ramsay-Algoma granitoid complex. These early plutons were coeval with, and have similar geochemical characteristics to, calc-alkaline volcanic rocks of the Pacaud assemblage, which Ayer et al. (2002a) bracketed between 2750 and 2735 Ma. The sampled Rice Lake and Round Lake tonalite bodies are geochemically comparable to most Superior province tonalite-trondhjemite-granodiorite (TTG) suites, which are now generally accepted to be the product of melting of subducted tholeiitic basalt at lower crustal or upper mantle depths in an arc environment (e.g., Sutcliffe et al., 1993, Beakhouse and Davis, 2005). Round Lake tonalite samples (ca. 2744 and 2714 Ma) are relatively enriched in light REE and have pronounced Nb depletions, whereas Rice Lake tonalites (ca. 2747 Ma) exhibit less fractionated REE, slight Eu enrichment, and only minor Nb depletion (Fig. 4). Although this could be interpreted to reflect less involvement of subducted sediments in the source region to the Rice Lake tonalites, we caution that such interpretations are currently equivocal due to our limited geochemical data and lack of information on tectonomagmatic setting and the composition of the putative crustal contaminant(s) in the Rice Lake magmas.

The tonalite bodies probably were emplaced as tabular intrusions into Pacaud greenstone crust, as demonstrated by the resolvable age difference between tonalite at the northern margin of the Round Lake batholith (2743.6 ± 0.9 Ma; this study) and nearby felsic tuff (2746.9 ± 0.8 Ma; Mortensen, 1993a). This relationship is also demonstrated by field and U-Pb data at a location a few kilometers south of the Rice Lake batholith where Pacaud assemblage rocks have been intruded by an older plutonic unit of the Ramsay-Algoma granitoid complex (Heather and Shore, 1999). Where not subsequently modified by faults or intrusion of younger plutons, these oldest plutons remain in contact with Pacaud volcanics, which are the lowest units of the preserved stratigraphy. A combination of regional folding, inflation of the batholiths by younger granitoid bodies, and gravitational uplift of the batholiths relative to overlying dense greenstones is suggested to be responsible for the present-day exposure of >2740 Ma plutonic rocks with their Pacaud assemblage mantles (Ayer et al., 2002a; Becker and Benn, 2003; Benn, 2005). Although the extent of this old crust is unknown, Corfu (1993) suggested that ca. 2740 Ma plutonic and volcanic rocks of the Temagami greenstone belt, located 70 km south of the Round Lake plutonic complex, might be related to Pacaud magmatism.

Crustal growth in the southwest Abitibi—influence of >2.8 Ga Wawa crust?

In general, geochemical and isotopic data from Abitibi supracrustal rocks do not suggest the presence of older continental crust in the source region (e.g., Jackson and Sutcliffe, 1990; Kerrich et al., 1999; Wyman et al., 2002), and xenocrystic zircons older than 2750 Ma are largely unknown (Ayer et al., 2002a; see however Bleeker, 2002). These data have been used by numerous workers to infer an ocean basin setting, with interaction of plume- and subduction-related magma sources typically being specified. However, our data suggest that continental crust at least 100 m.y. older than the oldest Abitibi volcanic and plutonic rocks locally interacted at various times with juvenile magmas in the western part of the subprovince. This older crustal influence is suggested by U-Pb, Hf, and Nd isotope data from the Rice Lake area but is generally not indicated for the Round Lake area. Given that the Rice Lake area is only 50 km away from the Wawa subprovince where sialic crust as old as 2.92 Ga is documented (Moser et al., 1996), it is logical to explore the possibility that Wawa continental crust may have been the source of xenocrystic zircons and juvenile magma contamination.

The Abitibi-Wawa subprovince boundary is marked by the Ivanhoe Lake fault zone (Fig. 1), which represents the eastern boundary of the high-grade Kapuskasing structural zone. Movement on this and other Kapuskasing faults is postulated at various times during the latest Archean and Proterozoic, with both thrust and transcurrent displacements suggested (e.g., Halls et al., 1994). Lithoprobe geophysical surveys, in particular seismic reflection and gravity profiles (Percival et al., 1989; Green et al., 1990; Atekwana et al., 1994), indicate that the Archean-Proterozoic thrust system responsible for exhuming mid- to deep-crustal rocks is dominated by ramp-flat geometry. Although subvertical brittle faults that postdate ductile uplift are known within the Kapuskasing structural zone (Bursnall et al., 1994), a steeply dipping crustal-scale boundary between the Wawa and Abitibi subprovinces is not inferred by most workers. However, a boundary between >2.8 Ga crust of the Wawa subprovince and <2.75 Ga Abitibi crust must exist somewhere in this region.

Gneissic tonalite dated at 2925 ± 35 Ma occurs in the Wawa gneiss domain roughly 50 km west of the Kapuskasing structural zone (Moser et al., 1996). Unfortunately these rocks cannot be readily distinguished from ca. 2.7 Ga tonalite in the field, and in general there is little primary age data for units of the Kapuskasing structural zone (Percival and West, 1994). However, Krogh and Moser (1994) reported the occurrence of 2826 ± 2 Ma zircon in tonalite gneiss sampled 1 km west of the Ivanhoe Lake fault zone. A similar tonalitic unit also located just west of this fault zone contains zircon with a minimum age of 2765 Ma (Percival and Krogh, 1983). The Nd isotope data of Shaw et al. (1994) neither confirm nor rule out the presence of 2.9 to 2.8 Ga crust within the Kapuskasing zone. Thus, although additional U-Pb dating is required, it appears that >2.8 Ga rocks could occur as far east as the Ivanhoe Lake fault zone.

Lithoprobe seismic reflection profiles (e.g., Percival et al., 1989; Percival and West, 1994) indicate that Wawa crust may extend at mid- and deep crustal levels (i.e., beneath the level of the Kapuskasing thrust detachment) eastward into the Abitibi subprovince, although exactly how far is uncertain due to limited penetration of the reflection survey into the Abitibi. As this mid-level crust is essentially that exposed within the Kapuskasing structural zone, continuation of Wawa crust at depth with its complement of >2.8 Ga rocks beneath the western Abitibi subprovince appears to be plausible. At a higher crustal level, a westward-tapering wedge of relatively nonreflective crust lying beneath reflections correlated with the Ivanhoe Lake fault zone extends to about 12-km depth at the eastern end of line 2 (Percival and West, 1994, figs. 8, 9). Beneath this wedge, both easterly and westerly dipping reflectors are observed. In an earlier interpretation, Percival et al. (1989) correlated the less-reflective crustal volume with volcanic rocks of the Swayze greenstone belt. We agree with this assessment and suggest that the lower surface of this wedge corresponds to the Abitibi-Wawa boundary at depth. Hence, beneath the surface trace of the Ivanhoe Lake fault zone, a westward-tapering wedge of Abitibi crust appears to overlie an eastward-tapering wedge of Wawa crust.

Despite suggestions that much of the Abitibi formed in an intraoceanic setting, there is growing evidence for the involvement of older sialic crust during Abitibi crustal genesis (Bleeker, 2002). In the northeastern Abitibi subprovince, Mortensen (1993b) dated a number of inherited zircons with U-Pb ages between 2805 to 2762 Ma in a 2759 Ma felsic volcanic unit. In the southwestern Abitibi, a xenocrystic zircon with a minimum age of 2926 Ma occurs in the 2694 Ma Coté township tonalite, located 90 km north of the Rice Lake batholith (Barrie and Davis, 1990; loc. a, Fig. 1). Just east of this pluton, galena with anomalously radiogenic Pb characterizes the Kam Kotia massive sulfide deposit (Thorpe, 1999), which could reflect this older crustal influence. In the same region, Nd isotope data for the Montcalm gabbroic complex and nearby granitic bodies (locs. b and c, respectively, Fig. 1) also suggest contamination by older crustal material (Barrie and Shirey, 1991). Within the Swayze greenstone belt, Cattell (1987) used geochemical and Nd istope data to demonstrate significant contamination of komatiitic basalts by <200-m.y.-old sialic crust (loc. d, Fig. 1). Finally, recently dated volcanic rocks from two locations north of the Kenogamissi plutonic complex provide new zircon inheritance evidence of an older crustal influence. An intermediate volcanic unit of Kidd-Munro age (U-Pb zircon age of 2712 Ma; loc. e, Fig. 1) yielded a concordant, 2861 Ma single zircon fraction (Ayer et al., 2005; see also Hathway et al., 2004). U-Pb data for a felsic tuff also of Kidd-Munro age (2712.8 ± 1.2 Ma; Ayer et al., 2002a) similarly included a discordant zircon fraction with a $^{207}Pb/^{206}Pb$ age of 2854 Ma (Ayer et al., 2005; loc. f, Fig. 1). These are the first volcanic samples from the southwestern Abitibi for which xenocrystic zircon ages older than ca. 2.75 Ga have been reported.

Based on our data and the information cited above, it seems probable that >2.8 Ga continental crust underlies a portion of the southwestern Abitibi subprovince and was in place from 2747 Ma onward. However, this older crustal influence appears to be spatially limited and currently is confidently detected only within ~75 km of the Abitibi-Wawa boundary

(Fig. 1). We suggest that this indicates at least a 75-km overlap of Abitibi crust onto a Wawa continental substrate during volcanic and plutonic construction of the former, an interpretation that is consistent with available seismic data. A large quantity of geochemical and inherited zircon U-Pb data from more easterly Abitibi greenstone assemblages suggests that ancient Wawa crust is unlikely to extend much farther east than this ~75-km-wide zone, at least in the region of Figure 1.

In general, our whole-rock geochemical data are too few to clearly support or refute the hypothesis of an older crustal contaminant in the Rice Lake but not the Round Lake magmas. Other factors that inhibit such an evaluation are a lack of information on the composition of the contaminant, and, in the possible case of a tonalitic contaminant, little ability to geochemically distinguish this material from the host tonalitic and granodioritic magmas. A more robust approach in this instance may be to consider other isotopic data in addition to those discussed above. In Figure 10, the regional ε_{Nd} data of Ayer et al. (2002a) and this paper (Table 6) are reevaluated with respect to location east or west of the proposed isotopic line shown in Figure 1. A histogram of ε_{Nd} data for plutonic and volcanic samples collected west of this line is characterized by a relatively broad range of ε_{Nd}. In contrast, the histogram for samples located east of the line is distinguished by a much tighter clustering of ε_{Nd} values. Although this does not represent a rigorous test of our crustal model, the Nd data do continue to support the absence of an older crustal contaminant in the east, in contrast to Nd isotope hints for its presence in the west.

Tectonomagmatic model

Indication of an eastward-tapering wedge of Wawa crust underlying the southwestern Abitibi subprovince suggests that the Archean and Proterozoic tectonic evolution of the region should be revisited. Jackson and Sutcliffe (1990) noted that the Swayze greenstone belt has characteristics of both an ensimatic and ensialic arc, with true ensimatic (Abitibi) and ensialic (Michipicoten) greenstone belts located to either side (Fig. 10). These workers further suggested that regional differences in volcanic setting may have been important in determining the location of the Kapuskasing structural zone. More recently, Bleeker (2002) suggested that Abitibi crustal growth occurred within a highly extended rift or marginal basin, with both rifted Wawa and Opatica tonalitic crust locally forming basement to overlying volcanic sequences. This is in accord with suggestions that the Swayze and Montcalm areas (Fig. 1) have features consistent with autochthonous or parautochthonous crustal development (Barrie and Shirey, 1991; Heather, 1998; Thurston, 2002; Ayer et al., 2002a). The concept of older crustal fragments within a dominantly mafic volcanic regime has an analogue in the modern Kerguelen oceanic plateau of the southern Indian ocean. Isotopic and geochronological data suggest the presence at depth of continental lithosphere that was likely derived from India during rifting and ocean basin development (Hassler and Shimizu, 1998; Nicolaysen et al., 2001; Weis et al., 2001). This is consistent with, but differs in detail from, the scenario envisaged here for development of the southwestern Abitibi subprovince.

Based on our proposed crustal architecture, a possible tectonomagmatic evolution involves the following progression (Fig. 10):

1. Growth of tonalitic and greenstone crust in the southeastern Wawa subprovince (and likely elsewhere in this subprovince) began at 2.93 Ga and probably continued until 2.82 Ga.
2. This crust was rifted to form an ocean basin and an east-facing Wawa continental margin. Alternately, this continental margin may have a different origin.
3. Mantle plume- and subduction-related growth of Wawa and southern Abitibi crust began at ca. 2.75 Ga, with contamination of Abitibi magmas with older sialic crust near the Wawa continental margin (e.g., Rice Lake area). The exact nature and polarity of tectonomagmatic events are not known.
4. Predominantly south-vergent collisional shortening within the Abitibi and Wawa subprovinces began at ca. 2.7 Ga (e.g., Jackson et al., 1994).
5. Beginning in the Late Archean and continuing during the Paleoproterozoic, east- and southeast-directed thrusting occurred within the Kapuskasing structural zone.

Because of the limited extent of older crust at depth beneath the Abitibi subprovince and the rheologically weak, highly faulted nature of rifted continental margins, we suggest that the former rifted margin may have played a fundamental role in determining the location of the Kapuskasing structural zone. The role of older tectonic features in controlling the location and growth of new structures is well documented and has been termed "tectonic inheritance" by Thomas (2006). A preexisting crustal influence on the location of the Kapuskasing structural zone has also been suggested by earlier workers (e.g., Jackson and Sutcliffe, 1990). Significant north-south compressional tectonic activity within the Abitibi subprovince beginning at ca. 2.7 Ga occurred at a high angle to this margin, and therefore the first-order geometry of older lithosphere to the west and juvenile lithosphere to the east would not have been destroyed during collisional shortening. It is interesting to speculate that this progression and geometry of events may have left the Abitibi-Wawa boundary relatively fertile for intracratonic reactivation at a later time.

Evidence presented here suggests that models that call for tectonic underplating of older crustal material or sediment subduction to account for evolved Abitibi isotopic signatures (e.g., Jackson and Sutcliffe, 1990; Bédard and Ludden, 1997) are not universally applicable. If our model is correct, then Wawa crust underlay the southwestern edge of the Abitibi during its entire growth history from 2750 Ma onward, and contamination of juvenile magmas by older crust was due to an autochthonous rather that allochthonous relationship. This suggests that the Abitibi subprovince formed in a pericontinental setting adjacent to (and partly on top of) older Wawa sialic crust, quite possibly as a result of extension and rifting of this crust. Earliest Abitibi magmatism may have been related to a mantle plume that resulted from, or perhaps was responsible for, rifting of the Wawa protocraton. The intracratonic Kapuskasing structure, which is an atypical feature of

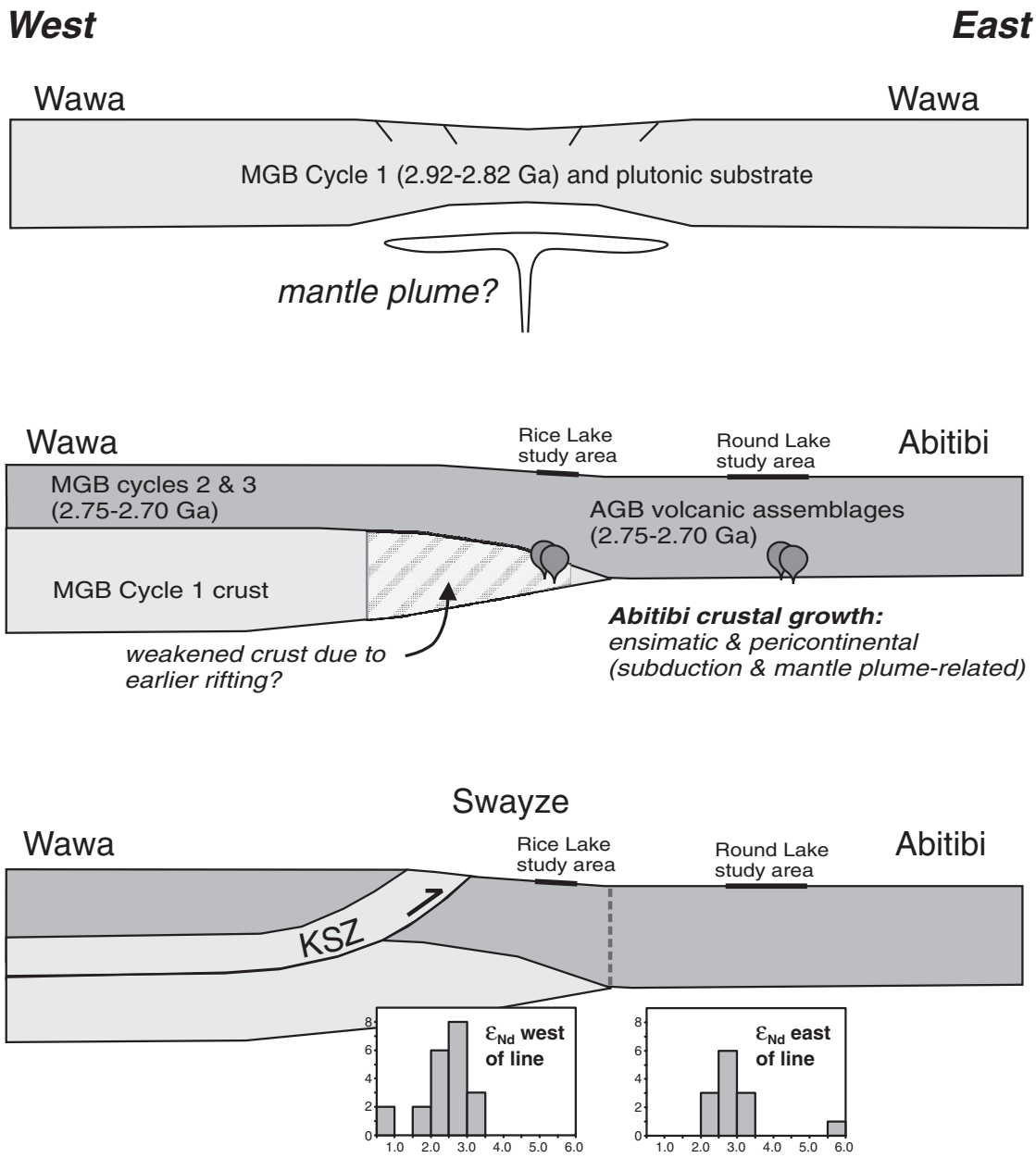

FIG. 10. Schematic illustration of Archean crustal development in the vicinity of the present-day Abitibi-Wawa subprovince boundary. Note the east-west orientation of these cross sections. Top panel: Crustal development in the Wawa subprovince began at ca. 2.93 Ma with initial growth of the Michipicoten greenstone belt (MGB) and contemporaneous felsic plutonic activity. We postulate the growth of an early continental block that may have been subsequently rifted to form an east-facing (present-day coordinates) continental margin. The age of this rifting event, if it occurred, is unknown, and a mantle plume-related cause is entirely speculative. Middle panel: Continued crustal growth in the eastern Wawa subprovince and initial crustal development of the Abitibi subprovince. This 2.75 to 2.70 Ga period witnessed comparable volcanic and plutonic activity in both subprovinces, and a variety of tectonic settings have been postulated by earlier workers. Based on new and existing isotopic data, older crust of the Wawa subprovince likely underlay the southwestern edge of the Abitibi subprovince from ca. 2.75 Ga onward and locally contributed to Abitibi crustal growth. If the Wawa continental margin was formed by rifting, inherent structural weaknesses may have remained following this period of crustal growth. AGB = Abitibi greenstone belt. Bottom panel: Beginning in the Late Archean and culminating at ca. 1.9 Ga (see Percival and West, 1994, and references therein), tectonic activity exhumed midcrustal rocks of the Wawa subprovince within the the Kapuskasing structural zone (KSZ), the eastern margin of which forms the present-day Abitibi-Wawa boundary. The locus of KSZ deformation may have been controlled in part by older structural features (perhaps rift related). Tectonic activity within the Abitibi beginning at ca. 2.7 Ga was predominantly related to north-south compression, and therefore the first-order features of the middle panel were likely preserved to some degree until subsequent Kapuskasing tectonic activity. Seismic reflection data from the KSZ are compatible with the hypothesis of older Wawa crust remaining beneath the Swayze greenstone belt. Histograms of the regional ε_{Nd} isotope data of Ayer et al. (2002a) and this paper suggest that these data generally support the concept of an older crustal influence during crustal growth along the southwestern margin of the Abitibi subprovince.

Archean cratons worldwide, suggests that a major lithospheric weakness remained following these events.

Our evolutionary model may also help to explain why the Swayze, Montcalm, and Michipicoten greenstone belts are less well-endowed in volcanic massive sulfide (VMS) deposits compared to the Abitibi belt east of the isotopic line shown in Figure 1. A similar lack of VMS deposits is also known in regions of the Slave and Superior provinces that are underlain by older continental crust. This may be because extensive synvolcanic rifting in areas without underlying older crust might allow greater heat transfer to the upper crust, as potentially indicated by more voluminous synvolcanic upper crustal melts such as the FII and FIII rhyolites of the Abitibi (Hart et al., 2004). Higher upper crustal temperatures would generate more widespread hydrothermal activity and potentially could also increase the likelihood of VMS deposition.

Conclusions

Volcanic and plutonic assemblages of the southwestern Abitibi subprovince formed between 2750 and 2670 Ma. Most researchers assume that the early stages of this crustal growth occurred in tectonic settings isolated from older continental crust. However, the presence of ca. 2850 Ma inherited zircons in two samples from the Rice Lake batholith (part of the larger Kenogamissi plutonic complex) indicate the involvement of older crust in Abitibi magmatism beginning at 2747 Ma. Neodymium and hafnium isotope data (the latter obtained from igneous zircons) support this conclusion and, in conjunction with previously published data, suggest that an approximately 75-km-wide zone of Abitibi crust adjacent to the Wawa subprovince is underlain by older continental crust. The most likely source of magma contamination is an eastward-tapering wedge of lower Wawa crust that remained following earlier rifting and continental margin development. Existing seismic reflection data are generally consistent with this crustal model. Published U-Pb ages for Wawa crust are no older than 2.92 Ga, consistent with isotopic data, suggesting that the crustal contaminant is unlikely to be more than 100 to 200 m.y. older than the age of Abitibi magmatism. The Kapuskasing structural zone, which forms the present-day Abitibi-Wawa boundary, is a Late Archean and Paleoproterozoic feature that developed in an intracratonic setting. The locii of Kapuskasing deformation was probably controlled by a preexisting crustal weakness situated within the former transition zone between Abitibi and Wawa crust. Rifted older Wawa crust may have been an important contributor to this crustal weakness.

Plutonic complexes of the Abitibi subprovince have been the subject of far fewer studies than adjacent volcanic assemblages. However, these complexes may contain better evidence for the presence of older crust at depth than coeval volcanics due to the longer crustal residence times of unerupted magmas. Given that this should enhance opportunities for crustal interaction, we suggest that studies of the type reported here may represent an avenue for further research, particularly in regions where an older crustal influence is suspected. In situ dating and Hf isotope analysis of zircon facilitates the discovery of inherited zircons and may permit a range of transient Hf isotope compositions (linked to source rock compositions) during magma generation and accumulation to be identified.

Acknowledgments

We gratefully acknowledge the assistance of staff of the various isotopic and geochemical laboratories who produced or contributed to the data presented here. Access to the unpublished data of Kevin Heather and his collaborators is particularly appreciated. Keith Benn is thanked for his support and advice during an early stage of this study. Jens Becker acknowledges financial support from the German Research Foundation (DFG) and an Ontario Geological Survey-University of Ottawa Collaborative Project Agreement. The manuscript benefitted from reviews by John Percival, Fernando Corfu, Ilka Kleinhanns, and an anonymous reviewer. This paper is published with permission of the Senior Manager, Precambrian Geoscience Section, Ontario Geological Survey. This is Geological Survey of Canada contribution 2005100. This is also contribution 543 from the ARC National Key Centre for Geochemical Evolution and Metallogeny of Continents (www.es.mq.edu.au/GEMOC). This study used instrumentation funded by ARC LIEF and DEST Systemic Infrastructure Grants, Macquarie University, and Industry.

REFERENCES

Amelin, Y., Lee, D.-C., and Halliday, A.N., 2000, Early-middle Archaean crustal evolution deduced from Lu-Hf and U-Pb isotope studies of single zircon grains: Geochimica et Cosmochimica Acta, v. 64, p. 4205–4225.

Andersen, T., 2002, Correction of common lead in U-Pb analyses that do not report ^{204}Pb: Chemical Geology, v. 192, p. 59–79.

Andersen, T., Griffin, W.L., and Pearson, N.J., 2002, Crustal evolution in the SW part of the Baltic Shield: The Hf isotope evidence: Journal of Petrology, v. 43, p. 1725–1747.

Atekwana, E.A., Salisbury, M.H., Verhoef, J., and Culshaw, N.G., 1994, Ramp-flat geometry within the central Kapuskasing uplift? Evidence from potential field modeling results: Canadian Journal of Earth Sciences, v. 31, p. 1027–1041.

Ayer, J.A., Amelin, Y., Corfu, F., Kamo, S., Ketchum, J., Kwok, K., and Trowell, N.F., 2002a, Evolution of the southern Abitibi greenstone belt based on U-Pb geochronology: Autochthonous volcanic construction followed by plutonism, regional deformation and sedimentation: Precambrian Research, v. 115, p. 63–95.

Ayer, J.A., Ketchum, J.W.F., and Trowell, N.F., 2002b, New geochronological and neodymium isotopic results from the Abitibi greenstone belt, with emphasis on the timing and the tectonic implications of Neoarchean sedimentation and volcanism: Ontario Geological Survey, Summary of Field Work and Other Activities 2002, Open File Report 6100, p. 5–1 to 5–16.

Ayer, J.A., Thurston, P.C., Bateman, R., Dubé, B., Gibson, H.L., Hamilton, M.A., Hathaway, B., Hocker, S., Houlé, M., Hudak, G., Lafrance, B., Lesher, C.M., Ispolatov, V., MacDonald, P.J., Péloquin, A.S., Piercey, S.J., Reed, L.E., and Thompson, P.H., 2005, Overview of results from the Greenstone Architecture Project: Discover Abitibi initiative: Ontario Geological Survey Open File Report 6154, 146 p.

Barrie, C.T., and Davis, D.W., 1990, Timing of magmatism and deformation in the Kamiskotia-Kidd Creek area, western Abitibi subprovince, Canada: Precambrian Research, v. 46, p. 217–240.

Barrie, C.T., and Shirey, S.B., 1991), Nd- and Sr-isotope systematics for the Kamiskotia-Montcalm area: Implications for the formation of the Late Archean crust in the western Abitibi subprovince, Canada: Canadian Journal of Earth Sciences, v. 28, p. 58–76.

Beakhouse, G., and Davis, D.W., 2005, Evolution and tectonic significance of intermediate to felsic plutonism associated with the Hemlo greenstone belt, Superior province, Canada: Precambrian Research, v. 137, p. 61–92.

Becker, J.K., and Benn, K., 2003, The Neoarchean Rice Lake batholith and its place in the tectonomagmatic evolution of the Swayze and Abitibi granite-greenstone belts, northeastern Ontario: Ontario Geological Survey Open File Report 6105, 42 p.

Bédard, L.P., and Ludden, J.N., 1997, Nd-isotope evolution of Archaean plutonic rocks in the southeastern Superior province: Canadian Journal of Earth Sciences, v. 34, p. 286–298.

Belousova, E.A., Griffin, W.L., O'Reilly, S.Y., and Fisher, N.I., 2002, Igneous zircon: Trace-element composition as an indicator of source rock type: Contributions to Mineralogy and Petrology, v. 143, p. 602–622.

Benn, K., 2005, Late Archean Kenogamissi complex, Abitibi subprovince, Ontario: Doming, folding and deformation-assisted melt remobilization during syntectonic batholith emplacement: Geological Society of America Special Paper 389, p. 297–307.

Black, L.P., and Gulson, B.L., 1978, The age of the Mud Tank carbonatite, Strangways Range, Northern Territory: BMR Journal of Australian Geology and Geophysics, v. 3, p. 227–232.

Bleeker, W., 2002, Archaean tectonics: A review, with illustrations from the Slave craton: Geological Society of London Special Publication 199, p. 151–181.

Blichert-Toft, J., and Albarède, F., 1997, The Lu-Hf isotope geochemistry of chondrites and the evolution of the mantle-crust system: Earth and Planetary Science Letters, v. 148, p. 243–258.

Bursnall, J.T., Leclair, A.D., Moser, D.E., and Percival, J.A. 1994, Structural correlation within the Kapuskasing uplift: Canadian Journal of Earth Sciences, v. 31, p. 1081–1095.

Calvert, A.J., and Ludden, J.N., 1999, Archean continental assembly in the southeastern Superior province of Canada: Tectonics, v. 18, p. 412–429.

Cattell, A., 1987, Enriched komatiitic basalts from Newton Township, Ontario: Their genesis by crustal contamination of depleted komatiite magma: Geological Magazine, v. 124, p. 303–309.

Chown, E.H., Harrap, R., and Moukhsil, A., 2002, The role of granitic intrusions in the evolution of the Abitibi belt, Canada: Precambrian Research, v. 115, p. 291–310.

Corfu, F., 1993, The evolution of the southern Abitibi greenstone belt in light of precise U-Pb geochronology: Economic Geology, v. 88, p. 1323–1340.

Corfu, F., and Davis, D.W., 1992, A U-Pb geochronological framework for the western Superior Province, Ontario: Ontario Geological Survey Special Volume 4/2, p. 1335–1346.

Corfu, F., and Noble, S.R., 1992, Genesis of the southern Abitibi greenstone belt, Superior province, Canada: Evidence from zircon Hf isotope analyses using a single filament technique: Geochimica et Cosmochimica Acta, v. 56, p. 2081–2097.

Corfu, F., and Stone, D., 1998, The significance of titanite and apatite U-Pb ages: Constraints for the post-magmatic thermal-hydrothermal evolution of a batholithic complex, Berens River area, northwestern Superior province, Canada: Geochimica et Cosmochimica Acta, v. 62, p. 2979–2995.

Corfu, F., Hanchar, J.M., Hoskin, P.W.O., and Kinny, P., 2003, Atlas of zircon textures: Reviews in Mineralogy and Geochemistry, v. 53, p. 468–500.

Cousens, B.L., 2000, Geochemistry of the Archean Kam Group, Yellowknife greenstone belt, Slave province, Canada: Journal of Geology, v. 108, p. 181–197.

DePaolo, D.J., 1980, Crustal growth and mantle evolution: Inferences from models of element transport and Nd and Sr isotopes: Geochimica et Cosmochimica Acta, v. 44, p. 1185–1196.

Desrochers, J.P., Hubert, C., Ludden, J.N., and Pilote, P., 1993, Accretion of Archean oceanic plateau fragments in the Abitibi greenstone belt, Canada: Geology, v. 21, p. 451–454.

Dimroth, E., Imreh, L., Goulet, N., and Rocheleau, M., 1982, Evolution of the south-central segment of the Archean Abitibi belt, Québec. Part I: Stratigraphy and paleogeographic model: Canadian Journal of Earth Sciences, v. 19, p. 1729–1758

Dostal, J., and Mueller, W.U., 1997, Komatiite flooding of a rifted Archean rhyolitic arc complex: Geochemical signature and tectonic significance of the Stoughton-Roquemaure Group, Abitibi greenstone belt, Canada: Journal of Geology, v. 105, p. 545–563.

Gagnevin, D., Daly, J.S., Poli, G., and Morgan, D., 2005, Microchemical and Sr isotopic investigation of zoned K-feldspar megacrysts: Insights into the petrogenesis of a granitic system and disequilibrium crystal growth: Journal of Petrology, v. 46, p. 1689–1724.

Goldstein, S.L., O'Nions, R.K., and Hamilton, P.J. 1984, A Sm-Nd-study of atmospheric dusts and particulates from major river systems: Earth and Planetary Science Letters, v. 70, p. 221–236.

Green, A.G., Milkereit, B., Mayrand, L.J., Ludden, J.N., Hubert, C., Jackson, S.L., Sutcliffe, R.H., West, G.F., Verpaelst, P., and Simard, A., 1990, Deep structure of an Archaean greenstone terrane: Nature, v. 344, p. 327–330.

Griffin, W.L., Pearson, N.J., Belousova, E., Jackson, S.E., van Achterbergh, E., O'Reilly, S.Y., and Shee, S.R. 2000, The Hf isotope composition of cratonic mantle: LAM-MC-ICPMS analysis of zircon megacrysts in kimberlites: Geochimica et Cosmochimica Acta, v. 64, p. 133–147.

Griffin, W.L., Wang, X., Jackson, S.E., Pearson, N.J., O'Reilly, S.Y., Xu, X., and Zhou, X. 2002, Zircon chemistry and magma mixing, SE China: In-situ analysis of Hf isotopes, Pingtan and Tonglu igneous complexes: Lithos, v. 61, p. 237–269.

Griffin, W.L., Pearson, N.J., Belousova, E.A., and Saeed, A. 2006, Comment: Hf-isotope heterogeneity in zircon 91500: Chemical Geology, v. 233, p. 358–363.

Halls, H.C., Palmer, H.C., Bates, M.P., and Phinney, W.C. 1994, Constraints on the nature of the Kapuskasing structural zone from the study of Proterozoic dyke swarms: Canadian Journal of Earth Sciences, v. 31, p. 1182–1196.

Harrap, R., and Helmstaedt, H., 1992, Structure and emplacement mechanics of the Round Lake batholith, south of Kirkland Lake, Ontario: Ontario Geological Survey Miscellaneous Paper 159, p. 38–46.

Hart, T.R., Gibson, H.L., and Lesher, C.M., 2004, Trace element geochemistry and petrogenesis of felsic volcanic rocks associated with volcanogenic massive Cu-Zn-Pb sulfide deposits: Economic Geology, v. 99, p. 1003–1013.

Hassler, D.R., and Shimizu, N., 1998, Osmium isotopic evidence for ancient subcontinental lithospheric mantle beneath the Kerguelen Islands, southern Indian Ocean: Science, v. 280, p. 418–421.

Hathway, B., Hudak, G., and Hamilton, M.A., 2004, Geological setting of volcanogenic massive sulphide mineralization in the Kamiskotia area: Ontario Geological Survey, Summary of Fieldwork and Other Activities, Open File Report 6145, p 38–1 to 38–8.

Heather, K.B., 1998, New insights on the stratigraphy and structural geology of the southwestern Abitibi greenstone belt: Implications for the tectonic evolution and setting of mineral deposits in the Superior province: The First Age of Giant Ore Formation: Stratigraphy, Tectonics and Mineralization in the Late Archean and Early Proterozoic: Prospectors and Developers Association of Canada Annual Convention, Toronto, p. 63–101.

Heather, K.B., and Shore, C.T., 1999, Geology, Swayze greenstone belt, Ontario: Geological Survey of Canada Open File 3384a.

Hoskin, P.W.O., and Schaltegger, U., 2003, The composition of zircon and igneous and metamorphic petrogenesis: Reviews in Mineralogy and Geochemistry, v. 53, p. 27–62.

Jackson, S.E., Pearson, N.J., Griffin, W.L., and Belousova, E.A. 2004, The application of laser ablation-inductively coupled plasma-mass spectrometry to in situ U-Pb zircon geochronology: Chemical Geology, v. 211, p. 47–69.

Jackson, S.L., and Fyon, A.J., 1991, The western Abitibi subprovince in Ontario: Ontario Geological Survey Special Volume 4/1, p. 405–482.

Jackson, S.L., and Sutcliffe, R.H., 1990, Central Superior province geology: Evidence for an allochthonous, ensimatic, southern Abitibi greenstone belt: Canadian Journal of Earth Sciences, v. 27, p. 582–589.

Jackson, S.L., Fyon, A.J., and Corfu, F. 1994, Review of Archean supracrustal assemblages of the southern Abitibi greenstone belt in Ontario, Canada: Products of microplate interaction within a large-scale plate-tectonic setting: Precambrian Research, v. 65, p. 183–205.

Jaffey, A.H., Flynn, K.F., Glendenin, L.E., Bentley, W.C., and Essling, A.M., 1971, Precision measurement of half–lives and specific activities of ^{235}U and ^{238}U: Physical Reviews, v. 4, p. 1889–1906.

Kerrich, R., Wyman, D., Hollings, P., and Polat, A., 1999, Variability of Nb/U and Th/La in 3.0 to 2.7 Ga Superior province ocean plateau basalts: Implications for the timing of continental growth and lithosphere recycling: Earth and Planetary Science Letters, v. 168, p. 101–115.

Krogh, T.E., 1973, A low contamination method for hydrothermal decomposition of zircon and extraction of U and Pb for isotopic age determinations: Geochimica et Cosmochimica Acta, v. 37, p. 85–94.

——1982, Improved accuracy of U-Pb ages by the creation of more concordant systems using an air abrasion technique: Geochimica et Cosmochimica Acta, v. 46, p. 637–649.

Krogh, T.E., and Moser, D.E., 1994, U-Pb zircon and monazite ages from the Kapuskasing uplift: Age constraints on deformation within the Ivanhoe Lake fault zone: Canadian Journal of Earth Sciences, v. 31, p. 1096–1103.

Ludden, J., Hubert, C., and Gariepy, C., 1986, The tectonic evolution of the Abitibi greenstone belt of Canada: Geological Magazine, v. 30, p. 357–372.

Ludwig, K.R., 2001, Isoplot/Ex rev. 2.49, a geochronological toolkit for Microsoft Excel: Berkeley Geochronology Center, Special Publication 1a.

Machado, N., Brooks, C., and Hart, S.R., 1986, Determination of initial $^{87}Sr/^{86}Sr$ and $^{143}Nd/^{144}Nd$ in primary minerals from mafic and ultramafic rocks: experimental procedure and implications for the isotopic characteristics of the Archean mantle under the Abitibi greenstone belt, Canada: Geochimica et Cosmochimica Acta, v. 50, p. 2335–2348.

McDaniel, D.K., Hemming, S.R., McLennan, S.M., and Hanson, G.N. 1994, Resetting of neodymium isotopes and redistribution of REEs during sedimentary processes: the Early Proterozoic Chelmsford Formation, Sudbury basin, Ontario, Canada: Geochimica et Cosmochimica Acta, v. 58, p. 931–941.

Mortensen, J.K., 1993a, U-Pb geochronology of the eastern Abitibi subprovince. Part 2: Noranda-Kirkland Lake area: Canadian Journal of Earth Sciences, v. 30, p. 29–41.

——1993b, U-Pb geochronology of the eastern Abitibi subprovince. Part 1: Chibougamau-Matagami-Joutel region: Canadian Journal of Earth Sciences, v. 30, p. 11–28.

Moser, D.E., Heaman, L.H., Krogh, T.E., and Hanes, J.A., 1996, Intracrustal extension of an Archean orogen revealed using single-grain U-Pb zircon geochronology: Tectonics, v. 15, p. 1093–1109.

Nicolaysen, K., Bowring, S., Frey, F., Weis, D., Ingle, S., Pringle, M.S., and Coffin, M.F., 2001, Provenance of Proterozoic garnet-biotite gneiss recovered from Elan Bank, Kerguelen Plateau, southern Indian Ocean: Geology, v. 29, p. 235–238.

Patchett, P.J., 1983, Importance of the Lu-Hf isotopic system in studies of planetary chronology and chemical evolution: Geochimica et Cosmochimica Acta, v. 47, p. 81–91.

Percival, J.A., and Krogh, T.E., 1983, U-Pb zircon geochronology of the Kapuskasing structural zone and vicinity in the Chapleau-Foleyet area, Ontario: Canadian Journal of Earth Sciences, v. 20, p. 830–843.

Percival, J.A., and West, G.F., 1994, The Kapuskasing uplift: A geological and geophysical synthesis: Canadian Journal of Earth Sciences, v. 31, p. 1256–1286.

Percival, J.A., Green, A.G., Milkereit, B., Cook, F.A., Geis, W., and West, G.F., 1989, Seismic reflection profiles across deep continental crust exposed in the Kapuskasing uplift structure: Nature, v. 342, p. 416–420.

Scherer, E., Munker, C., and Mezger, K., 2001, Calibration of the lutetium-hafnium clock: Science, v. 293, p. 683–687.

Shaw, D.M., Dickin, A.P., Li, H., McNutt, R.H., Schwarcz, H.P., and Truscott, M.G., 1994, Crustal geochemistry in the Wawa-Foleyet region, Ontario: Canadian Journal of Earth Sciences, v. 31, p. 1104–1121.

Shirey, S.B., and Hanson, G.N., 1984, Mantle-derived Archean monzodiorites and trachyandesites: Nature, v. 310, p. 222–224.

——1986, Mantle heterogeneity and crustal recycling in Archean granite-greenstone belts: Evidence from Nd isotopes and trace elements in the Rainy Lake area, Superior province, Ontario, Canada: Geochimica et Cosmochimica Acta, v. 50, p. 2631–2651.

Smithies, R.H., and Champion, D.C., 2000, The Archaean high-Mg diorite suite: Links to tonalite-trondhjemite-granodiorite magmatism and implications for early Archaean crustal growth: Journal of Petrology, v. 41, p. 1653–1671.

Söderlund, U., Patchett, P.J., Vervoort, J.D., and Isachsen, C.E., 2004, The ^{176}Lu decay constant determined by Lu-Hf and U-Pb isotope systematics of Precambrian mafic intrusions: Earth and Planetary Science Letters, v. 219, p. 311–324.

Stacey, J.S., and Kramers, J.D., 1975, Approximation of terrestrial lead isotopic evolution by a two-stage model: Earth and Planetary Science Letters, v. 26, p. 207–221.

Stern, R.A., 1997, The GSC sensitive high resolution ion microprobe (SHRIMP): Analytical techniques of zircon U-Th-Pb age determinations and performance evaluation: Geological Survey of Canada, Current Research 1997–F, p. 1–31.

Stern, R.A., Hanson, G.N., and Shirey, S.B., 1989, Petrogenesis of mantle-derived, LILE-enriched Archean monzodiorites and trachyandesites (sanukitoids) in southwestern Superior province: Canadian Journal of Earth Sciences, v. 26, p. 1688–1712.

Stevenson, R., Henry, P., and Gariépy, C., 1999, Assimilation-fractional crystallization origin of Archean sanukitoid suites: Western Superior province, Canada: Precambrian Research, v. 96, p. 83–99.

Sutcliffe, R.H., Barrie, C.T., Burrows, D.R., and Beakhouse, G.P., 1993, Plutonism in the southern Abitibi subprovince: A tectonic and petrogenetic framework: Economic Geology, v. 88, p. 1359–1375.

Theriault, R.J., 1990, Methods for Rb-Sr and Sm-Nd isotopic analyses at the Geochronology Laboratory, Geological Survey of Canada: Geological Survey of Canada Paper 89–2, p. 3–6.

Thomas, W.A., 2006, Tectonic inheritance at a continental margin: GSA Today, v. 16(2), p. 4–11.

Thorpe, R.I., 1999, The Pb isotope linear array for volcanogenic massive sulfide deposits of the Abitibi and Wawa subprovinces, Canadian Shield: Economic Geology, Monograph 10, p. 555–575.

Thurston, P.C., 1991, Archean geology of Ontario: Introduction: Ontario Geological Survey Special Volume 4/1, p. 73–78.

——2002, Autochthonous development of Superior province greenstone belts?: Precambrian Research, v. 115, p. 11–36.

Tomlinson, K.Y., Bowins, R., and Hechler, J., 1998, Refinement of Hf and Zr analysis by improvement in the sample digestion procedure: Ontario Geological Survey Miscellaneous Paper 169, p. 189–192.

Van Achterbergh, E., Ryan, C.G., Jackson, S.E., and Griffin, W.L., 2001, Data reduction software for LA-ICP-MS: Mineralogical Association of Canada Short Course Series, v. 29, p. 239–243.

van Breemen, O., Heather, K.B., and Ayer, J.A., 2006, U-Pb geochronology of the Neoarchean Swayze sector of the southern Abitibi greenstone belt: Geological Survey of Canada Current Research 2006–F1, 32 p.

Vervoort, J.D., and Blichert-Toft, J., 1999, Evolution of the depleted mantle: Hf isotopic evidence from juvenile rocks through time: Geochimica et Cosmochimica Acta, v. 63, p. 533–556.

Vervoort, J.D., White, W.M., and Thorpe, R.I., 1994, Nd and Pb isotope ratios of the Abitibi greenstone belt: New evidence for very early differentiation of the Earth: Earth and Planetary Science Letters, v. 128, p. 215–229.

Vervoort, J.D., Patchett, P.J., Gehrels, G.E., and Nutman, A.P., 1996, Constraints on early Earth differentiation from hafnium and neodymium isotopes: Nature, v. 379, p. 624–627.

Waight, T.E., Maas, R., and Nicholls, I.A., 2000, Fingerprinting feldspar phenocrysts using crystal isotopic composition stratigraphy: Implications for crystal transfer and magma mingling in S-type granites: Contributions to Mineralogy and Petrology, v. 139, p. 227–239.

Walker, R.J., and Stone, W.E., 2001, Os isotopic constraints on the origin of the 2.7 Ga Boston Creek flow, Ontario, Canada: Chemical Geology, v. 175, p. 567–579.

Walker, R.J., Shirey, S.B., and Stecher, O., 1988, Comparative Re-Os, Sm-Nd and Rb-Sr isotope and trace element systematics for Archean komatiite flows from Munro Township, Abitibi belt, Ontario: Earth and Planetary Science Letters, v. 87, p. 1–12.

Weis, D., Ingle, S., Damasceno, D., Frey, F.A., Nicolaysen, K., and Barling, J., 2001, Origin of continental components of Indian Ocean basalts: Evidence from Elan Bank (Kerguelen plateau, ODP Leg 183, Site 1137): Geology, v. 29, p. 147–150.

White, W.M., and Patchett, J., 1984, Hf-Nd-Sr isotopes and incompatible element abundances in island arcs: Implications for magma origins and crust-mantle evolution: Earth and Planetary Science Letters, v. 67, p. 167–185.

Wiedenbeck, M., Allé, P., Corfu, F., Griffin, W.L., Meier, M., Oberli, F., von Quadt, A., Roddick, J.C., and Spiegel, W., 1995, Three natural zircon standards for U-Th-Pb, Lu-Hf, trace element and REE analyses: Geostandards Newsletter, v. 19, p. 1–23.

Wyman, D.A., Kerrich, R., and Groves, D.I., 1999, Lode gold deposits and Archean mantle-plume-island arc interaction, Abitibi subprovince, Canada: Journal of Geology, v. 107, p. 715–725.

Wyman, D.A., Kerrich, R., and Polat, A. 2002, Assembly of Archean cratonic mantle lithosphere and crust: Plume-arc interaction in the Abitibi-Wawa subduction-accretion complex: Precambrian Research, v. 115, p. 37–62.

APPENDIX

Analytical Methods

Whole-rock geochemical analysis

Analytical results for 15 representative samples from the Rice Lake batholith, Somme pluton, and Round Lake plutonic complex are presented in Table 1. All work was completed using the facilities and methods of the Geoscience Laboratories of the Ontario Geological Survey, Sudbury. Samples were powdered using an agate mill. Major and minor element values were determined by wavelength-dispersive X-ray fluorescence spectrometry (WD-XRFS) of fused glass disks. Loss-on-ignition was determined gravimetrically. Trace element analyses were performed by inductively coupled plasma-mass spectrometry using closed-beaker sample digestion (Tomlinson et al., 1998). Nb, Y, Zr, and Cr concentrations were also determined through WD-XRFS of pressed powder pellets, and Be, Cr, Co, Cu, Li, Ni, Sc, Sr, V, W, and Zn were determined by inductively coupled plasma-atomic emission spectrometry.

TIMS U-Pb zircon and titanite dating

Most samples collected for U-Pb geochronology were processed and initially dated by TIMS at the Jack Satterly Geochronology Laboratory, Royal Ontario Museum, Toronto. Standard crushing and mineral separation techniques (e.g., heavy-liquid density separation, Frantz magnetic separator) were used to isolate zircon-bearing heavy mineral separates. Good-quality, least paramagnetic zircons representing the common morphological types in each sample were chosen and given an air-abrasion treatment (Krogh, 1982) prior to final grain selection. Each fraction (typically a single grain) was weighed prior to addition of a ^{205}Pb-^{235}U mixed spike and dissolution in Teflon minicapsules (Krogh, 1973). Due to the small fraction sizes, isolation of U and Pb following dissolution is not essential and was not carried out. Dissolved titanite fractions required HBr column chemical separation (Corfu and Stone, 1998).

The dissolved fractions were dried down in phosphoric acid and loaded with silica gel onto outgassed single Re filaments. Isotopic compositions of Pb and U were measured using a single Daly collector with a pulse-counting detector in a solid source VG354 mass spectrometer. Total common Pb in zircon fractions was below 1 pg in most cases and was assigned the isotopic composition of the lab blank (see footnote to Table 2). Any common Pb in excess of the laboratory blank was assigned the model isotopic composition of Stacey and Kramers (1975). All uncertainties in the text, tables, and concordia diagrams are given at the 95 percent confidence level. The ISOPLOT program (Ludwig, 2001) was used to calculate weighted average $^{207}Pb/^{206}Pb$ ages, discordia lines, and concordia intercept ages.

Additional zircons from all but one sample collected for TIMS dating were mounted in epoxy discs and polished to reveal grain interiors. These grains were analyzed at the Geochemical Analysis Unit, Macquarie University, as described next.

Zircon imaging and electron microprobe analysis

The polished zircons were imaged and then analyzed for SiO_2, ZrO_2, HfO_2, U_2O_3, ThO_2, and Y_2O_3, using a Cameca SX-50 electron microprobe. Under typical instrument operating conditions, zircon imaging involves the detection of both backscattered electrons and cathodoluminescence (Belousova et al., 2002; Jackson et al., 2004). Hence the zircon images are composite BSE and/or CL images. U and Th concentrations were determined during LA-ICPMS by calibration of the observed counts of masses 238 and 232 against within-run analyses of the GJ-1 standard. These concentrations are more precise than the equivalent electron microprobe measurements. Yb and Lu concentrations were determined by LA-MC-ICPMS from the measured $^{176}Yb/^{177}Hf$ and $^{176}Lu/^{177}Hf$ ratios (see below), using the electron microprobe-determined Hf concentration as an internal standard. Zircon compositional data are reported in Table 7.

LA-ICPMS U-Pb zircon dating

LA-ICPMS zircon dating was carried out using a Agilent HP4500 series 300 quadrupole instrument coupled to a New Wave Research/Merchantek EO LUV 213-nm laser. Analytical protocols and methods followed Jackson et al. (2004). Analysis location was chosen based on zircon microstructures and zoning observed in BSE and/or CL images and also took into account the planned location of a subsequent Hf isotope analysis. Laser operating conditions were 5-Hz repetition rate, 0.1-mJ incident pulse energy, and 50-μm spot size. The calibration standard used to correct for fractionation of Pb and U and instrumental drift was GJ-1 (609 Ma; Jackson et al., 2004). Standard zircons 91500 (Wiedenbeck et al., 1995) and Mud Tank (Black and Gulson, 1978) were also analyzed during each analytical run (typically comprising ~20 standards and unknowns) to ensure data quality. The data were processed offline using GLITTER (Van Achterbergh et al., 2001), with the time-resolved isotopic ratios examined for variations due to the influence of inherited cores, metamorphic overgrowths, common Pb, atypical elemental fractionation, and/or Pb loss. Where such heterogenity existed, care was taken to select only isotopically coherent segments of the signal so as to avoid obtaining mixed Pb/U, Pb/Pb, and Pb/Th ages. This strategy is important as concordancy in Pb/U space can be falsely obtained in some cases. Common lead corrections were performed using the algorithm of Andersen (2002), assuming recent Pb loss, and were made for only three of 82 unknown zircons.

SHRIMP U-Pb zircon dating

Two plutonic samples were dated using the SHRIMP II ion microprobe at the Geological Survey of Canada in Ottawa. Standard operating procedures are described by Stern (1997). Approximately 150 grains with an average size of 100 μm were selected at random from the least magnetic fractions and mounted on 2.5-cm epoxy disks along with fragments of the international zircon standard BR 266. The polished zircons were imaged with a scanning electron microscope in either backscatter electron or cathodoluminescence mode to guide primary beam placement for ion probe analysis. Polished mounts were evaporatively coated with 10 nm of high-purity Au for ion probe analysis. Selected areas of the zircons were

sputtered using a mass-filtered O^- primary beam operating in Kohler mode. Primary beam currents ranged from 2 to 6 nA, generating elliptical pits of ca. 20-μm maximum diameter. Pits were <1 μm deep after completion of 10-min analyses. Correction of the measured isotopic ratios for common Pb was estimated from monitored ^{204}Pb, and the corrected ratios and ages are reported with 1σ analytical errors (68% confidence) in Table 4. In Figure 8, analyses are shown at the 1σ level. Age uncertainties cited in the text for all U-Pb data regardless of analytical method are at the 2σ level.

LA-MC-ICPMS Hf isotope analysis of zircon

Hf isotope data for zircons were obtained using a New Wave Research/Merchantek UP 193-nm excimer laser attached to a Nu Plasma MC-ICPMS. Analytical methods and details of instrument operating conditions, standards, and correction for isobaric interferences are discussed in detail by Griffin et al. (2000, 2002) and Andersen et al. (2002). The excimer laser was operated at 2-Hz repetition rate, 0.1- to 0.2-mJ/pulse, and 80- to 100-μm spot size. Total Hf signals were typically 0.5 to 1.5 V, a somewhat low range for these laser operating conditions. It was subsequently discovered that a damaged mirror was responsible for the low signal strength. The within-run precision (1 standard error) for ^{176}Hf/^{177}Hf averages ±0.00003 for all samples but is approximately half this for some samples.

Hf analysis sites were normally chosen to analyze material comparable to that sampled for U-Pb. For example, in oscillatory-zoned zircons, Hf ablation was normally performed "along-strike" from the U-Pb laser ablation site. He was used to transport ablated material from the laser ablation cell via an Ar-He mixing chamber to the ICPMS torch. Following a 30-s background measurement, ablation was initiated and signals were collected for ~170 s. The Nu Plasma software allows time-resolved analysis of the individual signals and isotopic ratios. Isotopically stable, high signal-strength data were chosen for calculation of the final results; this generally involved all data from approximately 10 s after the initiation of ablation to the end of the analysis. Shorter intervals were selected when significant isotopic variation was noted or signal strength decreased markedly toward the end of an analysis. The selected interval was divided into 25 replicates for the calculation of standard errors.

The ^{176}Lu decay constant of 1.865×10^{-11} yr^{-1} (Scherer et al., 2001) and present-day chondritic values of Blichert-Toft and Albarède (1997; ^{176}Hf/^{177}Hf = 0.282772, ^{176}Lu/^{177}Hf = 0.0332) were used. The decay constant of Scherer et al. (2001) is derived from the analysis of well-dated terrestrial samples and is supported by both decay counting experiments and the more recent work of Söderlund et al. (2004) who obtained a similar value of 1.867×10^{-11} yr^{-1}. The Scherer et al. (2001) value is preferred here over that of Blichert-Toft and Albarède (1997; λ^{176}Lu = 1.93×10^{-11} yr^{-1}) because for some of our zircons, the latter yields initial ε_{Hf} values that are up to six ε_{Hf} units above the model depleted mantle curve. This discrepancy is reduced by about two ε_{Hf} units using the Scherer et al. (2001) decay constant. Depleted mantle evolution is calculated using present-day ^{176}Hf/^{177}Hf = 0.28325 (e.g., Griffin et al., 2000) and ^{176}Lu/^{177}Hf = 0.0386.

Uncertainties on the calculation of initial ^{176}Hf/^{177}Hf in zircon (i.e., ^{176}Hf/^{177}Hf at the time of zircon crystallization) stem almost entirely from analytical error in the measured ^{176}Hf/^{177}Hf ratio (Amelin et al., 2000). This error has been propagated in the calculation of ε_{Hf}, which is also sensitive to age due to the age dependence of the chondritic reference value. However, precise age data exist for most of our samples and therefore age-related uncertainties in ε_{Hf} will be negligible.

Both the Mud Tank and 91500 zircons were analyzed as external standards; however the latter appears to be somewhat heterogeneous in ^{176}Hf/^{177}Hf (Griffin et al., 2006) and therefore was used primarily as a monitor of instrument operating conditions. During our analytical sessions we obtained ^{176}Hf/^{177}Hf = 0.282537 ± 0.000060 (2σ, n = 20) for Mud Tank, with an average one standard error of the mean (within-run) of 0.000018.

Whole-rock Nd isotope analysis

Samples were analyzed at either the Geological Survey of Canada or at Carleton University (both in Ottawa). At the Geological Survey of Canada, sample powders were spiked with a mixed ^{148}Nd-^{149}Sm solution and dissolved in an HF-HNO_3 mixture in Savillex Teflon beakers. Separation and purification of Sm and Nd followed cation exchange and HDEHP (Di[2-ethylexyl]) orthophosphoric acid-teflon powder chromatography. Mass analysis was carried out on an MAT-261 solid source mass spectrometer in static multicollection mode. Additional details can be found in Thériault (1990).

Analytical procedures at Carleton University are similar to those at the Geological Survey of Canada. Total procedural blanks for Nd are <400 pg and are insignificant. The ^{147}Sm/^{144}Nd ratios are reproducible to 1 percent. Samples were loaded with 1N HNO_3 on one side of an Re double filament and analyzed in a Finnigan MAT261 thermal ionization mass spectrometer at temperatures of 1,780° to 1,820° C. Isotope ratios are normalized to ^{146}Nd/^{144}Nd = 0.72190. The internal 2σ uncertainties of the means of Nd analyses were typically 0.002 percent, and external reproducibilities based on replicate runs were 0.004 percent. Analyses of two standards in the Carleton laboratory have provided the follow results. The USGS standard BCR-1 yielded Nd = 29.02 ppm, Sm = 6.68 ppm, and ^{143}Nd/^{144}Nd = 0.512668 ± 20 (n = 4). Twenty-two runs of the La Jolla standard averaged ^{143}Nd/^{144}Nd = 0.511877 ± 18. Additional details of the procedure are described by Cousens (2000).

Initial ε_{Nd} values were calculated assuming CHUR ^{147}Sm/^{144}Nd = 0.1967 and present-day ^{143}Nd/^{144}Nd = 0.512638. The uncertainty in the initial ε_{Nd} values is typically ±0.5 to 1.0 ε units. T_{DM} model ages were calculated according to the parameters of Goldstein et al. (1984) in which the present-day–depleted mantle (with ε_{Nd} = 10 and ^{147}Nd/^{144}Nd = 0.2138) has evolved linearly from 4.5 Ga, and the parameters of DePaolo (1980). The latter model may better fit with estimated ε_{Nd} values (3.2–1.8) for the Late Archean-depleted mantle composition of the Abitibi greenstone belt (Machado et al., 1986; Vervoort et al., 1994).